GDAŃSK UNIVERSITY
OF TECHNOLOGY

GDAŃSK UNIVERSITY OF TECHNOLOGY
FACULTY OF CIVIL AND ENVIRONMENTAL ENGINEERING

The author of the PhD dissertation: Kamila Mikina
Scientific discipline: Civil Engineering

DOCTORAL DISSERTATION

Title of PhD dissertation: Direct design of Controlled Modulus Columns (CMC) based on in-situ testing

Title of PhD dissertation (in Polish): Projektowanie bezpośrednie kolumn CMC na podstawie badań polowych

Supervisor *signature*	Second supervisor *signature*
Lech Bałachowski, Ph.D., D.Sc.	
Auxiliary supervisor *signature*	Cosupervisor *signature*
Jakub Konkol, PhD	

Gdańsk, 2022

GDAŃSK UNIVERSITY OF TECHNOLOGY
FACULTY OF CIVIL AND ENVIRONMENTAL ENGINEERING

STATEMENT

The author of the PhD dissertation: Kamila Mikina

I, the undersigned, agree/do not agree* that my PhD dissertation entitled:
Direct design of Controlled Modulus Columns (CMC) based on in-situ testing
may be used for scientific or didactic purposes.[1]

Gdańsk,..... .....
signature of the PhD student

Aware of criminal liability for violations of the Act of 4th February 1994 on Copyright and Related Rights (Journal of Laws 2006, No. 90, item 631) and disciplinary actions set out in the Law on Higher Education (Journal of Laws 2012, item 572 with later amendments),[2] as well as civil liability, I declare, that the submitted PhD dissertation is my own work.

I declare, that the submitted PhD dissertation is my own work performed under and in cooperation with the supervision of Lech Bałachowski, the auxiliary supervision of Jakub Konkol.

This submitted PhD dissertation has never before been the basis of an official procedure associated with the awarding of a PhD degree.

All the information contained in the above thesis which is derived from written and electronic sources is documented in a list of relevant literature in accordance with art. 34 of the Copyright and Related Rights Act.

I confirm that this PhD dissertation is identical to the attached electronic version.

Gdańsk,..... .....
signature of the PhD student

I, the undersigned, agree/do not agree* to include an electronic version of the above PhD dissertation in the open, institutional, digital repository of Gdańsk University of Technology, Pomeranian Digital Library, and for it to be submitted to the processes of verification and protection against misappropriation of authorship.

Gdańsk,..... .....
signature of the PhD student

[1] Decree of Rector of Gdansk University of Technology No. 34/2009 of 9th November 2009, TUG archive instruction addendum No. 8.

[2] Act of 27th July 2005, Law on Higher Education: Chapter 7, Criminal responsibility of PhD students, Article 226.

Abstract

In this paper, the serviceability limit state and bearing capacity of tension screw displacement piles were analyzed using the results of static pile load tests, carried out on the test plot near the Elbląg city, and field, and laboratory tests. The paper presents the methodology of determining the pile load-settlement curve using different types of t-z transfer functions. The new method of constructing the pile load-settlement curves using the trilinear transfer curves, analogous to the functions developed by Frank and Zhao (1982) based on pressuremeter test, is proposed taking into consideration the results of flat dilatometer test. The analogy between pile shaft friction mobilization and direct shearing of the concrete-soil interface was used. The proposed method was derived from 44 shear-displacement curves of cohesionless, cohesive and organic soils in tests performed in a direct shear apparatus on rough or smooth concrete interfaces. The maximum shear stresses on interface were determined, and the slope of skin friction mobilization was expressed as a function of constrained modulus from DMT. Separate friction mobilization functions were proposed for coarse-grained soils (sands), fine-grained (cohesive), and organic soils. The proposed transfer curves takes into account the installation effects, i.e. the applied pile technology. The soil parameters and stress state before and after pile installation were evaluated using the results of CPTU and DMT soundings. The proposed method was validated using the results of eight static load pull-out tests on screw displacement piles performed on the trial test plot. The study is also focused on the determination of soil parameters before and after pile installation using the results of CPT and DMT soundings. The results of uplift static pile load tests were analyzed and the influence of pile length and the after their construction (set-up) on bearing capacity was studied. Currently used CPT-based methods (direct methods) for pile bearing capacity were discussed in this thesis. They were applied then to estimate the bearing capacities of three piles of different lengths. The results were compared with the bearing capacities obtained from the method elaborated by the author. In conclusion, the possibilities for future research to expand the proposed method were presented and its limitations were discussed.

Streszczenie

W niniejszej pracy przeanalizowano stan graniczny użytkowalności i nośności wyciąganych pali przemieszczeniowych formowanych świdrem. Wykorzystano wyniki próbnych obciążeń statycznych pali przeprowadzonych na poletku badawczym w okolicy Elbląga, oraz badań polowych i laboratoryjnych. W pracy przedstawiono metodologię wyznaczania krzywej osiadania pali z wykorzystaniem funkcji transformacyjnych t-z. Zaproponowano autorską metodę budowania pełnej krzywej osiadania pala przy wykorzystaniu funkcji transformacyjnych trzyliniowych, analogiczną do funkcji opracowanych przez Frank'a i Zhao (1982) dla badań presjometrycznych, ale wykorzystującą wyniki badań dylatometrycznych. W tym celu zastosowano analogię między mobilizacją tarcia na pobocznicy pala, a badaniami kontaktu beton-grunt w aparacie bezpośredniego ścinania. Zaproponowana metoda powstała na podstawie 44 krzywych mobilizacji oporów tarcia w badaniach przeprowadzonych w aparacie bezpośredniego ścinania w gruntach niespoistych, spoistych oraz organicznych z wykorzystaniem gładkiego i szorstkiego kontaktu. Wyznaczone zostały maksymalne naprężenia ścinające pomiędzy gruntem i betonem, a nachylenie krzywej mobilizacji tarcia przedstawiono w zależności od wartości modułu ściśliwości z badania dylatometrycznego. Zaproponowano oddzielne funkcje transformacyjne dla gruntów gruboziarnistych (piasków) oraz gruntów drobnoziarnistych i organicznych. Proponowane funkcje transformacyjne uwzględniają efekty instalacji pala, a zatem wpływ technologii wykonywanych pali. Parametry gruntowe oraz stan naprężenia w gruncie przed i po instalacji pali wyznaczono na podstawie badań CPTU i DMT. Do walidacji metody wykorzystano wyniki próbnych obciążeń statycznych ośmiu pali wyciąganych wykonanych na analizowanym poletku badawczym. Przeanalizowano wyniki próbnych obciążeń statycznych pali wyciąganych o różnych długościach, badając wpływ długości pali oraz czasu od ich wykonania na ich nośność. W pracy omówiono również aktualnie stosowane metody bezpośrednie wyznaczania nośności pali oraz wykorzystano te metody do oszacowania nośności trzech pali o różnych długościach na podstawie sondowań statycznych metodą CPTU. Wyniki analiz porównano z nośnością pali uzyskaną z zaproponowanej metody autorskiej. W podsumowaniu przedstawiono możliwości przyszłych badań w celu rozbudowania zaproponowanej metody oraz podano również jej ograniczenia.

Contents

List of figures

List of photographs

List of tables

Notation

All symbols and abbreviations used in this thesis are provided and defined directly in text, figures or they are enclosed to the equations. Here, the full notation is additionally submitted.

Latin letters

a - cone correction factor
a - soil - type parameter
b - soil - type parameter
c - soil - type parameter
c_u - undrained shear strength
d - pile diameter
d_{aver} - pile average diameter
f_p - unit shaft resistance
f_s - friction sleeve
f_{sol} - soil dependent function
h_i -soil layer thickness
k - stiffness
k_t - initial slope of the t-z diagrams
k_q - initial slope of the q-z diagrams
k_1 - empirical coefficient
k - initial slopes
n - number of soil layers
p_0 - pressure applied to the soil at the start of the membrane expansion
p_1 - pressure applied to the soil at the end of the membrane expansion
q_b - limit unit base resistance derived from the MPM (or CPT) method
q_c - cone tip resistance
q_s - limit unit shaft friction derived from the MPM (or CPT) method
q_{si} - pile shaft resistance corresponding to *i* layer
$q_{s,ult.}$ - the ultimate resistance
q_t - corrected cone resistance
q_t - average corrected cone resistance
r_m - radius at which the shear stress in the soil becomes negligible
s - pile head displacement
s_s - actual displacement

u_0 - hydrostatic pore water pressure
u_2 - pore water pressure measured at shoulder filter position
Δu - the increment of the normal displacement
Δu_2 - excess pore water pressure
$s_{s,lim}$ - limit settlement
$q_{s;ult}$ - ultimate unit resistance at pile shaft
q_{ref} - reference stress
q_c - cone resistance from CPTU
w_c - water content
A_{si} - pile shaft area corresponding to the *i* layer
C_{se} - side correlation coefficient
C_1 - slope of the linear plot corresponding to the inverse of the asymptotic value of the ultimate resistance Q_f
C_2 - a constant corresponding to the initial slope of the load settlement curve plotted in linear coordinates
D - pile diameter
D_{50} - mean grain size
E_D - dilatometer modulus
E_M - pressuremeter modulus
E_p - pressuremeter modulus
F_r - normalized friction ratio
G - shear modulus
G_s - specific soil gravity
I_D - material index
K - coefficient of earth pressure
K_D - horizontal stress index
LL - liquid limit
LOI - Loss On Ignition
M - stress ratio
M - the shaft flexibility factor
M_{DMT} - vertical drained constrained modulus from DMT
N - design pile load capacity
N_{kt} - cone factor
OCR - overconsolidation ratio
PI - plasticity index
Q - the applied load on the pile head
$R_{d,t}$ - design pile bearing capacity in tension
R_M - correction factor
R^2 - coefficient of determination
S - normalized undrained shear strength

Greek letters

α - empirical friction coefficient depending on soil type and pile category
β - coefficient dependent on the pile type.
γ_{gm} - model factor
γ_{Rd} - model factor
$\gamma_{s;t}$ - partial safety factor
γ_t - the resistance factor
κ_τ - parameter describing the slopes of the different parts of the t-z curve
ν - Poisson's ratio

ρ - soil density
σ'_h - effective horizontal stress
$\Delta\sigma_n$ - increment of the normal stress
σ_v - total vertical stress
σ'_v - effective vertical stress
σ'_{v0} - vertical effective stress [kPa].
τ_{max} - maximum skin friction

Abbreviations

API - American Petroleum Institute
AVG - Average
BP - Before the Present
CD - Consolidated Drained
CL - clay of low plasticity
CMC - Controlled Modulus Columns
CNL - Constant Normal Load
CNS - Constant Normal Stiffness
CPT - Cone Penetrations Test
CPTu - Cone Penetration Test with pore water pressure measurement
CU - Consolidated Undrained
CV - Constant Volume
DMT - Dilatometer Test
ESCS - European Soil Classification System
ML - silt of low plasticity
MPM - Menard Pressuremeter Test
OH - organic soil of high plasticity
OL - organic soil of low plasticity
PCC - cast-in-situ concrete thin-wall pipe pile
Pt - peat
SD - Standard Deviation
SM - silty sand
SLT - Static Load Tests
SW - well-graded sand
USCS - Unified Soil Classification System

Chapter 1
Introduction

1.1 Background

The analysis concerning CMC (controlled modulus columns) installed on the trial field near the S-7 motorway embankment is the subject of this thesis. These concrete columns were formed in the soft soils of Vistula Marshlands using screw auger technology. The same type of columns was also used for subsoil reinforcement under S-7 embankment. In this study, the complex analysis of the columns below the embankment, including interaction between column, soil, transmission layer and embankment, was not considered. The scope of this thesis is limited to the behavior of a single column on the trial field under axial loading. That is why it can be considered as the behavior of the displacement pile installed with screw auger and the term 'pile' is often used in this thesis together with CMC column.

The bearing capacity of a pile in compression is the sum of the bearing capacity of the base and shaft of the pile. In case of tension piles, only the shaft capacity is generally considered. Two approaches can be used to estimate the ultimate bearing capacity of the pile. The first traditional group of design methods is based on results of laboratory and field soil investigation, where the shear strength parameters are determined and then used in calculation codes. The second approach, more efficient, consists on the use of in-situ soil investigation methods and the analogy between the penetration tool behavior and the pile work. Currently, there are many methods for estimating bearing capacity based on field tests such as cone penetration testing CPT, dilatometer soundings DMT and pressuremeter testing PMT. The cone penetration induces large deformations in the surrounding soil, so the results of this tests are more oriented towards bearing capacity or soil stability problems. On the other hand the penetration of flat dilatometer blade and the inflation of steel membrane generate intermediate level of deformation in the surrounding soil. Similar level of soil deformation can be also expected during expansion of pressuremeter. One should notice that the results of these two tests are sensitive to the stress history and the level of lateral stress in the soil. That is why the results of DMT and PMT tests are more oriented towards deformation analysis. Most of the direct methods are based on CPT soundings due to theirs frequent usage and ease of performing the test. Moreover, the cone penetrometer can be considered as a mini-pile, in which the measured cone resistance corresponds to the bearing capacity of the pile base and the bearing capacity of the shaft of the pile can be estimated using corresponding cone resistance or even sleeve friction in some of the methods. DMT sounding results are less frequently applied in the direct design of piles, even though the basic parameters measured in DMT,

p_0 and p_1, are well suited for calculation of shaft and toe pile resistance (Togliani and Reuter, 2015). Taking into account the horizontal direction of membrane expansion, the results of DMT can be applied in the direct design of piles subjected to horizontal loads, sheet pile walls or slurry walls. In this thesis the constrained modulus from DMT will be used to describe the shaft friction mobilization in form of transfer function t-z. The proposed t-z curves will also be used to predict loading-head displacement curve (Q-s diagrams) in terms of initial displacements as an alternative to existing methods e.g. (Chin, 1970; Gwizdala, 1984; Hansen, 1970; Więcławski, 2015)

The current existing design methods are mainly dedicated to drilled piles, driven piles and offshore piles. Screw displacement piles, which are the subject of this thesis, in terms of bearing capacity can be classified somewhere between drilled and driven piles. These piles are formed by inserting a specially designed spiral auger segment into the soil using both vertical force and torque moment. The soil, with minimal excavation, is displaced laterally and the resulting void is filled with grout or concrete. Screw displacement piles are often an ideal alternative in case where the installation of driven piles is not advisable. The advantages of screw displacement piles are:

- ease of construction with minimal vibration and noise;
- minimum amount of excavated material ;
- high bearing capacity resulting from partial or full displacement of the soil surrounding the pile;
- possibility of piling with this method in almost any soil conditions, including compressible, organic and anthropogenic soils.

The screw auger technology can be also used to form CMC (controlled modulus columns). These are an ideal alternative for pilings and structural slabs, useful for buildings with a conventional or slab-on-grade foundation. They are suitable for highly loaded structures such as highways, industrial and commercial buildings, storage tanks, terminals, residential buildings, etc.

1.2 Outline and aims of the research

The purpose of this dissertation is to analyze ultimate bearing capacity and displacements of screw displacement piles subjected to tension loading together with estimation of load-head displacement Q-s curve. Comprehensive in-situ soil investigations were performed on the trial field using CPTU and DMT before piles installation to monitor initial soil characteristics like strength and deformation parameters together with stress history. The CPTU and DMT carried out tests in some series after piles construction permitted to estimate the pile installation effects including the changes in soil constrained modulus or lateral stress.

The ultimate bearing capacity of selected piles in tension was estimated using the results of static load test and compared to the calculations based on six different direct design methods with CPTU. The load-head displacement curve was predicted including local friction mobilization curves t-z elaborated using the results of interface direct shear tests and DMT.

Important aim of this research is to describe the local friction mobilization on the pile shaft. For this purpose, first, laboratory tests were conducted in a direct shear apparatus, determining the maximum shear stresses in the interface between soil and concrete. Here, an analogy between the skin friction mobilization on the pile segment and direct shear interface test is used. The normal stress applied to the box includes the effect of pile installation with higher lateral stress on the pile shaft. Then, the existing transfer functions using the pressuremeter modulus were rebuilt to take into account the constrained modulus from DMT. Different transfer functions were proposed for coarse-grained soils (sands), for fine-grained, cohesive and organic soils.

Finally the force-head displacement curve was calculated based on local t-z curves and the results were compared with static load tests on tension piles. The elaborated Q-s method was then validated using the results of static load tests.

1.3 Contents of the thesis

This thesis is divided into ten chapters, including an introduction.

Chapter 2 contains, a brief discussion of the methods used to design piles based on in-situ tests. From the numerous methods available in the literature, single, relatively new methods, originating from different countries, have been selected to be applicable to screw displacement columns. The LCPC, CPT 2012, Togliani, German, Unicone and SEU methods are discussed in detail, focusing on the bearing capacity of the shaft.

Chapter 3 describes the essence of transfer functions and discusses several existing methods, which differ in the type of curve used. The linear, trilinear, hyperbolic, point by point and root function methods are described in detail.

The soil conditions analyzed in this paper are presented in Chapter 4. The location of the test fields and the history of the local soil formation are described. The performed field investigations are discussed, and, based on them the soil profile was determined, as well as the basic parameters needed for further calculations, including: vertical drained constrained modulus M_{DMT}, coefficient of earth pressure K or effective horizontal stress σ'_h. Laboratory tests performed, physical characteristics, undrained shear strength and angle of internal friction are also discussed.

Chapter 5 describes the CMC column execution technology and its application. Schemes of test plots with installed columns, their length and loading scheme are presented here. The test loading procedure, its duration, and the results of maximum loads and displacements are described in detail. Then, the results of the test loads are presented in graphs along with the use of Chin's approximation method for estimation of ultimate bearing capacity of the piles. Finally, comparative analyses are conducted to check an eventual time effect (set-up), influence of the pile length and the loading scheme i.e. the influence of previous compression on the bearing capacity of tension columns.

Shear tests between soil and concrete are the subject of Chapter 6. Shear zones at the pile shaft in fine and granular soils are discussed as well as analogies between the localized shear band along a pile and a direct shear test with imposed stiffness. In order to represent the soil behavior in laboratory conditions, the normal stiffness of the tested soils was determined. The behavior of soil-concrete interface was however simplified as possible to be represented by constant normal load (CNL) tests. Two series of measurements were performed at different shear rates, testing both fine and granular soils in contact with smooth and rough concrete at normal stress corresponding to the normal stress acting on the pile shaft after installation. Additionally, one series of measurements was performed by shearing the specimens forward and backward. Shear stress results are presented and compared.

Chapter 7 concerns the formulation of new DMT method for pile design. Based on the transfer function method proposed by Frank & Zhao (Frank and Zhao, 1982) a scheme for creating transfer functions based on DMT is presented. The results, obtained from the direct shear apparatus, were approximated to trilinear functions, and the slopes of the individual curves were analyzed. On this basis, relationships with the vertical drained constrained modulus M_{DMT} were created for both smooth and rough interfaces. In order to make the proposed transfer curves applicable, it is also necessary to know the maximum shear stress values, preferably directly from field testing. Therefore, using the result of DMT soundings, a promising relation between the maximum shear stress and the pressure applied to the soil at the start of the expansion p_0 is found. Complementary analysis for backward shearing is also performed.

The verification of the proposed method is presented in Chapter 8. The results of DMT soundings performed in the pile axis prior to installation were used, as well as the results of static pullout load tests. Calculations were performed for floating piles and piles based on bearing soil layer, for both types of interfaces (smooth and rough). Additional analysis for compression-tension pile was also performed to check the effect of loading path.

The pile capacities obtained in Chapter 8, are then compared in Chapter 9 with the results obtained by other direct methods used for pile design, mentioned in Chapter 2.

Conclusions and comments on the achievements of this research were presented and possible further studies are briefly discussed in Chapter 10.

Chapter 2
Pile capacity – direct design methods

Indirect or direct methods can be used for pile/column design. Indirect methods are based on a multi-step approach, i.e., soil strength parameters (e.g., friction angle, undrained shear strength) determined from in-situ measurements or laboratory tests, and then, the estimation of pile bearing capacity is made.

Direct methods use in-situ measuring data. Most direct methods are based on the CPT (or CPTu) soundings, and thus use measurements of the cone resistance q_c, friction sleeve f_s (and pore water pressure measurements $u_2$from the CPTu test) i.e.(Aoki and Velloso, 1975; Bustamante and Gianeselli, 1982; Cai et al., 2011; Clausen et al., 2005; Eslami and Fellenius, 1997; Gwizdała, 1984; Igoe et al., 2011; Jardine et al., 2005; Kempfert and Becker, 2010; Lehane et al., 2005; Togliani, 2008; White and Bolton, 2005). There are also methods using PMT pressuremeter testing (mainly in French and Canadian practice)(i.e.(Baguelin et al., 2012; Burlon et al., 2014) or DMT (i.e.(Togliani and Reuter, 2015). Direct methods use relationships and algorithms based on probe readings in a one-step process to allow estimation of the bearing capacity of the pile base and shaft.

In this chapter the selected examples of direct methods based on CPT and CPTu testing are discussed. Since this thesis focuses on pullout piles, the base resistance is assumed to be zero as no suction is considered under pile base. Therefore, the formulas for calculating the base resistance are omitted in this chapter and only those for the shaft friction are described.

2.1 Methods for screw displacement piles – overview

2.1.1 LCPC method

The LCPC method is widely used. It is suitable for many pile types in different soil types. Unit shaft resistance f_p is calculated as (Bustamante and Gianeselli, 1982) :

$$f_p = \sum_{i=1}^{n} \frac{q_{ci}}{\propto_i} \tag{2.1}$$

where: q_c – cone tip resistance [MPa]; α - empirical friction coefficient [-], n number of soil layers [-].

Both values of empirical friction coefficient and maximum possible values of unit shaft resistance depend on the type of soil and pile. These values are summarized below in Table 2.1.

Table 2.1. Values of coefficients $\propto$ for calculating the limit skin friction f_p (after (Bustamante and Gianeselli, 1982))

		Category									
		Coefficients, α [-]				*Maximum limit of f_p [MPa]*					
		I		*II*		*I*		*II*		*III*	
Nature of soil	*q_c [MPa]*	*A*	*B*	*A*	*B*	*A*	*B*	*A*	*B*	*A*	*B*
Soft clay and mud	*<1*	*30*	*30*	*30*	*30*	*0.015*	*0.015*	*0.015*	*0.015*	*0.035*	*-*
Moderately compact clay	*1 to 5*	*40*	*80*	*40*	*80*	*0.035 (0.08)*	*0.035 (0.08)*	*0.035 (0.08)*	*0.035*	*0.08*	*≥0.12*
Silt and loose sand	*≤5*	*60*	*150*	*60*	*120*	*0.035*	*0.035*	*0.035*	*0.035*	*0.08*	*-*
Compact to stiff clay and compact silt	*>5*	*60*	*120*	*60*	*120*	*0.035 (0.08)*	*0.035 (0.08)*	*0.035 (0.08)*	*0.035*	*0.08*	*≥0.20*
Soft chalk	*≤5*	*100*	*120*	*100*	*120*	*0.035*	*0.035*	*0.035*	*0.035*	*0.08*	*-*
Moderately compact sand and gravel	*5 to 12*	*100*	*200*	*100*	*200*	*0.08 (0.12)*	*0.035 (0.08)*	*0.08 (0.12)*	*0.08*	*0.12*	*≥0.20*
Weathered to fragmented chalk	*>5*	*60*	*80*	*60*	*80*	*0.12 (0.15)*	*0.08 (0.12)*	*0.12 (0.15)*	*0.12*	*0.15*	*≥0.20*
Compact to very compact sand and gravel	*>12*	*150*	*300*	*150*	*200*	*0.12 (0.15)*	*0.08 (0.12)*	*0.12 (0.15)*	*0.12*	*0.15*	*≥0.20*

Category – IA: plain bored piles; mud bored piles; hollow auger bored piles; micropiles (grouted under low pressure); cast screwed piles; piers; berrettes.

IB: casted bored piles; driven cast piles

IIA: driven precast piles; prestressed turbular piles; jacket concrete piles.

IIB: driven metal piles; jacked metal piles.

IIIA: driven grouted piles; driven rammed piles

IIIB: high pressure grouted piles of large diameter > 250mm; micropiles (grouted under high pressure).

Note: maximum limit unit skin friction f_p: bracket value apply to careful execution and minimum disturbance of soil due to construction.

The design value for the skin friction is obtained by adopting a safety factor of 2. (Bustamante and Gianeselli, 1982)

2.1.2 CPT 2012

Revised CPT 2012 model was introduced to the new French standard for pile design according to Eurocode 7 (Frank, 2017a). It can be considered as an extension of LCPC method including recent pile technologies. This model uses only the measurements on the cone q_c from the CPT test.

The CPT 2012 model divides piles into 8 classes and 20 categories depending on geometrical properties (diameter, length), pile technology and grouting process (see Table 2.2.).

In 'CPT 2012' model, the pile unit shaft resistance q_s is given by formula (AFNOR NF P94-262:2012-07 (2012)):

$$q_s = \alpha \cdot f_{sol} \tag{2.2}$$

where: α – empirical coefficient depending on soil type and pile category [-] (Pile category is presented in Table 2.2, while the empirical coefficient *α* in Table 2.3); f_{sol} – soil dependent function [kPa].

Note that $q_s < q_{s.max}$ where $q_{s,max}$ is a maximum pile unit shaft resistance (see Table 2.4).

f_{sol} is soil-depended function (AFNOR NF P94-262:2012-07 (2012)):

$$f_{sol} = (a \cdot q_c + b)(1 - \exp(-c \cdot q_c)) \tag{2.3}$$

where: a, b, c - soil-type parameters (see Table 2.5).

Table 2.2. Classes and Categories of Piles ("AFNOR NF P94-262:2012-07 (2012)"; Frank, 2017)

Pile class	***Pile category***
C1: Bored Piles	*1: No support* *2: With Slurry* *3: Permanent casing* *4: Recoverable casing* *5: Dry bored pile/or slurry; bored pile with grooved sockets*
C2: CFA Piles	*6: CFA Piles*
C3: Screw Piles	*7: Screw cast-in-place pile* *8: Screw piles with casing*
C4: Closed-Ended driven Piles	*9: Pre-cast or pre-stressed concrete-driven pile* *10: Coated driven steel pile (coating: concrete, mortar, grout)* *11: Driven cast-in-place pile* *12: Driven steel pile ; closed ended*
C5: Open-ended driven Piles	*13: Driven steel pile ; open ended*
C6: Driven H Piles	*14: Driven H pile* *15: Driven grouted H pile*
C7: Driven Sheet Pile Walls	*16: Driven sheet pile*
C8: MicroPiles	*17: Micropile I (gravity pressure)* *18: Micropile II (low pressure)* *19: Micropile III (high pressure)* *20: Micropile IV (high pressure with TAM)*

Table 2.3. Values of installation factor α for 'CPT 2012' model ("AFNOR NF P94-262:2012-07 (2012)"; Frank, 2017)

Pile class	**Soil Type**					
	Silt and Clay % $CaCO_3$<30%	*Intermediate soil*	*Sand and gravel*	*Chalk*	*Marl and calcareous marl*	*Weathered rock*
1	*0.55*	*0.65*	*0.70*	*0.80*	*1.40*	*1.50*
2	*0.65*	*0.80*	*1.00*	*0.80*	*1.40*	*1.50*
3	*0.35*	*0.40*	*0.40*	*0.25*	*0.85*	*-*
4	*0.65*	*0.80*	*1.00*	*0.75*	*0.13*	*-*
5	*0.70*	*0.85*	*-*	*-*	*-*	*-*
6	*0.75*	*0.90*	*1.25*	*0.95*	*1.50*	*1.50*
7	*0.95*	*1.15*	*1.45*	*0.75*	*1.60*	*-*
8	*0.30*	*0.35*	*0.40*	*0.45*	*0.65*	*-*
9	*0.55*	*0.65*	*1.00*	*0.45*	*0.85*	*-*
10	*1.00*	*1.20*	*1.45*	*0.85*	*1.50*	*-*
11	*0.60*	*0.70*	*1.00*	*0.95*	*0.95*	*-*
12	*0.40*	*0.50*	*0.85*	*0.20*	*0.85*	*-*
13	*0.60*	*0.70*	*0.50*	*0.25*	*0.95*	*0.95*
14	*0.55*	*0.65*	*0.70*	*0.20*	*0.95*	*0.85*
15	*1.35*	*1.60*	*2.00*	*1.10*	*2.25*	*2.25*
16	*0.45*	*0.55*	*0.55*	*0.20*	*1.25*	*1.15*
17	*-*	*-*	*-*	*-*	*-*	*-*
18	*-*	*-*	*-*	*-*	*-*	*-*
19	*1.35*	*1.60*	*2.00*	*1.10*	*2.25*	*2.25*
20	*1.70*	*2.05*	*2.65*	*1.40*	*2.90*	*2.90*

Table 2.4. Values of $q_{s,max}$ for 'CPT 2012' model ("AFNOR NF P94-262:2012-07 (2012)"; Frank, 2017)

Pile class	**Soil Type**					
	Silt and Clay % $CaCO_3$<30%	*Intermediate soil*	*Sand and gravel*	*Chalk*	*Marl and calcareous marl*	*Weathered rock*
1	*90*	*90*	*90*	*200*	*170*	*200*
2	*90*	*90*	*90*	*200*	*170*	*200*
3	*50*	*50*	*50*	*50*	*90*	*-*
4	*90*	*90*	*90*	*170*	*170*	*-*
5	*90*	*90*	*-*	*-*	*-*	*-*
6	*90*	*90*	*170*	*200*	*200*	*200*
7	*130*	*130*	*200*	*170*	*170*	*-*
8	*50*	*50*	*90*	*90*	*90*	*-*
9	*130*	*130*	*130*	*90*	*90*	*-*
10	*170*	*170*	*260*	*200*	*200*	*-*
11	*90*	*90*	*130*	*260*	*200*	*-*
12	*90*	*90*	*90*	*50*	*90*	*-*
13	*90*	*90*	*50*	*50*	*90*	*90*
14	*90*	*90*	*130*	*50*	*90*	*90*
15	*200*	*200*	*380*	*320*	*320*	*320*
16	*90*	*90*	*50*	*50*	*90*	*90*
17	*-*	*-*	*-*	*-*	*-*	*-*
18	*-*	*-*	*-*	*-*	*-*	*-*
19	*200*	*200*	*380*	*320*	*320*	*320*
20	*200*	*200*	*440*	*440*	*440*	*500*

Table 2.5. Determination of the a ,b, c parameters ("AFNOR NF P94-262:2012-07 (2012); Frank, 2017a)

Parameter	**Soil Type**					
	Silt and Clay % $CaCO_3$<30%	*Intermediate soil*	*Sand and gravel*	*Chalk*	*Marl and calcareous marl*	*Weathered rock*
a	*0.0018*	*0.0015*	*0.0012*	*0.0015*	*0.0015*	*0.0015*
b	*0.1*	*0.1*	*0.1*	*0.1*	*0.1*	*0.1*
c	*0.4*	*0.25*	*0.15*	*0.25*	*0.25*	*0.25*

The total pile bearing capacity in tension R_t is as follows ("AFNOR NF P94-262:2012-07 (2012)," n.d.; Frank, 2017a):

$$R_t = \sum_{i=1}^{n} q_{si} A_{si} \tag{2.4}$$

where: q_{si} - pile shaft resistance corresponding to *i* layer and [kPa]; A_{si} - pile shaft area corresponding to the *i* layer.

In this model the design approach 2 and 'ground model' procedure is used. Consequently, the design value of pile resistance for tension can be expressed as follows ("AFNOR NF P94-262:2012-07 (2012)," n.d.; Frank, 2017a):

$$R_{d,t} = R_t/(\gamma_{Rd} \cdot \gamma_{gm} \cdot \gamma_t) \tag{2.5}$$

where, $R_{d,t}$ - design pile bearing capacity in tension [kN], γ_{Rd} γ_{gm} - model factors [-]; γ_t - the resistance factor [-]. The safety factors γ_{Rd} are defined within the AFNOR and they are presented in Table 2.5 for the 'CPT 2012' model. The ground model safe factor γ_{gm} is equal to 1.1 and the resistance factor γ_t on the total characteristic resistance is equal to 1.15 for tension piles.

Table 2.6. Model factor γ_{Rd} values for 'CPT 2012' model ("AFNOR NF P94-262:2012-07 (2012),"; Frank, 2017)

Pile type	***γ_{Rd} compression [-]***	***γ_{Rd} tension [-]***
All piles except listed below	*1.18*	*1.45*
Piles embedded in chalk	*1.45*	*1.75*
Coated and injected piles	*2.0*	*2.0*

2.1.3 Togliani method

This method is a kind of combination of the LCPC method and some previous recommendations for estimating the bearing capacity of tapered piles (Gambini, 1986). In this method, sleeve friction f_s is used to calculate the bearing capacity of the pile in addition to the cone resistance values q_c. This method is designed for both cylindrical displacement and non-displacement piles as well as tapered piles in all soil types (Niazi and Mayne, 2013).

The following equation is proposed for the lateral resistance of displacement piles (Togliani, 2008):

$$R_s = \sum_{i=1}^{n} [\pi \cdot d_{aver} \cdot h_i \cdot q_{si}] \tag{2.6}$$

$$q_{si} = k_1 \cdot q_c^{0.5} \tag{2.7}$$

where: h_i – layer thickness [m]; $d_{aver} = (d_{top} + d_{bottom})/2$ – pile average diameter [m]; q_c – tip resistance [kN]; k_1 – empirical coefficient [-].

Depending on the value of friction ratio R_f (Equation 2.8), k_1 is calculated from different equations (Table 2.7).

$$R_f = (f_s/q_c) \cdot 100 \tag{2.8}$$

Table 2.7. Dependencies for the k_1 coefficient

For $R_f < 1$	$k_1 = \beta \cdot [1.2 \cdot \left(0.8 + \frac{R_f}{8}\right)]$	(2.9)
For $R_f \geq 2$	$k_1 = \beta \cdot [1.1 \cdot (0.4 + ln(R_f)]$	(2.10)
For $1 < R_f < 2$	$k_1 = \beta \cdot [1.2 \cdot \left(0.8 + \frac{R_f}{8}\right) + 1.1 \cdot (0.4 + ln(R_f)]/2$	(2.11)

and: β – coefficient dependent on the pile type. $\beta = 1$ for driven displacement piles, 0.6 for non-displacement driven and CFA piles, 0.5 for bored piles (Niazi and Mayne, 2013).

With reference to the calculation of the allowable load, the author adopted the safety factors proposed by Bustamante and Gianeselli, which is 2 for ultimate shaft resistance.

2.1.4 German method

The German method included in the National German recommendation for piles "EA-Pfähle" takes into account recent pile technologies divided into 10 types.

The characteristic pile shaft capacity of a single pile is given (Kempfert and Becker, 2010):

$$R_s = \sum_{i=1}^{n} (q_{si} \cdot A_{s,i}) \tag{2.12}$$

where: $q_{s,i}$ – shaft resistance in layer i [kPa]; $A_{s,i}$ – area of pile shaft in layer i [m^2].

The design values of axial pile resistance in tension in the ultimate limit state result from:

$$R_{s;d} = R_s / \gamma_{s;t} \tag{2.13}$$

where: $\gamma_{s;t}$ – partial safety factor adopted from the German Handbook EC-7. For tension piles, based on empirical data, $\gamma_{s;t} = 1.50$ (Moormann, 2016; Pfähle, 2012).

The shaft resistance is determined from the nomograms shown in Figure 2.1 (Kempfert and Becker, 2007). In non-cohesive soils, knowledge of the cone resistance q_c is needed, while in cohesive soils, the shaft friction is defined by the undrained shear strength.

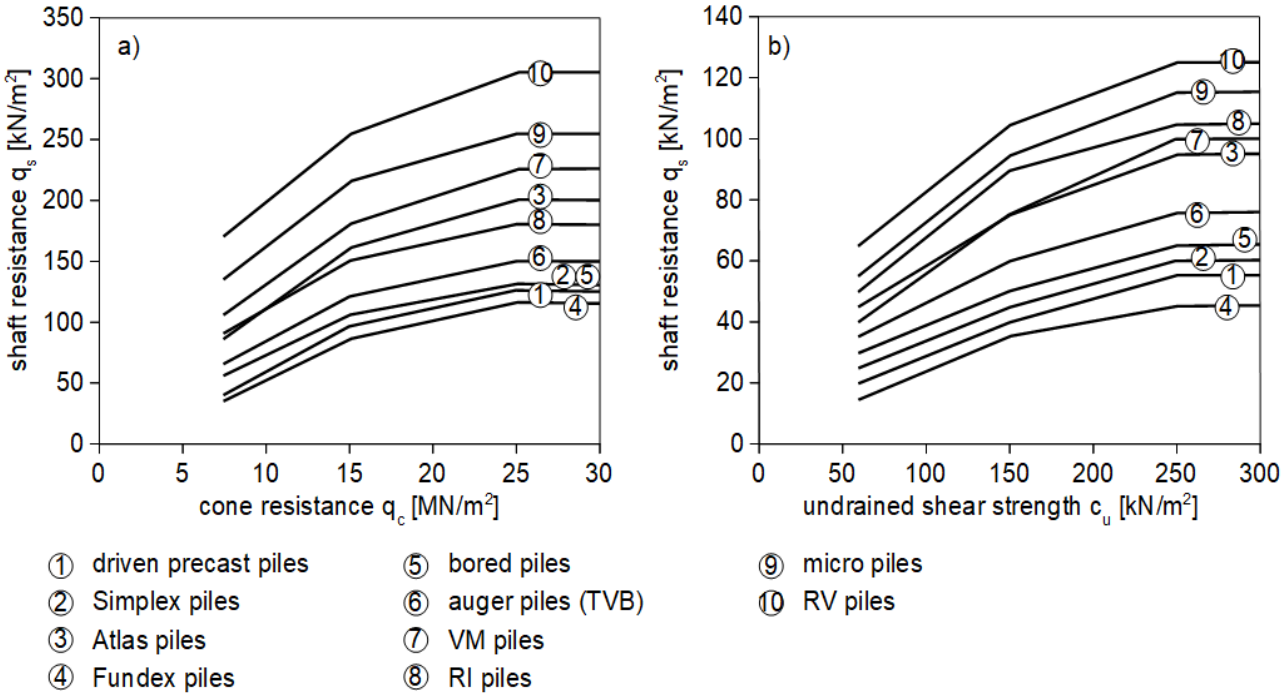

Figure 2.1. Lower empirical values of skin friction for different piles in a) noncohesive soils and b) cohesive soils (after (Kempfert and Becker, 2007))

2.1.5 Unicone method

The method is applicable to all types of piles in all types of soil. It is the first and currently the only method that uses all three measurements from CPTu sounding i.e. q_t, f_s and u_2. to estimate the pile bearing capacity.

The Unicone method uses soil classification based on sleeve friction f_s, and effective cone resistance q_E, using a soil profiling chart (Figure 2.2). The effective cone resistance is determined by the following formula (Eslami and Fellenius, 1997):

$$q_E = q_t - u_2 \tag{2.14}$$

where: q_t – corrected cone resistance, [kPa]; u_2 – hydrostatic mobilized pore water pressure measured behind the cone (shoulder filter measurement) [kPa].

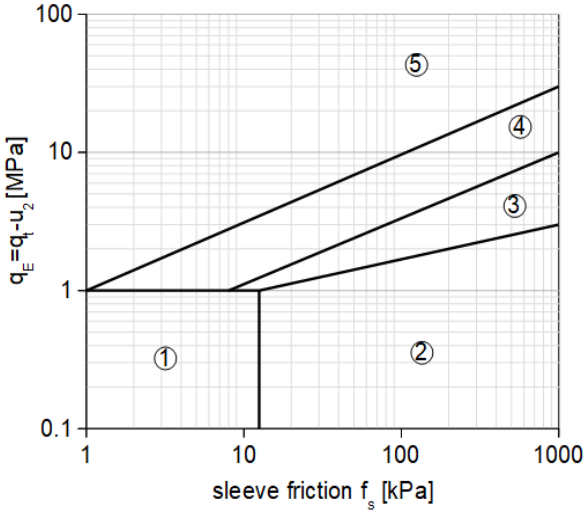

Zone No.	Soil Type	C_{se}
1	Soft sensitive clay	0.08
2	Soft clay and silt	0.05
3	Stiff clay and silt	0.025
4	Silty sand mix	0.01
5	Sand	0.004

Figure 2.2. Soil profiling chart in the Unicone method. (after (Eslami and Fellenius, 1997))

Each soil zone is assigned a side correlation coefficient C_{se}which is then used to calculate the unit shaft friction f_p in each soil layer:

$$f_p = C_{se} \cdot q_E \tag{2.15}$$

2.1.6 SEU method

The method was developed based on the results of 26 load tests on driven, jacked and cased piles and as well as CPTu data. The tests were conducted on Yangsu soft soil deposits in China (Niazi and Mayne, 2013). This is a method suitable for PCC (cast-in-situ concrete thin-wall pipe pile) thin-wall and high-strength caissons, cement fly-ash grave pile in soft clays (driven or jacked) (Niazi and Mayne, 2013). The SEU method is presented here due to the fact that the cement fly-ash grave piles is a similar technology to CMC columns.

The SEU method uses both the friction sleeve f_s and excess pore water pressure Δu_2 to estimate the shaft capacity. Relationships were created to calculate the unit shaft resistance f_p, which depends on pore water pressure (Cai et al., 2011).

For $\Delta u_2 < 200\ kPa$:

$$f_p = \left(\frac{\Delta u_2 + 380}{250}\right) \cdot f_s \tag{2.16}$$

For $200 < \Delta u_2 < 1000\ kPa$:

$$f_p = \left(\frac{\Delta u_2 + 100}{125}\right) \cdot f_s \tag{2.17}$$

where: $\Delta u_2 = u_2 - u_0$; u_0 – hydrostatic pore water pressure [kPa]; u_2 – pore water pressure measured behind the cone [kPa].

The total shaft capacity is calculated similarly to the previous methods (e.g. formula 2.4).

Chapter 3
Transfer curves – existing methods

Transfer curves describe the mobilization of resistance at the shaft (t-z curves) and base (q-z curves) of the pile as a function of axial displacement at a particular depth. They are particularly useful in computer analyses, where the pile is treated as an elastic rod with a constant stiffness along shaft, divided into a series of short elements. The soil is modeled as a collection of springs, described with nonlinear characteristics, distributed along the shaft and one spring under the base of the pile.

Transfer functions for axial loading were first developed over 60 years ago (Cambefort, 1964; Gambin, 1963; Seed and Reese, 1957). Since then, subsequent methods have been developed for specific pile types and soil situations. Curves vary in type, complexity, and number of parameters needed. There are linear functions (eg. Randolph and Wroth, 1979; Verbrugge, 1981), trilinear (e.g. Frank, 1985; Frank and Zhao, 1982), hyperbolic (e.g. Fleming, 1993; Hirayama, 1990; Zhang et al., 2010), point by point (e.g. API, 1993) and root curves e.g. (Krasiński, 2012; Vijivergiya, 1977).

In this paper, one example from each type of method is presented. The relatively simple ones based on a single parameters were selected. Only curves used for soil unit resistance along the pile shaft are discussed here, due to the fact that this work deals only with pullout piles.

3.1 Randolph & Wroth (1978) – linear curves

This is the simplest of the methods, using one deformation parameter to create the t-z curve: the shear modulus G, obtained by correlation from the parameters measured in-situ. The initial slope of the curve is represented by the equation below:

$$k = \frac{G}{\frac{D}{2} \cdot \ln\left(\frac{r_m}{\frac{D}{2}}\right)} \tag{3.1}$$

where: G- shear modulus [kPa]; D – pile diameter [m]; r_m – radius at which the shear stress in the soil becomes negligible [m](Frank, 1975).

The linear curve and is shown in Figure 3.1. and described by Equation 3.2.

$$q_s = min\left(\frac{G}{\frac{D}{2} \cdot \ln\left(\frac{r_m}{\frac{D}{2}}\right)} \cdot s; q_{ult}\right) \tag{3.2}$$

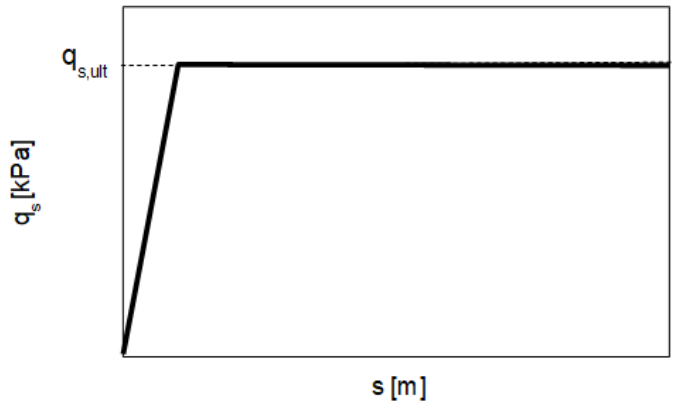

Figure 3.1. The shape of Randolph & Wroth t-z curve for shaft friction

This method, according to the authors, is designed for all types of piles, in all soil conditions.

3.2 Frank & Zhao (1982) and Frank (1985) – trilinear curves

This method is widely used in France. The stiffness of the t-z curve is derived from the pressuremeter modulus E_M from the MPM (Menard pressuremeter) test (Frank, 2017b). Figure 3.2 shows the course of this curve. The parameter κ_τ describing the slopes of the different parts of the curve depends on the E_M and for fine-grained soils is equal to:

$$\kappa_\tau = 2.0 \cdot E_M / D \tag{3.3}$$

and for granular soils:

$$\kappa_\tau = 0.8 \cdot E_M / D \tag{3.4}$$

where: D – pile diameter [m].

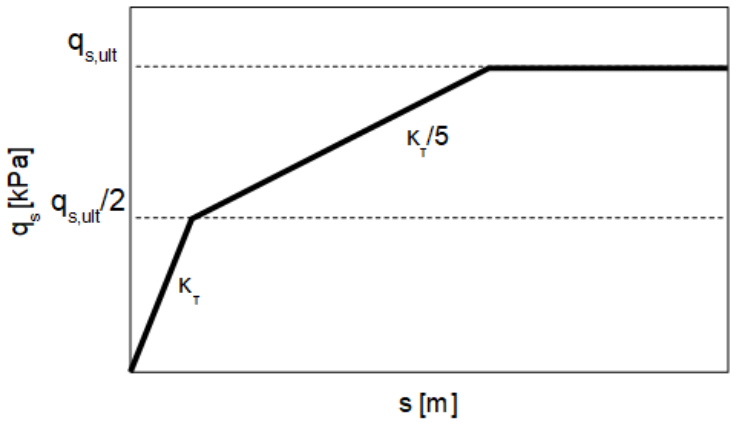

Figure 3.2. The shape of Frank & Zhao t-z curve for shaft friction

This method was developed mainly based on empirical correlations, but some theoretical background is also proposed by Frank (Frank, 1985). It is suitable for all types of piles in fine and coarse grained soils.

3.3 Fleming (1992) - hyperbolic curves

Hyperbolic curves were developed as an analogy to load-settlement curves obtained from pile load tests (Fleming, 1993). Regardless of soil or pile type, a load-settlement curve when plotted on hyperbolic axes (i.e. settlement/load vs. settlement) should give a straight line.

Defining a hyperbola requires two parameters: the first is the ultimate resistance $q_{s,ult.}$, and the second is a fixed parameter: the shaft flexibility factor M. The hyperbola is shown in Figure 3.3 and described by the Equation 3.5 below.

$$q_s = \frac{q_{s,ult} \cdot s_s}{M \cdot D + s_s} \tag{3.5}$$

where: D – pile diameter [m]; s_s – pile displacement [m]; $q_{s;ult}$ – soil ultimate resistance [kPa]; M – shaft flexibility parameter [-].

The parameter M takes values from 0.004 for soft to firm or relatively loose soils to 0.005 for very stiff soils or soft rocks. It should be noted, however, that this parameter decreases with increasing stiffness and, for example, in stiff overconsolidated clays can be as low as 0.001-0.002, with variations depending on soil type, quality of pile construction, and even time effects (Fleming, 1993).

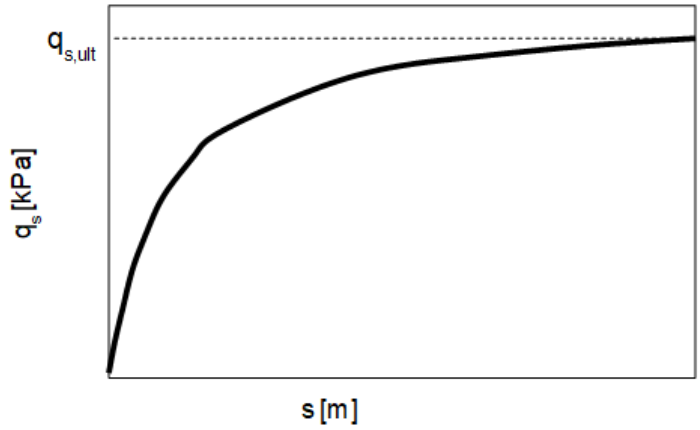

Figure 3.3. The shape of Fleming's t-z curve for shaft friction

This method is designed for all types of piles in all types of soil.

3.4 API (1993) - point by point curves

The method presented in the API (American Petroleum Institute) Standard uses fixed parameters, specifically the settlement limit defined as the settlement full resistance mobilization (API, 1993). There are two curves, one for sands and one for clays. These curves are shown in Fig. 3.4. The characteristic points of the curve for clays are shown in Table 3.1 and for sands in Table 3.2.

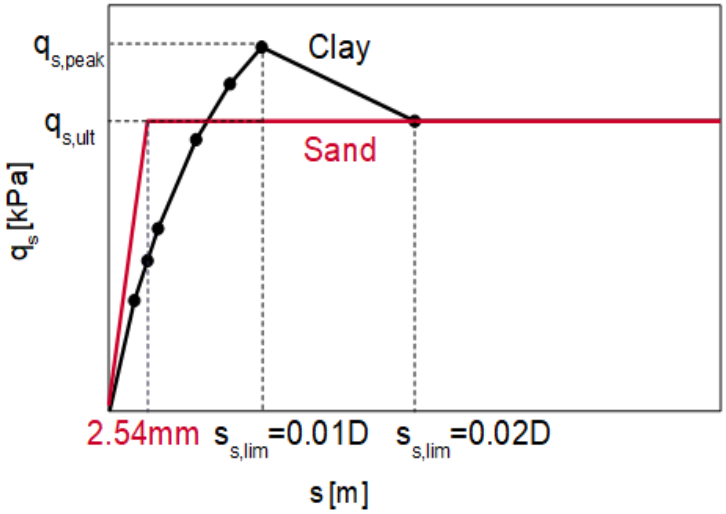

Figure 3.4. The shape of API t-z curve for shaft friction

Table 3.1. Characteristic points for clay curve in API method for transfer curves

Clay	
s_s/D	$q_s/q_{s;ult}$
0.0016	*0.30*
0.0031	*0.50*
0.0057	*0.75*
0.0080	*0.90*
0.0100	*1.00*
0.0200	*0.70 to 0.90*

∞	*0.70 to 0.90*

Table 3.1. Characteristic points for sand curve in API method for transfer curves

Sand	
s_s *[mm]*	$q_s/q_{s;ult}$
0.00	*0.00*
2.54	*1.00*
∞	*1.00*

Initial slopes k for clays and sands are given by the following formulas respectively:

$$k = \frac{q_{s,ult}}{0.0037D} \tag{3.6}$$

$$k = \frac{q_{s,ult}}{0.00254} \tag{3.7}$$

where: D – pile diameter [m]. Limit settlement $s_{s,lim} = 0.02 \cdot D$ for clay and 0.00254m (0.1 inch) fixed for sand.

This method is suitable for all pile types in clays and non-carbonate sands.

3.5 Krasiński (2012) – root curves

As in the previous method, Krasinski's method the limit displacement is used to describe the shape of the transfer curve. The method was developed based on several pile load tests of screw displacement piles (Krasiński, 2012) and is applicable only in sands. The appearance of the curve is shown in Fig. 3.5 and is described by the following equation:

$$q_s = min\left(53 \cdot \left(\frac{q_{s,ult}}{q_{ref}}\right)^{0.25} \cdot \left(\frac{s_s}{s_{s,lim}}\right)^{0.38}; q_{s,ult}\right) \tag{3.8}$$

where: $q_{s;ult}$ - ultimate unit resistance at pile shaft [MPa]; q_{ref} – reference stress, taken to be 1 MPa; s_s – actual displacement [m]; $s_{s,lim}$ – limit displacement equal to 10 mm.

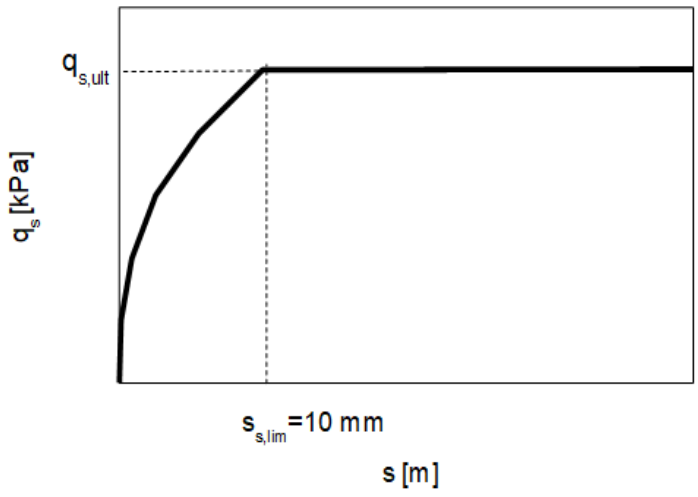

Figure 3.5. The shape of Krasiński's t-z curve for shaft friction

Chapter 4
Soil conditions in Vistula Marshlands – Jazowa testing site

4.1 Introduction

This chapter presents the description and localization of the testing site in Vistula Marshlands. The geotechnical profile, occurring on the examined plot, determined on the basis of static CPTu and dilatometer DMT soundings is described. Most of the soundings were made at the site before the installation of the columns. Thus they present the initial soil conditions. Some in-situ tests were also performed after the pile formation to check installation effects. The field tests were supplemented by a series of laboratory tests, which allowed to determine physical characteristics of the soil, its strength and deformation parameters.

4.1.1 Localization and history of the Vistula Marshlands

The research area is located in northern Poland, in the area of the Vistula Marshlands, 50 km southeast from Gdańsk, near the city of Elbląg. It was carried out during the works related to the construction of the S7 expressway. The exact location and the plot are shown in Figure 4.1 and Photograph 4.1. The research plot is located in the close vicinity of the Nogat River, in the most recent part of the delta not far away from the Vistula lagoon. The soil conditions at the site could be considered as a representative for Vistula Marshlands due to geological history.

The Vistula Marshlands cover an area of about 1700 km², of which 450 km² are located below sea level. Formation of the Vistula's delta started about 6000 BP during the Littorina Sea phase, being a period of transgression and maximum salinity in warmer Atlantic period. The ancient post glacial bay in the mouth of the Vistula river was getting filled with fluvial deposits. It was closed with the sandy Vistula spit formed by marine currents and eolien transport. In this way the majority of the fluvial debris was deposited in the inner delta. The process of the inner delta formation was very complex, with general development trend initially in north-western and then in north-eastern direction (Makowski, 1997).

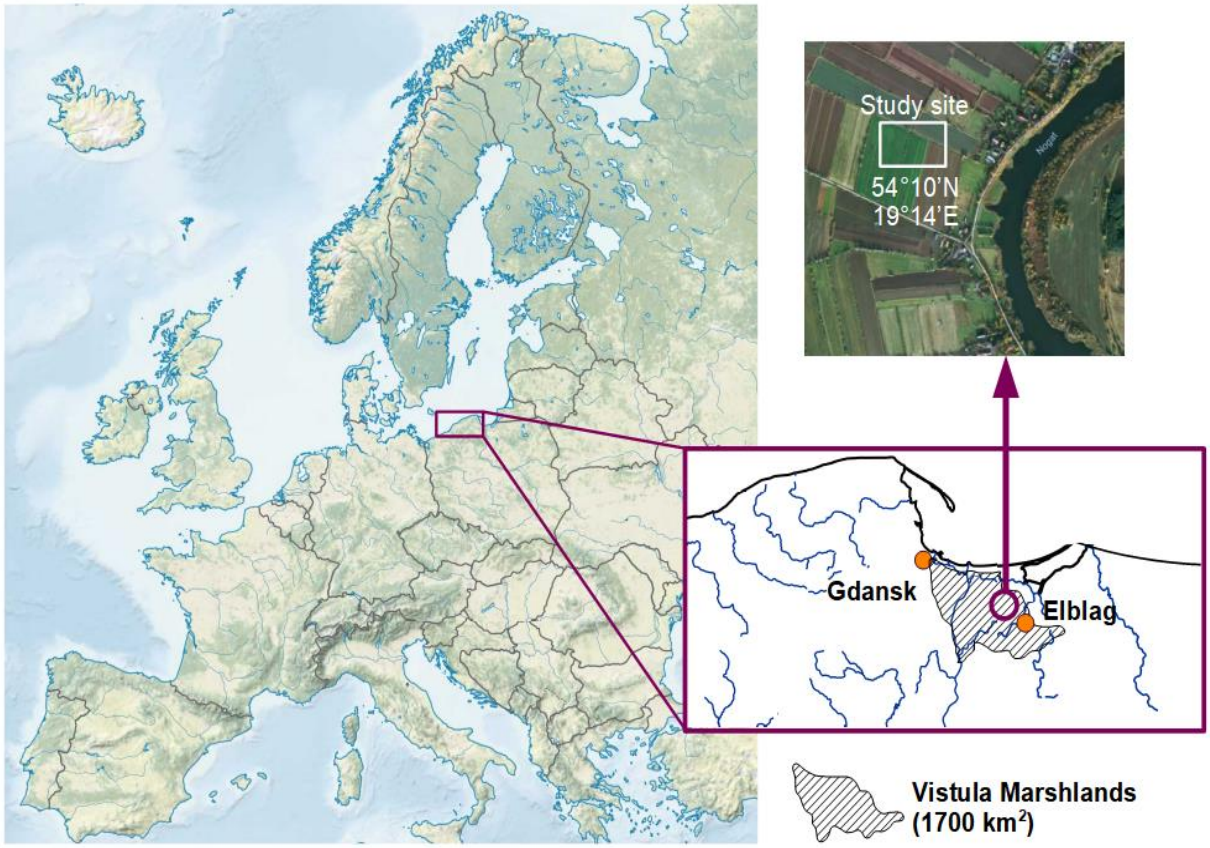

Figure 4.1. Location of the testing site (Konkol et al., 2019)

Photograph 4.1. Testing site (author: Jakub Konkol)

4.1.2 Geotechnical investigations at the testing site

All of the soundings conducted on the test plots are shown in Figure 4.2. The subscripts next to the test designation indicate when a given test was performed, i.e. the subscript '0' means that a given test was performed before pile installation, and e.g. the subscript '8' means that a given test was performed 8 weeks after pile installation.

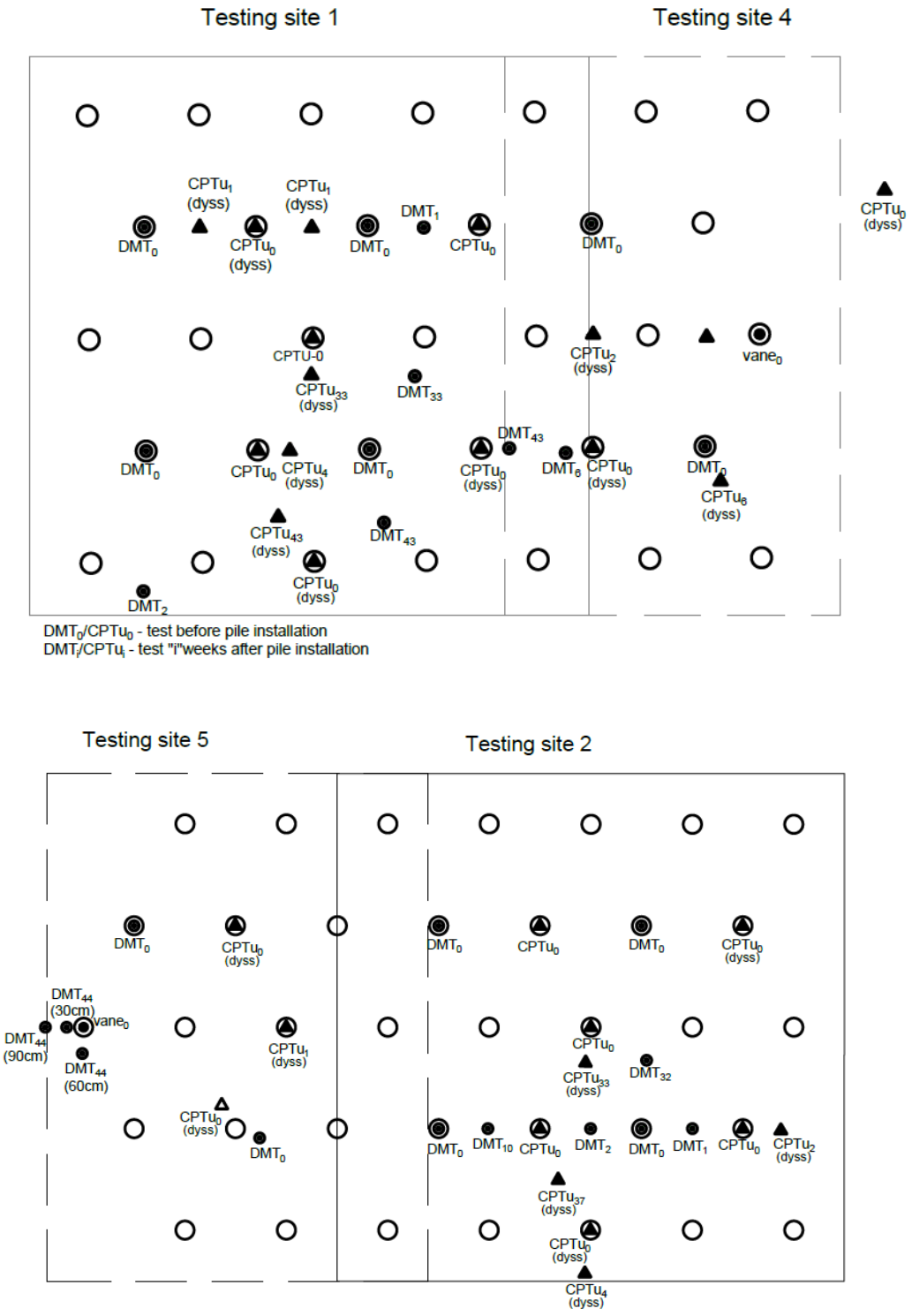

Figure 4.2. CPT and DMT soundings performed on testing site

Before the pile installation, 15 CPTu soundings with a 10 cm^2 electric piezocone were carried out down to approximately 20 m depth. The soundings were carried out at a standard speed of 20 mm/s according to ASTM D5778 (2012). The results are shown with grey lines in Figure 4.3. The results obtained directly from static probing were: cone resistance q_c, friction sleeve f_s and pore water pressure u_2.The cone resistance values were corrected for the net cone base area according to Formula 4.1:

$$q_t = q_c + (1 - a) \cdot u_2 \tag{4.1}$$

where: q_c = cone resistance [kPa], u_2 = pore water pressure measured at shoulder filter position [kPa], a = cone correction factor (equal to 0.84 for a given cone) [-].

Moreover, 8 dilatometer probings were performed on the research plots before the piles installation in accordance with ASTM D6634 (2015) (Fig.4.3). Readings from the DMT soundings were taken every 20 cm and standard pressure readings, p_0 and p_1 ,which are applied to the soil at the start and at the end of the membrane expansion, were obtained. Then, using the equations 4.2-4.4 (Marchetti, 1980), the following parameters were determined:

— horizontal stress index

$$K_D = \frac{p_0 - u_0}{\sigma'_{v0}} \tag{4.2}$$

— dilatometer modulus

$$E_D = 34.7 \cdot (p_1 - p_0) \tag{4.3}$$

— material index

$$I_D = \frac{p_1 - p_0}{p_0 - u_0} \tag{4.4}$$

where: p_0 – pressure applied to the soil at the start of the membrane expansion [kPa]; p_1 – pressure applied to the soil at the end of the membrane expansion [kPa]; u_0 – hydrostatic pore water pressure [kPa]; σ'_{v0} - vertical effective stress [kPa].

During field tests, samples were also taken for laboratory tests with the Piston Sampler ST:1 equipped with three 170 mm long liners and an inner diameter of 50 mm. Depths of sampling are shown in Figures 4.3 and 4.4.

4.1.3 Laboratory investigation

The laboratory tests, carried out for the purposes of this PhD, included primarily determination of basic physical parameters and interfaces testing (discussed extensively in Chapters 6 and 7). Additionally, strength and compressibility parameters were also examined, as described in (Bałachowski et al., 2018; Konkol et al., 2019; Międlarz et al., 2019).

The basic physical soil properties such as water content (ASTM D2216, 2010), soil unit weight (ASTM D7263, 2009) and specific gravity (ASTM D854, 2014) have been distinguished for characteristic soil depths. i.e. at the sampling depths. Additionally, in order to classify soils in accordance with Unified Soil Classification System (USCS) (ASTM D2487 (2017)) the consistency limits were determined in terms of ASTM D4318 (2017) on thirteen selected specimens.

Several triaxial compression tests were also performed to determine the angle of internal friction. Organic silty clay and organic silt samples taken from 3.2-4.0m and 9.5-10.5m depth and peat sampled

from the approx. 14m depth were tested. The CU (consolidated undrained) (ASTM D4767, 2011) and CD (consolidated drained) (ASTM D7181, 2011) tests were conducted.

4.2 Soil profile

Soil layers were separated on the basis of CPTu and DMT sounding results (Fig.4.2-4.3) and classified according to the Unified Soil Classification System (Fig. 4.4).

The soil profile of Jazowa site is as follows:

- 0.00–0.70 m – a layer of silty sand (working platform),
- 0.70–1.80 m – low plasticity silt,
- 1.80–2.70 m – high plastic, organic silty clay (mud),
- 2.70–4.00 m – organic silty clay (mud) / peat,
- 4.00–7.05 m – silty sand (loose to medium dense),
- 7.05–12.15 m - low to high plastic, organic silt (mud) intersected with thin sand layer
- 12.15-14.45 m – peat / inclusions of organic silt
- below 14.45 m – well-graded sand layer.

The water table is located at the shallow depth of approx. 1.7 m below surface level. The soft soil is generally normally consolidated with slight overconsolidation in the upper part of deposits due to water level changes and climate action.

4.2.1 CPTu probings

The results of CPT probings are shown in Figure 4.3 b-d with grey lines. The black line shows the averaged values of individual parameters.

As shown in the figure below, the soundings are repeatable, proving the regularity of subsoil structure.

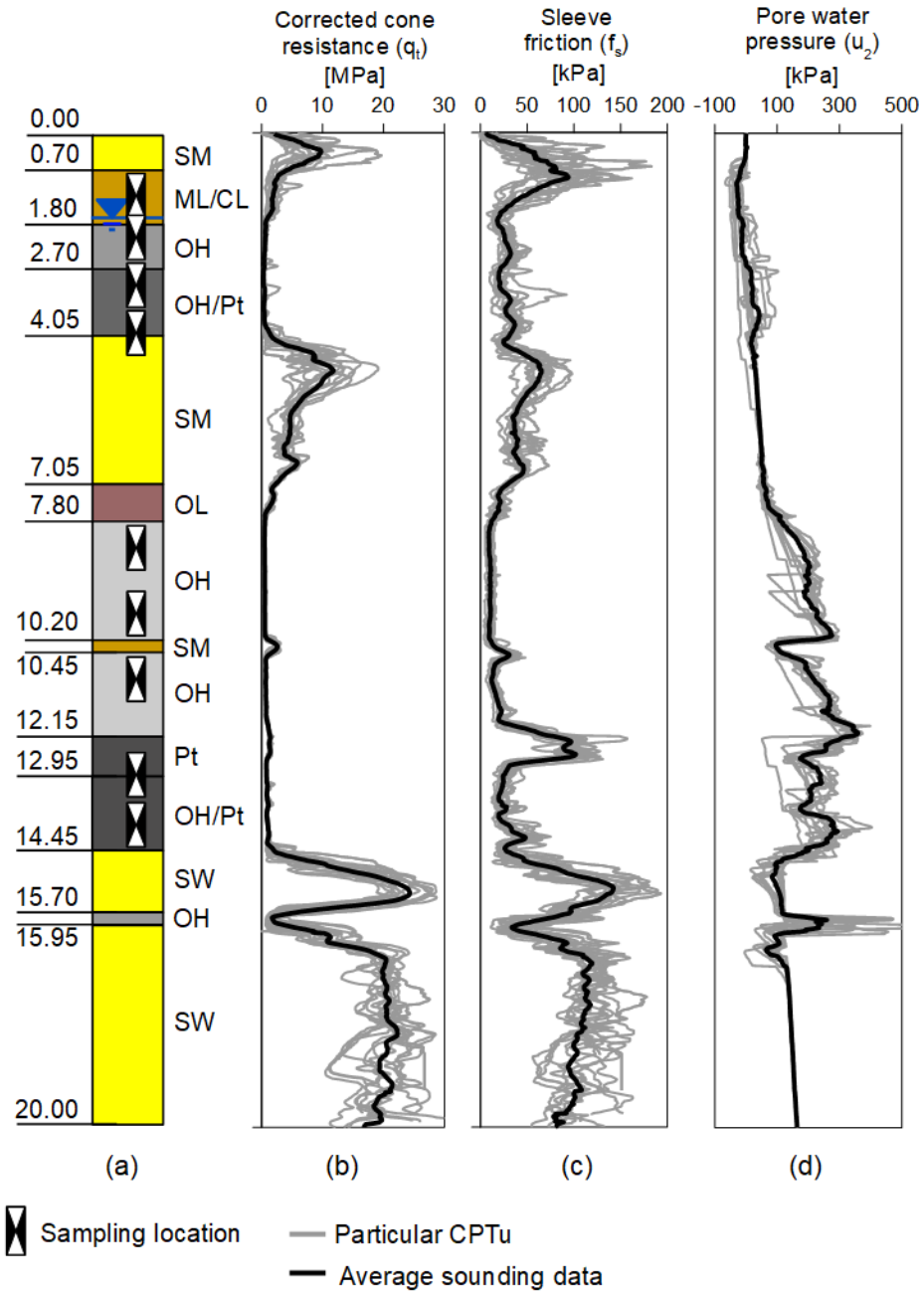

Figure 4.3. (a) Jazowa site soil profile, (b)-(d) CPTU probing results

Based on the sounding results, values of parameters q_t, f_s i u_2 in particular layers were averaged (AVG) and their standard deviations (SD) are given and summarized in Table 4.1.

Table 4.1. Averaged CPTu parameters with standard deviations

Soil layer	q_t AVG	q_tSD	f_s AVG	f_s SD	u_2AVG	u_2 SD
	[MPa]	[MPa]	[kPa]	[kPa]	[kPa]	[kPa]
SM	6.85	3.64	48.53	26.63	-3.02	5.88
ML/CL	1.99	0.86	53.39	18.76	-23.39	14.89
OH	0.54	0.17	28.25	6.73	-9.49	19.74
Pt/OH	0.51	0.28	29.54	8.74	25.77	27.89
SM	6.00	1.79	46.52	10.32	39.11	8.32
OL	1.37	0.26	21.14	4.44	76.82	16.06
OH	0.55	0.05	10.7	2.62	198.37	38.23
SM	2.22	0.48	17.36	5.55	106.7	20.3
OH	0.83	0.09	25.16	5.61	249.99	34.08
Pt	1.07	0.11	71.86	13.99	231.95	66.51
OH/Pt	1.05	0.26	28.73	8.06	231.59	58.83
SW	15.46	4.02	103.31	23.97	109.24	26.46
OH	2.57	1.93	65.8	24.8	213.68	118.86
SW	17.37	2.71	98.63	15.89	153.86	7.97

4.2.2 DMT probings

The results of DMT soundings are presented in Fig. 4.4. As in the case of CPTu , the results of individual tests are presented with grey lines, while the black line shows the averaged profile.

The values of parameters $I_D, K_D$and E_D have been averaged for individual layers and are presented in Table 4.2 as well as standard deviations.

Table 4.2. Averaged DMT parameters with standard deviations

Soil type	I_D AVG	I_D SD	K_D AVG	K_D SD	E_D AVG	E_D SD
	[-]	[-]	[-]	[-]	[MPa]	[MPa]
SM	-	-	-	-	-	-
ML/CL	1.84	0.55	10.51	4.14	13.32	5.33
OH	0.82	0.32	4.42	0.63	3.90	1.20
Pt/OH	0.38	0.14	3.47	0.58	1.74	0.68
SM	2.93	0.66	4.18	1.21	21.93	6.80
OL	1.58	0.39	1.79	0.20	8.00	2.16
OH	0.26	0.05	2.17	0.18	1.601	0.26
SM	2.02	1.27	1.84	0.37	11.74	7.75
OH	0.35	0.06	2.09	0.19	2.46	0.37
Pt	0.37	0.06	3.59	0.61	4.73	0.87
OH/Pt	0.49	0.19	2.54	0.49	4.34	1.51
SW	2.14	0.74	6.38	2.28	56.65	21.72
OH	1.88	1.13	3.86	2.41	35.61	28.54
SW	2.51	0.32	5.84	0.70	69.22	5.68

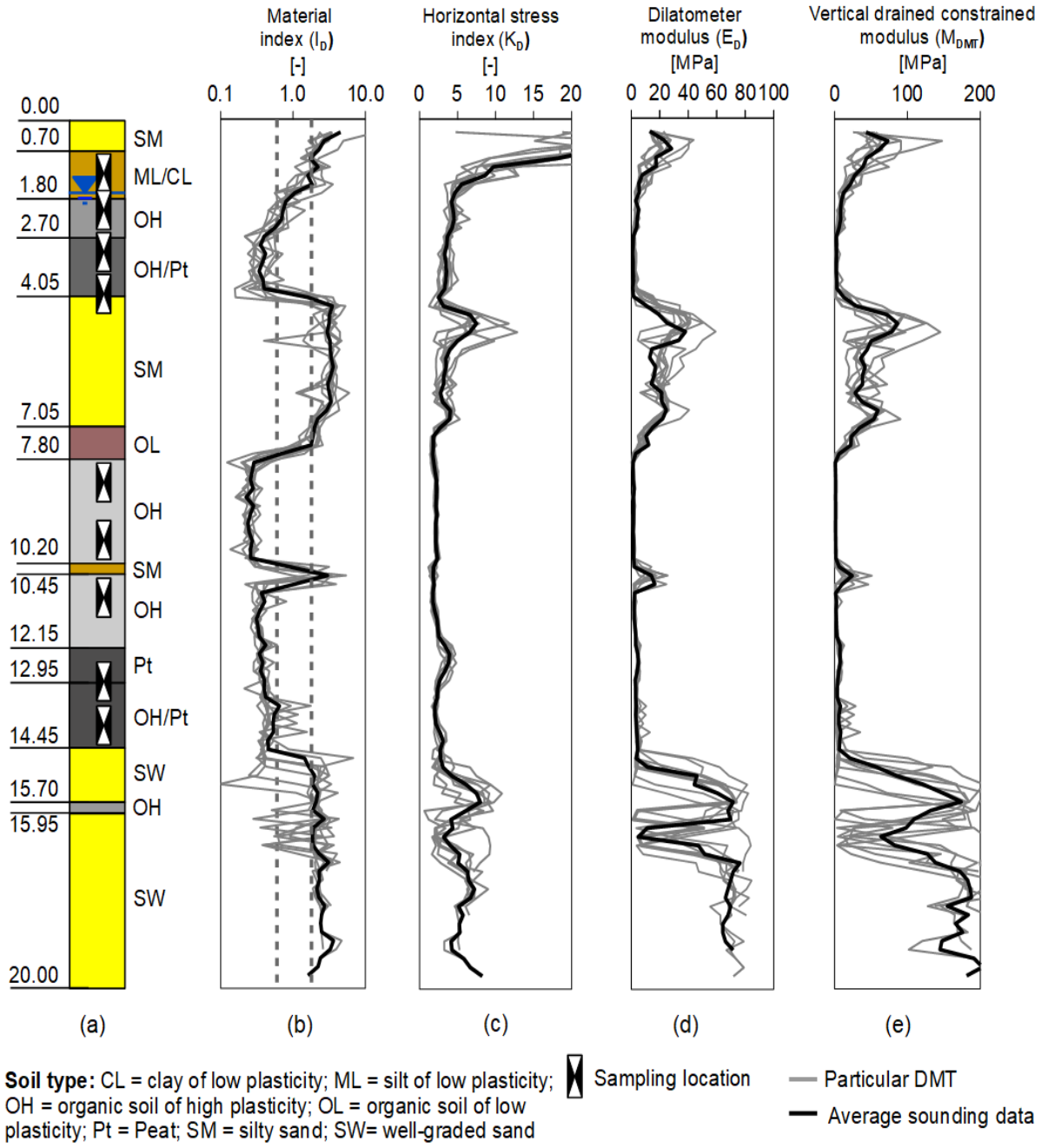

Figure 4.4. (a) Jazowa site soil profile, (b)-(d) DMT probing results

For further calculations, vertical drained constrained modulus M_{DMT} was determined using Formulas 4.5-4.10 (Marchetti, 1980).

$$M_{DMT} = R_M \cdot E_D \tag{4.5}$$

where: R_M – correction factor [-], E_D – dilatometer modulus [kPa].

The values of R_M depend on the density index of soil I_D and the horizontal stress index K_D and should be taken according to the Table 4.3.

Table 4.3. Dependencies for the R_M correction factor

For $I_D \leq 0.6$	$R_M = 0.14 + 2.36 \cdot logK_D$	(4.6)
For $I_D \geq 3$	$R_M = 0.5 + 2logK_D$	(4.7)
For $0.6 < I_D < 3$	$R_M = R_{M,0} + (2.5 - R_{M,0})logK_D$	(4.8)
	$R_{M,0} = 0.14 + 0.15(I_D - 0.6)$	(4.9)
For $K_D > 10$	$R_M = 0.32 + 2.18logK_D$	(4.10)

Note that, R_M should always be greater than 0.85.

On the basis of the results from CPT and DMT soundings, the value of the effective horizontal stress acting in particular soil layers was also calculated in order to determine stress levels in the middle of each soil layer. The effective horizontal stress σ'_h was estimated as:

$$\sigma'_h = K \cdot \sigma'_v \tag{4.11}$$

$$\sigma'_v = \sigma_v - u_0 \tag{4.12}$$

where: σ'_v – effective vertical stress [kPa], σ_v – total vertical stress [kPa], K - coefficient of earth pressure [-], u_0 – pore pressure measured in CPTu [kPa].

For cohesive soils Equation 4.13 (Marchetti, 1980) was used, whereas for non-cohesive soils equation 4.14 (Hossain and Andrus, 2016) was applied.

$$K = \left(\frac{K_D}{1.5}\right)^{0.47} - 0.6 \tag{4.13}$$

$$K = 0.72 + 0.456 \cdot logOCR + 0.035 \cdot K_D - 0.194 \cdot \log\left(\frac{q_c}{\sigma'_v}\right) \tag{4.14}$$

where:q_c – cone resistance from CPTU [kPa], OCR – overconsolidation ratio [-], K_D – horizontal stress index [-].

The overconsolidation ratio was estimated using Equation 4.15 for cohesive soils (Marchetti, 1980) and Equation 4.16 for non-cohesive soils (Monaco et al., 2014).

$$OCR = (0{,}5 \cdot K_D)^{1{,}56} \tag{4.15}$$

$$OCR = -0.0135 \cdot K_D^2 + 0.4959 \cdot K_D - 0.0359 \tag{4.16}$$

Using the above Equations the values of $M_{DMT}, K_0, OCR, \sigma'_v$ and σ'_h were determined and presented in Table 4.4. Due to the large thickness of sand layers at the depths of 4.05-7.05 m and 15.95-19.00 m, these layers were additionally divided into half.

Table 4.4. The values of $M_{DMT}, K, OCR, \sigma'_v$ and σ'_h for particular soil layers

Depth of soil layer [m]		Soil type	M_{DMT} initial	OCR	K_0	σ'_v	σ'_h
top	bottom		[MPa]	[-]	[-]	[kPa]	[kPa]
0.00	0.70	SM	-	-	-	-	-
0.70	1.80	ML/ CL	15.6	19.08	1.80	20.26	36.47
1.80	2.70	OH	6.0	3.48	1.06	32.5	34.45
2.70	4.05	Pt/ OH	2.3	2.40	0.88	38.14	33.56
4.05	5.55	SM	67.9	4.29	0.64	49.18	31.25
5.55	7.05		31.8	3.56	0.52	61.78	32.05
7.05	7.80	OL	-	0.84	0.48	72.58	35.08
7.80	10.20	OH	1.5	1.14	0.59	82.19	48.39
10.20	10.45	SM	17.8	0.92	0.50	90.81	45.00
10.45	12.15	OH	2.1	1.09	0.57	96.12	54.32
12.15	12.95	Pt	7.7	2.53	0.90	102.70	92.47
12.95	14.45	OH/Pt	3.8	1.50	0.67	108.85	72.92
14.45	15.70	SW	140.1	4.03	0.73	114.52	83.06
15.70	15.95	OH	5.7	3.25	0.89	120.82	107.91
15.95	17.50	SW	137.4	4.03	0.70	128.92	90.34
17.5	19.00		148.1	4.03	0.64	143.32	91.29

4.3 Soil properties

4.3.1 Physical properties

Tested soil samples are mainly organic silts, organic clays and peats. The basic physical parameters were tested in the laboratory on the specimens taken during field testes. All results are presented in Table 4.5 below.

The specific gravity of muds is about 2.57 g/cm^3, and for peats it is much lower, between 1.6 and 1.7 g/cm^3. These values are within the commonly known ranges (e.g. (Cheng et al., 2007)). The bulk density of the soil was also determined, on the basis of which the values of vertical stresses in the subsoil structure were then estimated.

The natural moisture content for pre-consolidated clay is about 30%, for muds it ranges from 47% to 76%, while for peats it exceeds 170%.

Due to the origin of the analyzed soils, the content of organic matter (LOI - Loss on Ignition) was also examined (ASTM D2974, 2014).

Sands from the deepest layer were not sampled. Based on CPTu and boreholes it is known that sand was very dense. Based on engineering judgement maximum bulk density was assumed and full saturation of the soil.

Table 4.5. Selected index properties of Jazowa soft soil deposits

Soil symbol	Sampling depth	$\rho^{(1)}$	$G_s^{(1)}$	$w_c^{(1)}$	PI	LL	$LOI^{(2)}$
	[m]	[g/cm^3]	[g/cm3]	[%]	[%]	[%]	[%]
ML	1.3÷1.6	1.74	2.65	30.6	21.4	49.9	5.8
ML/OH	1.85	1.79	-	45.4	-	-	4,4
OH	2.2	-	-	54.4	49.7	90.4	-
OH	2.45	1.73	-	68.9	-		8,3
OH	2.3÷2.6	1.45	2.54	75.9	63.7	119.0	11.4
OH	3.2÷4.2	1.48	2.61	64.4	54.8	100.3	16.2
Pt	~4	1.18	1.71	264.1	-	-	69.9
SM	4.5	1.90	2.65	20.3	-	-	-
OH	8.10	1.72	-	46.8	-	-	6,7
OH	8.1÷8.9	1.60	2.59	46.3	23.3	57.1	4.2
OH	8.65	1.72	-	57.3	-	-	4.5
OH	9.5÷10.5	1.66	2.67	45.4	27.5	55.8	-
OH	11.1÷11.9	1.59	2.54	49.8	15.7	53.7	7.1
OH	13.0	-	-	41.8	37.4	31.5	-
OH	~13.4	1.62	-	77.2	28.5	87.1	7.0
Pt	~14	1.07	1.57	179.2	-	-	87.2
SW	not applicable	2.07	2.65	20.3	-	-	-

(1) = average value, (2) = point value, w_c = water content, ρ = soil density, G_s = specific soil gravity, PI = plasticity index, LOI= Loss on Ignition

As mentioned before, the results of plasticity index and liquid limit were used for soil classification according to the Unified Soil Classification System (ASTM D2487, 2017)(ASTM D2487, 2017), using the Casagrande's plasticity chart (Figure 4.4). The soil layer from 0.7÷1.8 m has a liquid limit (LL) of less than 50% and lies below the A-line and can be defined as low plastic silt (ML). Soils sampled from the 2.3÷4.05 m and most of the samples from 7.8÷14.45 m have a liquid limit exceeding 50%, and are classified as organic silts (OH). Samples taken from approximately 4 m and 14 m are classified as peats (Pt) due to their high organic matter content (Table 4.6). The layers at 2.7÷4.05 m and 12.95÷14.45 m contain mixtures of interlaying muds and peats and are denoted as OH/Pt.

Cohesionless soils were classified on the basis of the CPTu results and archive boreholes.

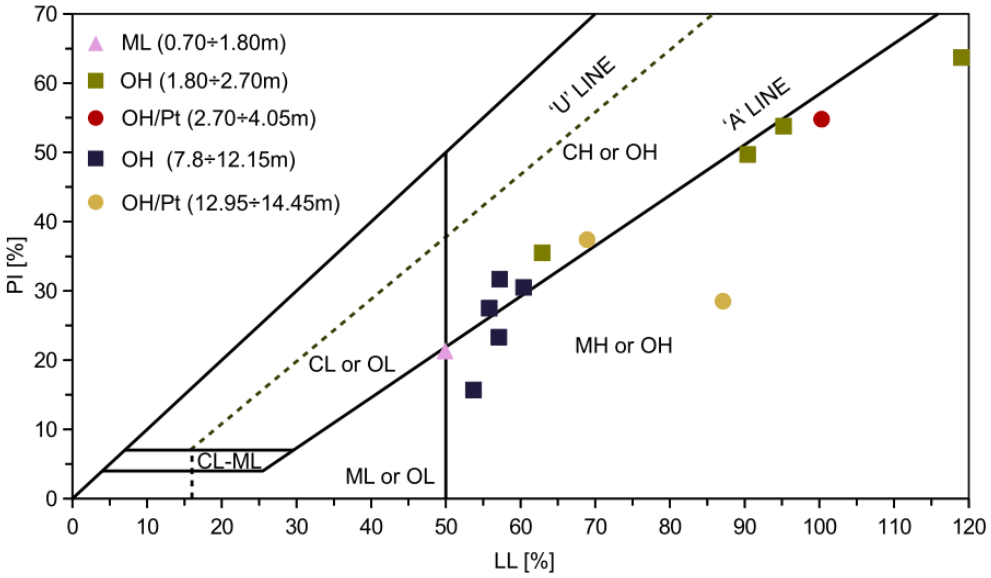

Figure 4.4. Classification of layers according to ASTM D2487 (2017) (Konkol et al., 2019)

4.3.2 Undrained shear strength

Undrained shear strength values c_u in fine-grained soils were also estimated from the soundings. The $c_u$values from DMT soundings were determined using the (Marchetti et al., 2001) proposition:

$$\frac{c_u}{\sigma'_{v0}} = 0.22 \cdot (0.5 \cdot K_D)^{1.25} \tag{4.17}$$

where: c_u - undrained shear strength [kPa]; σ'_{v0}- effective vertical stress [kPa]; K_{DMT}- horizontal stress index [-], and (Lechowicz, 1997) equation:

$$\frac{c_u}{\sigma'_{v0}} = S \cdot (0.45 \cdot K_D)^{1.20} \tag{4.18}$$

where c_u - undrained shear strength [kPa]; σ'_{v0}- effective vertical stress [kPa]; S - normalized undrained shear strength for normally consolidated state equal to 0.4 for organic soils [-](Lechowicz 1997); K_D - horizontal stress index [-].

The following relationship was used to estimate c_u from the CPT results (Lunne et al., 1997):

$$N_{kt} = \frac{(q_t - \sigma_{v0})}{c_u} \tag{4.19}$$

where: q_t - average corrected cone resistance [kPa]; σ_{v0} - total vertical stress [kPa]; c_u - undrained shear strength [kPa]; N_{kt} - cone factor, determined from the correlation proposed for the analyzed soils (Bałachowski et al., 2018)

$$N_{kt} = 1.242 \cdot F_r + 7.803 \tag{4.20}$$

and F_r - normalized friction ratio [-].

The results obtained are shown below in Figure 4.5. Two field vane tests were also performed from which the undrained shear strength is obtained directly. The results are also plotted in Fig. 4.5

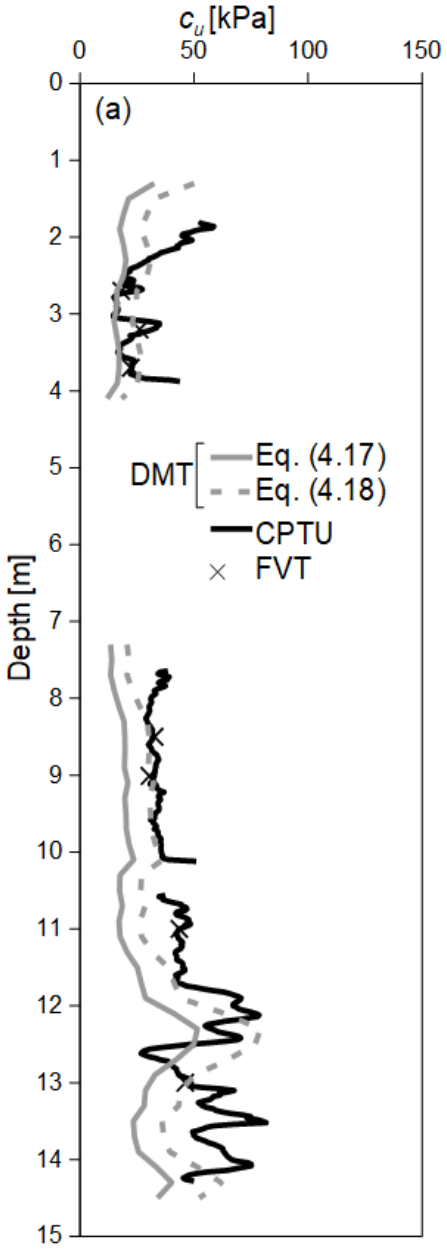

Figure 4.5. Undrained shear strength of Jazowa soft soil deposits estimated with different methods

4.3.3 Friction angle

Several tests of soft soils in triaxial compression apparatus were also carried out. The derived stress ratio M, in consolidated undrained conditions, equals 0.904 in silty clay which corresponds to the effective angle of internal friction of 23.1°. For organic silt stress ratio M at failure is equal to 1.255 which results in the angle of internal friction equal to 31.3°. The CU test on peat taken from approx. 14m depth

confirmed the high angle of internal friction equal to 55.7° (Międlarz et al., 2019). The results are shown in Figure 4.6.

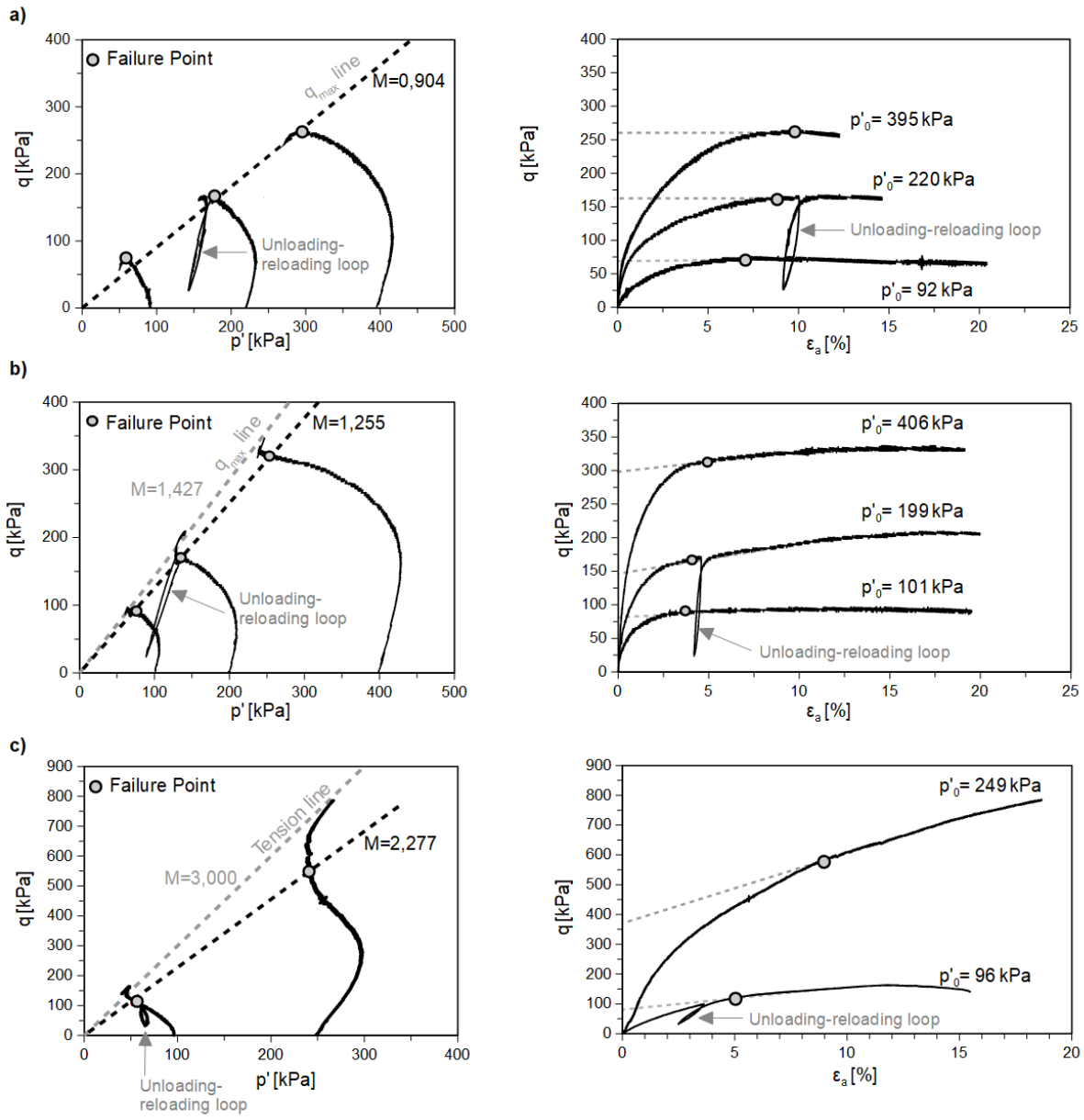

Figure 4.6. The CU tests results for (a) organic silty clay, (b) organic silt and (c) peat.

4.4 Parameters after pile installation

After about 6 weeks from the pile installation, three soundings were made at a distance of 0.30, 0.60 and 0.90 m from the column 5_13 axis (Figure 8.1). The location of the soundings are indicated in Figure 4.2. The results were compared with the soundings made before pile installation. In the case of cohesive soils, the horizontal stress index K_D and M_{DMT} practically did not change after the pile installation and no clear effect of the distance from the pile axis on the results was observed. In some layers K_D increased as the distance from the pile axis decreased, in others it decreased. Additional studies would be needed to determine this relationship. In this study, in soft soil layers the K_D on the pile

shaft was assumed to be the same as the initial one. On the other hand, in the case of non-cohesive soils, an clear increase of those parameters was observed in the direct vicinity of the pile shaft. As a distance from the pile axis increased, a decrease was observes up to the values measured before the pile installation. For the peat layer, the K_D value decreases slightly near the shaft, which may be due to the effect of structure disturbance during drilling.

The values of K_D for particular soil layers are presented in Table 4.6 and value of M_{DMT} are in Table 4.7. Values of K_D and M_{DMT} on the pile shaft were linearilly extrapolated using the corresponding values at 90 cm, 60 cm and 30 cm from the pile shaft.

Table 4.6. The values of σ'_v and K_D for particular soil layers

Depth of soil layer [m]		Soil type	σ'_v	q_c	K_D initial	K_D from the pile axis			
						90	60	30	on the pile shaft (assumed)
top	bottom		[kPa]	[MPa]	[-]	[-]	[-]	[-]	[-]
0.00	0.70	SM	-	6.85	-	-	-	-	-
0.70	1.80	ML/ CL	20.26	1.99	10.51	10.73	11.46	11.41	10.51
1.80	2.70	OH	32.5	0.54	4.42	4.94	6.26	5.38	4.42
2.70	4.05	Pt/ OH	38.14	0.51	3.47	4.18	4.24	3.64	3.47
4.05	5.55	SM	49.18	7.16	5.19	7.33	9.49	11.97	14.24
5.55	7.05		61.78	4.55	3.00	4.14	4.92	8.29	9.94
7.05	7.80	OL	72.58	1.37	1.79	2.04	2.73	2.56	1.79
7.80	10.20	OH	82.19	0.55	2.17	1.67	2.12	1.71	2.17
10.20	10.45	SM	90.81	1.74	1.84	2.01	2.14	2.01	2.05
10.45	12.15	OH	96.12	0.83	2.09	2.76	2.08	2.52	2.09
12.15	12.95	Pt	102.7	1.07	3.59	2.66	3.82	2.65	3.59
12.95	14.45	OH/Pt	108.85	1.05	2.54	2.67	2.94	2.60	2.54
14.45	15.70	SW	114.52	14.07	6.38	7.65	8.84	10.87	12.35
15.70	15.95	OH	120.82	2.57	3.86	not measured			As initial 3.86
15.95	17.50	SW	128.92	17.04	6.07	not measured			12.35 (assumed after layer 14.45-15.70m)
17.5	19.00		143.32	21.03	5.22	not measured			

M_{DMT} at the pile shaft was assumed the same as at 30cm distance

Table 4.7. The values of M_{DMT}, K, OCR and σ'_h for particular soil layers.

Depth of soil layer [m]		Soil type	M_{DMT} initial	M_{DMT} from the pile axis				K	σ'_h
				90	60	30	on the pile shaft (assumed)		
top	bottom		[MPa]	[MPa]	[MPa]	[MPa]	[MPa]	[-]	[kPa]
0.00	0.70	SM	-	-	-	-	-	-	-
0.70	1.80	ML/CL	15.6	51.8	46.4	47.6	44.4	1.80	36.47
1.80	2.70	OH	6.0	7.7	10.1	10.4	10.4*	1.06	34.45
2.70	4.05	Pt/OH	2.3	3.3	3.3	2.7	2.5	0.88	33.56
4.05	5.55	SM	67.9	85.3	109.0	136.9	161.8	1.09	53.46
5.55	7.05		31.8	51.1	64.6	120.4	147.7	0.96	59.13
7.05	7.80	OL	-	23.4	12.6	16.2	10.3	0.48	35.08
7.80	10.20	OH	1.5	1.1	0.7	1.3	1.3	0.59	48.39
10.20	10.45	SM	17.8	11.4	19.1	34.2	44.2	0.53	47.52
10.45	12.15	OH	2.1	5.9	3.6	5.9	5.1	0.57	54.32
12.15	12.95	Pt	7.7	4.4	4.8	5.1	5.4	0.90	92.47
12.95	14.45	OH/Pt	3.8	6.3	5.3	6.0	5.6	0.67	72.92
14.45	15.70	SW	140.1	199.3	209.4	204.0	208.9	1.02	117.14
15.70	15.95	OH	5.7	Not measured			-	0.89	107.91
15.95	17.50	SW	137.4	Not measured			208.9 (assumed after layer 14.45-15.70m)	1.02	131.08
17.5	19.00		148.1	Not measured				1.02	144.46

Chapter 5
Static pile load tests at Jazowa testing site

5.1 Introduction

At the beginning, it is important to distinguish between displacement and non-displacement piles. The construction of non-displacement piles consists of removing soil with specialized augers and filling the resulting borehole with concrete. An ideal non-displacement pile is installed in the place of previously removed soil without disturbing the surrounding soil or changing the stress state nor density at any point of the surrounding soil (Loukidis and Salgado, 2008). On the other hand typical displacement piles (driven or pushed-in) induce large strains in the surrounding soil mass and increase the soil density and the stress level.

CMC (Controlled Modulus Columns) in form of concrete screw displacement piles is a technology patented by Menard in the early 90s. The speed of execution, lack of excavated material and small settlements are just some of the features that distinguish CMC columns from other technologies of column execution. In addition, due to its high load-bearing capacity, the CMC concrete column quickly became an economical alternative method of traditional piling (menard.pl).

The screw displacement piles used in this study are constructed by specially designed displacement auger, installed on a machine equipped with a high torque and static vertical load head, which moves the ground in a horizontal direction to the axis of the hole. After moving the soil outside the pile (column), the concrete mixture is injected under pressure (Fig.5.1). The concrete mixture is designed in a special way that allows to achieve a predetermined stiffness ratio of the column to the surrounding soil. As a result, a composite structure containing the soil and columns is obtained, characterized with increased bearing capacity and reduced compressibility. The process of making the column does not cause practically any damage to the ground surface and does not generate vibrations dangerous for nearby structures.

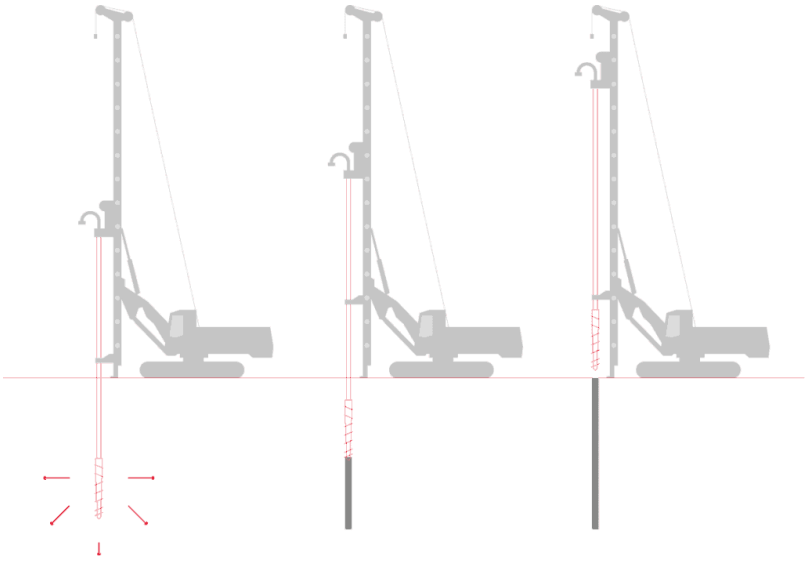

Figure 5.1. Controlled Modulus Column execution scheme (menard.pl, 2021)

5.2 Pile configuration and testing procedures

69 CMC columns with a diameter of 0.40m were made on 4 trial fields in Jazowa, using full displacement auger. Of all the columns, 27 were subjected to static load tests (SLT), while the remaining ones were used as anchor piles. The arrangement of the columns on the test sites is shown in Figure 5.2.

Figure 5.2. Arrangement of columns on testing sites

5.2.1 Column configuration

Three types of columns were made according to the arrangement of soil layers. The shortest ones, 8 and 11 m long, were drilled in the soft soil layers as so-called floating columns. These are not embedded in bearing soil layers (sands). Another type with a length of about 14.6 m was made to the top of the bearing layer. These columns are based on a bearing layer. The longest columns of 15.5, 17 and 18 meters were embedded in compacted sands. Here, the use of different column lengths will allow to estimate the effect of embedment into the bearing layer. This issue is however outside the scope of this thesis.

5.2.2 Testing program

For the assessment of the bearing capacity of the constructed piles, static load tests (SLT) using hydraulic jack method were used.

Static load tests were carried out in four schemes:

- tension test;
- compression test;
- tension-compression test;
- compression-tension test.

On the basis of such schemes, an attempt to estimate the friction during pile tension and compression will be made as well as check whether tension affects the results from compression or conversely. In this thesis only the columns subjected to tension loading were analyzed. They include the columns under tension tests only, subjected first to tension and then to compression tests and the case of columns subjected first to compression and then to tension tests. One should point out that the study focuses on the pull-out resistance of columns. The further compression test is thus not analyzed. The effect of previous compression test is however studied on the column behavior in tension, at the second stage of the loading scheme.

Static load tests, were carried out at different times from the columns execution. First columns were tested about 20-30 days after installation. The next tests took place after about 50 days and the last one after about 115 days. The purpose of testing the columns after different periods of time was to check the influence of the time elapsed from the column execution on its behavior (set-up effect).

5.2.3 Loading procedures

The test load was carried out in steps of 1/8N (pushing in) or 1/10N (pulling out) (where N - design pile load capacity). During the test, the load value was increased (the next load step started) in 10-minute periods. First cycle of the test was carried out to the value of N. After the settlements at the last load step of a given cycle was stabilized, the pile was unloaded with steps of 0.25 N and stabilized after complete unload. Then the second cycle was carried out by overloading the column to the value of Q_{max} = 1.50 N. The second cycle is not analyzed in this thesis. The displacement of the test pile was measured using four SLS 130 type telescopic displacement sensors with a measurement accuracy of 0.01 mm. The sensors were connected to a reference frame, located at a distance of 3.0 m from the shaft of the tested pile. The displacement of the tested pile was determined on the basis of the average reading of the four sensors. The force was measured using a load cell type W15192, with an accuracy of ± 0.5%. The load cell was calibrated in the range up to 5000 kN. The test stand and measurement system are shown in Photos 5.1 a and b.

Based on the load test results, the load-displacement curves (the Q-s curves) can be determined, as well as the load-time and displacement-time characteristics.

Photograph 5.1 a) The stand in pull-out test b) The measurement system

Table 5.1 lists all columns subjected to static load test, taking into account load schemes, testing time after column installation, column lengths, as well as the results obtained from the SLT.

Columns that have reached displacements of up to 5 mm were not included in further calculations due to significant difficulties in determining their behavior in the range of larger displacements. Some columns were also rejected due to errors during SLT. In addition, since the further part of the work focuses on the shaft friction, only the piles working in tension are analyzed. Table 5.1 shows in bold the columns that will be used to analyze the SLT results.

Table 5.1. List of columns subjected to static load tests.

Column designation	*Days from execution to SLT*	*Length*	*Loading scheme*	*SLT duration*		*Maximum displacement from the SLT*		*Maximum load from the SLT*	
				compression	*tension*	*compression*	*tension*	*compression*	*tension*
[-]	*[-]*	*[m]*	*[-]*	*[min]*	*[min]*	*[mm]*	*[mm]*	*[kN]*	*[kN]*
FLOATING COLUMNS									
S5C5	***31***	***8***	***tension***	***-***	***250***	***-***	***2.46***	***-***	***300***
S5C10*	***112***	***8***	***tension***	***-***	***245***	***-***	***13.62***	***-***	***450***
S5C13*	***56***	***11***	***tension***	***-***	***260***	***-***	***32.44***	***-***	***650***
S4C8*	***34***	***11***	***tension-compression***	***910***	***195***	***22.24***	***11.78***	***700***	***600***

S5C9*	***113***	***11***	***tension-compression***	***295***	***445***	***31.00***	***7.14***	***800***	***600***
COLUMNS RESTED ON THE BEARING LAYER									
S4C3*	***31***	***14.6***	***tension-compression***	***145***	***650***	***20.71***	***5.26***	***1200***	***480***
S1C17	*51*	*14.65*	*tension-compression*	*1170*	*180*	*20.27*	*2.59*	*1340*	*300*
S4C4*	***57***	***14.6***	***tension-compression***	***206***	***865***	***25.86***	***10.94***	***1300***	***600***
S5C8*	***116***	***14.6***	***tension-compression***	***210***	***490***	***19.48***	***8.04***	***1100***	***540***
S1C14	***117***	***14.75***	***tension-compression***	***120***	***1045***	***12.68***	***2.19***	***1304***	***450***
S2C14	***118***	***14.72***	***tension-compression***	***135***	***755***	***13.47***	***2.07***	***1303***	***450***
S4C7	***120***	***14.6***	***compression-tension***	***575***	***355***	***21.77***	***38.70***	***1200***	***650***
COLUMNS EMBEDDED IN THE BEARING LAYER									
S1C9	*20*	*17.04*	*compression*	*270*	*-*	*5.42*	*-*	*1040*	*-*
S2C9	*21*	*18.05*	*compression*	*115*	*-*	*2.74*	*-*	*1040*	*-*
S1C8	*35*	*17.09*	*compression*	*265*	*-*	*5.32*	*-*	*1040*	*-*
S2C8	*35*	*18.11*	*compression*	*140*	*-*	*3.71*	*-*	*1040*	*-*
S2C5	*51*	*18*	*compression*	*135*	*-*	*4.13*	*-*	*1040*	*-*
S1C5	*112*	*17.08*	*compression*	*175*	*-*	*4.14*	*-*	*1040*	*-*
S2C3	*112*	*18.02*	*compression*	*132*	*-*	*2.43*	*-*	*1040*	*-*
S1C3	*114*	*17.02*	*compression*	*300*	*-*	*5.13*	*-*	*1040*	*-*
S2C23	*42*	*18.01*	*tension-compression*	*167*	*128*	*3.34*	*1.15*	*1340*	*300*
S2C17	*47*	*16.52*	*tension-compression*	*1005*	*132*	*8.30*	*1.27*	*1560*	*300*
S1C23	*50*	*17.24*	*tension-compression*	*220*	*110*	*9.43*	*1.19*	*1560*	*300*
S1C22	*115*	*17.21*	*tension-compression*	*335*	*110*	*9.31*	*1.52*	*1560*	*450*
S2C22	*117*	*18.08*	*tension-compression*	*180*	*125*	*5.22*	*2.02*	*1490*	*450*
*S5C3**	*30*	*15.5*	*compression-tension*	*505*	*240*	*8.73*	*6.44*	*1560*	*650*
S5C4	*118*	*15.5*	*compression-tension*	*425*	*195*	*14.99*	*29.18*	*1650*	*517*

**columns used for model verification (Chapter 8)*

During the static load tests, only some of the columns have achieved significant displacement during pull-out, thus providing the basis for further calculations. Only 7 columns tested in tension were selected to be used for model verification (Chapter 8). Knowing the duration of the test load of these columns and their final displacements, it was estimated that the average pull-out speed was about 0.06 mm/min. At this speed, interface direct shear tests were performed in laboratory (see Chapter 6 for more details).

As part of the additional research, the columns tested in the compression-tension scheme will also be analyzed in order to check the influence of previous compression on the further behavior of the column subjected to tension. For the calculations presented in Chapter 8, one column (S5C3) was also selected, which was first subjected to compression and then to tension, to verify the two-direction model.

5.3 Static load test results

The static load test is considered satisfactory primarily when it is possible to determine the ultimate load capacity of the pile. In the case of the analyzed columns, most of them have reached small displacements during the SLT, and the test loads have not been taken to failure. The Chin method (Chin, 1970b) was used to estimate the ultimate load capacity of the floating columns and columns rested on the bearing layer. This is a mathematical and graphical approach to estimate the shape of the Q-s curve for larger displacements until the ultimate capacity is reached.

5.3.1 Estimation of ultimate bearing capacity of the columns with Chin method

The Chin method is considered to be the simplest method based on the assumption that the Q-s curve is approximately hyperbolic. It has been expressed by Chin (Chin, 1970b) in the form (Eq.5.1):

$$\frac{s}{Q} = C_1 \cdot s + C_2 \tag{5.1}$$

where: Q – the applied load on the pile head [kN]; s – pile head displacement [mm], C_1 – the slope of the linear plot corresponding to the inverse of the asymptotic value of the ultimate resistance Q_f, C_2 – a constant corresponding to the initial slope of the load settlement curve plotted in linear coordinates..

The Chin's method is presented in Figure 5.3a.

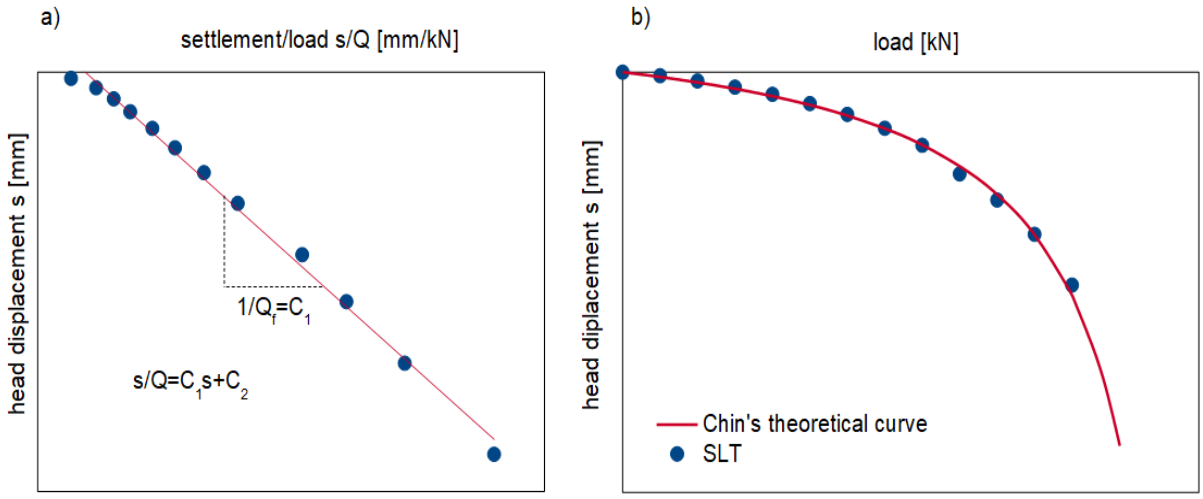

Figure 5.3. Assumptions of the Chin's method

Using the Chin method, C_1 and C_2 values were determined, as well as the ultimate bearing capacity of all analyzed columns. The ultimate value is determined as an asymptote to the graph, i.e., as $1/C_1$. The results are summarized in Table 5.2. In the following section, ultimate capacities of the Chin method and the resulting Q-s curves will be used to compare the bearing capacities. Example of such comparison is shown in Figure 5.3b.

Table 5.2. Ultimate load capacities in tension prediction of analyzed columns with the use of the Chin method.

Column designation	Days from execution to	Length	Loading scheme	Maximum displacement from the SLT	s/D	Maximum load from the SLT	Chin method		
							C_1	C_2	Q_f
[-]	[-]	[m]	[-]	[kN]	[%]	[kN]	[-]	[-]	[kN]
FLOATING COLUMNS									
S5C5	31	8	tension	2.46	6.15	300	0.0021	0.0031	476
S5C10	112	8	tension	13.62	34.05	450	0.0020	0.0039	510
S5C13	56	11	tension	32.44	81.10	650	0.0014	0.0043	706
S4C8	34	11	tension-compression	11.78	29.45	600	0.0013	0.0046	749
S5C9	113	11	tension-compression	7.14	17.85	600	0.0014	0.0021	699
COLUMNS BASED ON THE BEARING LAYER									
S4C3	31	14.6	tension-compression	5.26	13.15	480	0.0014	0.0034	696
S4C4	57	14.6	tension-compression	10.94	27.35	600	0.0013	0.0043	749
S5C8	116	14.6	tension-compression	8.04	20.10	540	0.0014	0.0040	717
S1C14	117	14.75	tension-compression	2.19	5.48	450	0.0016	0.0018	625
S2C14	118	14.72	tension-compression	2.07	5.18	450	0.0019	0.0011	526
S4C7	120	14.6	compression-tension	38.7	96.75	650	0.0008	0.0270	1203

5.3.2 Time effect on the bearing capacity of the tension columns

According to literature studies (Komurka et al., 2003; Lim and Lehane, 2015, 2014; Ng et al., 2013; Tovar-Valencia et al., 2018b) the set-up effect in full displacement pile bearing capacity is related principally to shaft friction increase. This effect was mainly observed for driven piles both in sands (Lim and Lehane, 2015, 2014) and clays (Ng et al., 2013). The aim of this study was to check if this phenomena occurs also in case of screw displacement piles. On the basis of Table 5.2, several load capacity comparisons have been prepared for the pull-out piles of identical lengths but tested after different time periods from the columns installation.

Figure 5.4 shows two 8-metre floating columns, tested after 31 and 113 days. Figure 5.5 shows three floating, 11-metre columns tested after 34, 56 and 113 days.

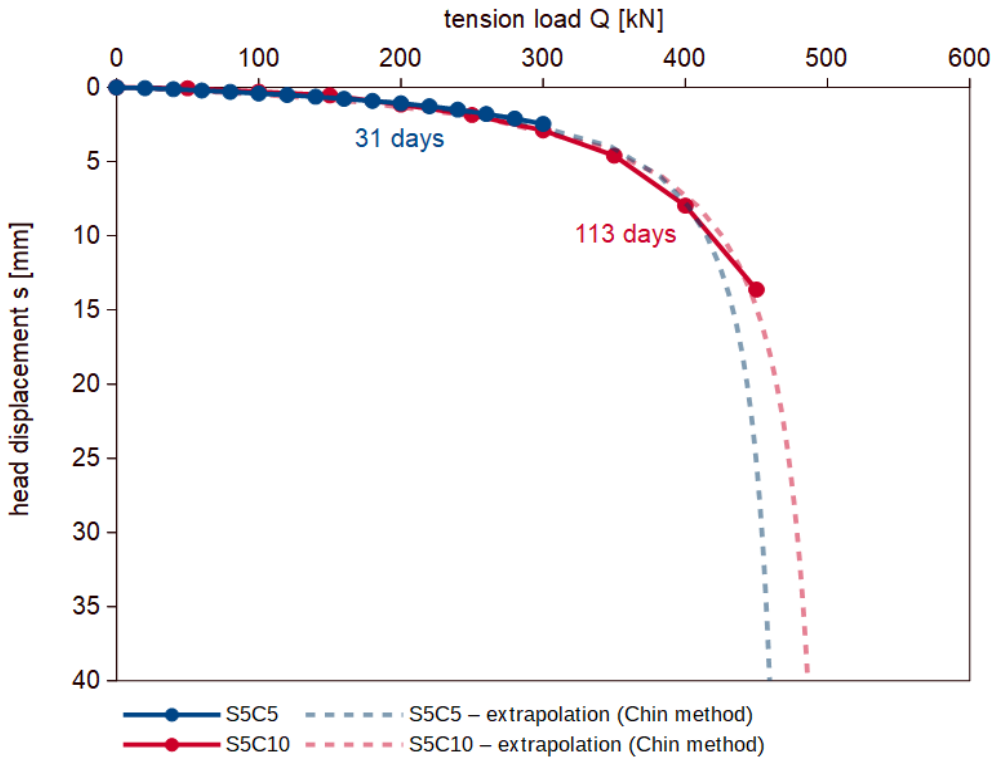

Figure 5.4. Comparison of the load capacities of 8-meter columns

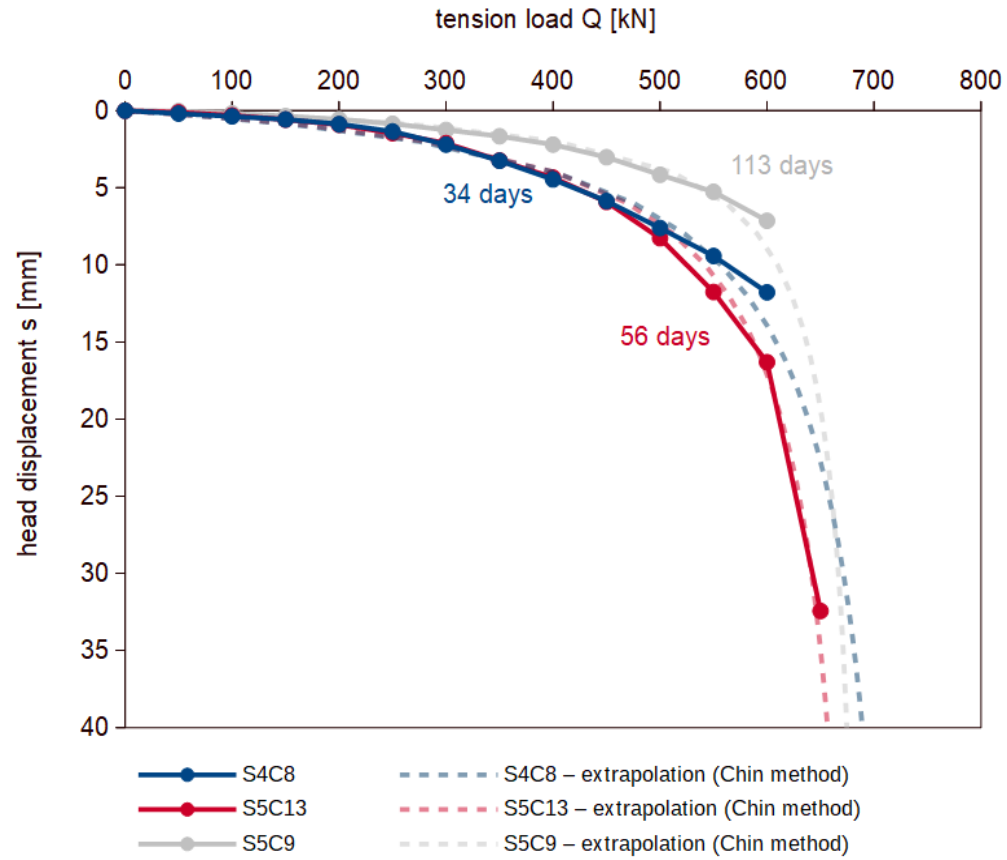

Figure 5.5. Comparison of the load capacities of 11-meter columns

The estimated ultimate bearing capacities at a displacement of 40 mm (10% of the pile diameter) are approx. 450 and approx. 650 kN for 8 and 11-metre columns, respectively.

As one can see, there are no clear differences in the behavior of these piles, which indicates that in given soil conditions the impact of time is negligible. Thus set-up effect for screw displacement piles can be neglected in normally consolidated clays and organic soils and loose to medium dense sands.

Figure 5.6 shows five, 14.6-metre columns, based on the bearing soil layer. One of them was examined after 31 days, one after about 50 days and three after over 116 days. The load capacities of the three columns overlap, while the two latest tested columns, that achieved the smallest displacements, diverge from the rest. In this case, there is also no distinct effect of time on the pile capacity but larger scatter of the results is observed.

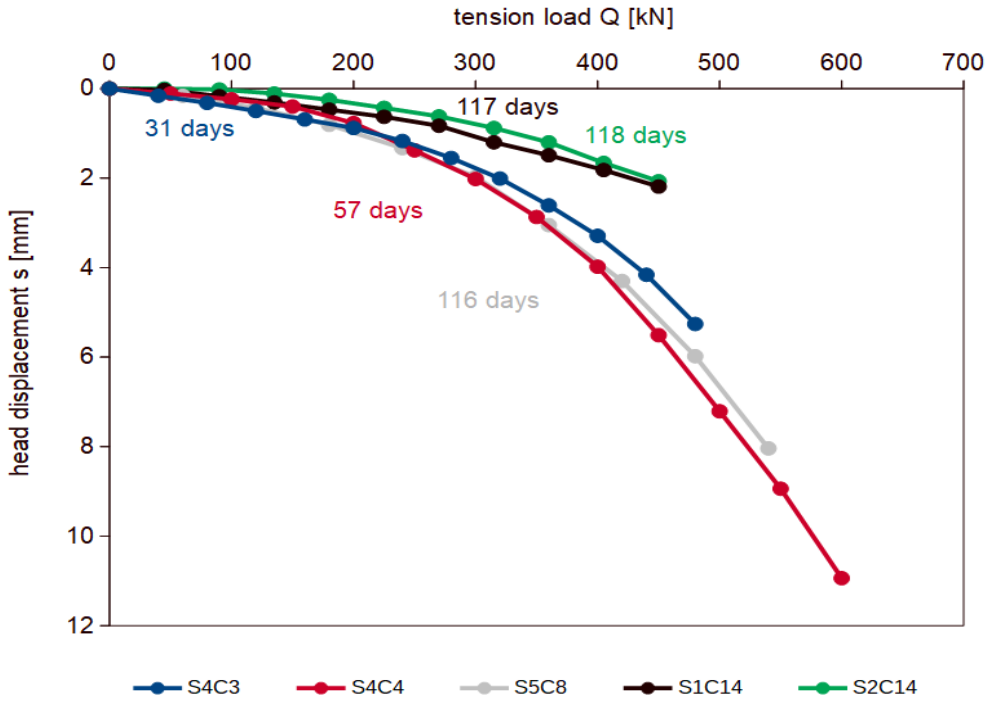

Figure 5.6. Comparison of the load capacities of 14.6-meter columns

The following Figures, 5.7 and 5.8, show two columns of 17 and 18 meters each, respectively, examined after about 40-50 and 115 days. The columns are embedded in the bearing layer. These columns achieved a maximum displacement of 2 mm during the test loads. However, from the data obtained it can be seen that the columns tested after about 115 days, in the low displacement range, achieved higher load capacities than the columns loaded after about 6 weeks. In case of 17-metre columns the difference is almost 50%. This could be related to set-up effect in shaft friction. However, further tests are needed to confirm this hypothesis.

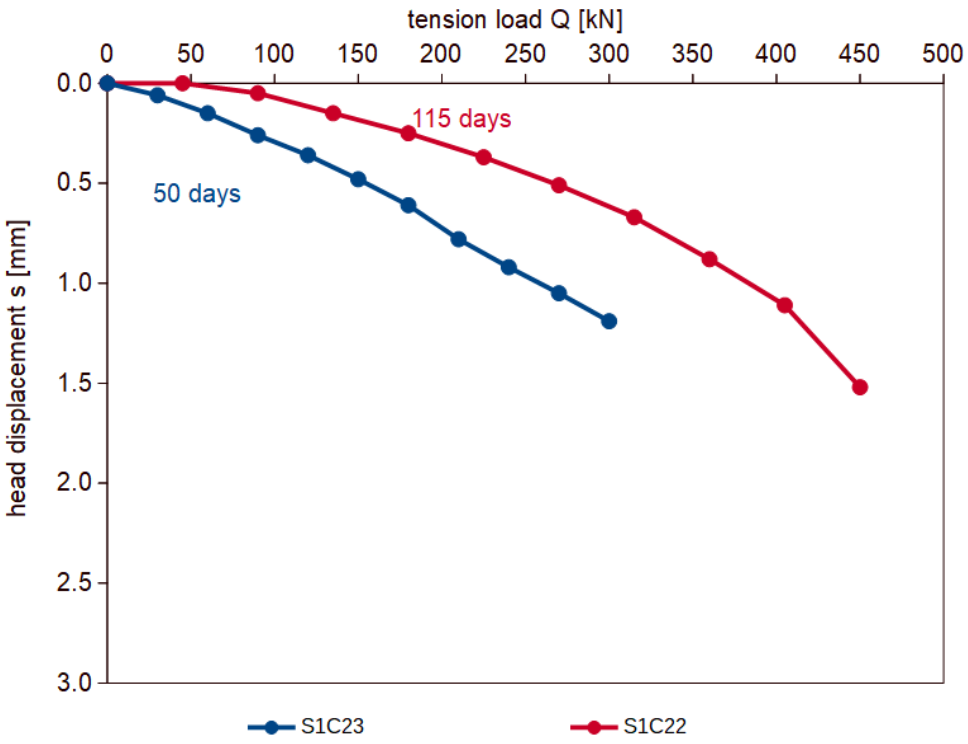

Figure 5.7. Comparison of the load capacities of 17-meter columns

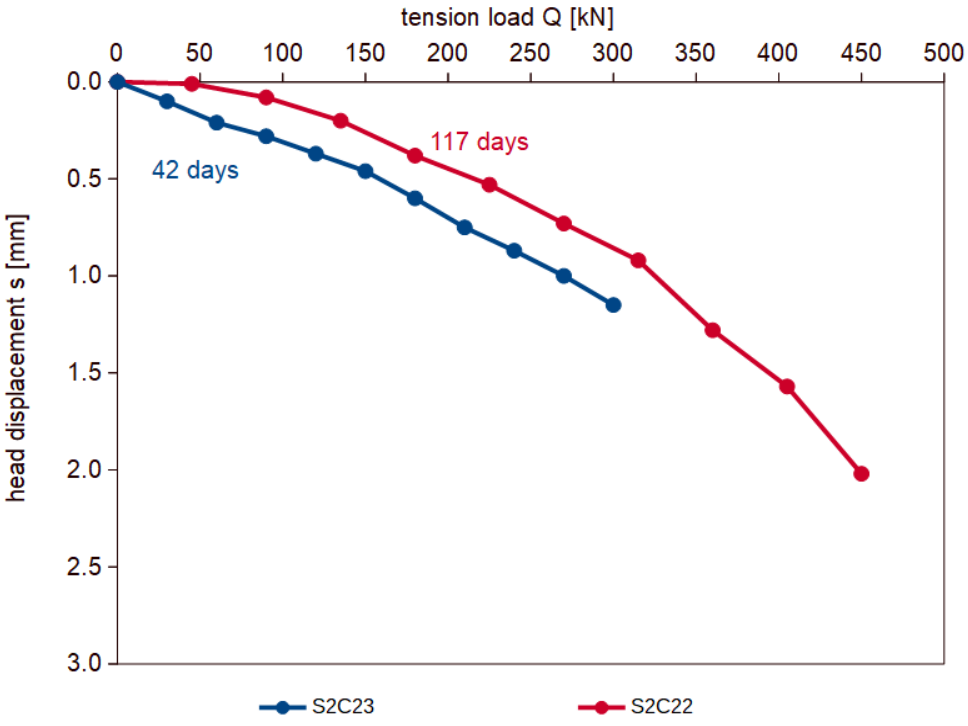

Figure 5.8. Comparison of the load capacities of 18-meter columns

5.3.3 Influence of the pile length on the bearing capacity of tension columns

In order to check the effect of pile length on the load capacity of tension columns, columns tested after approx. 30 days are presented in Figure 5.9 and after approx. 115 days in Figure 5.10 (see Table 5.2).

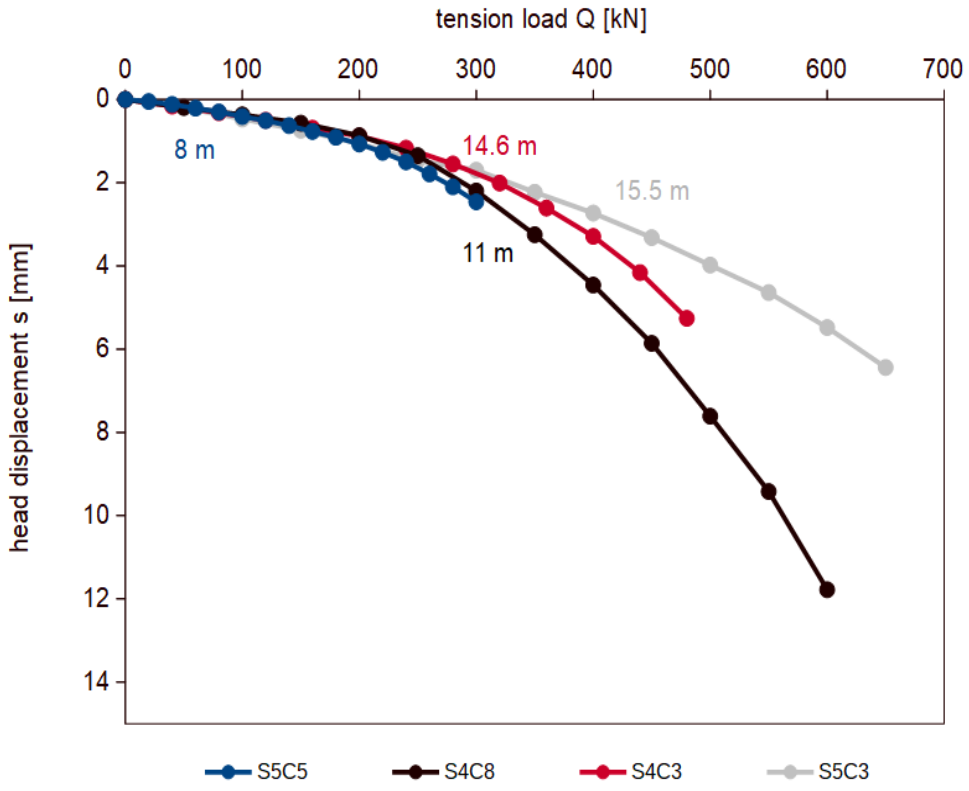

Figure 5.9. Influence of the pile length on the pull-out capacity - columns tested after 30 days

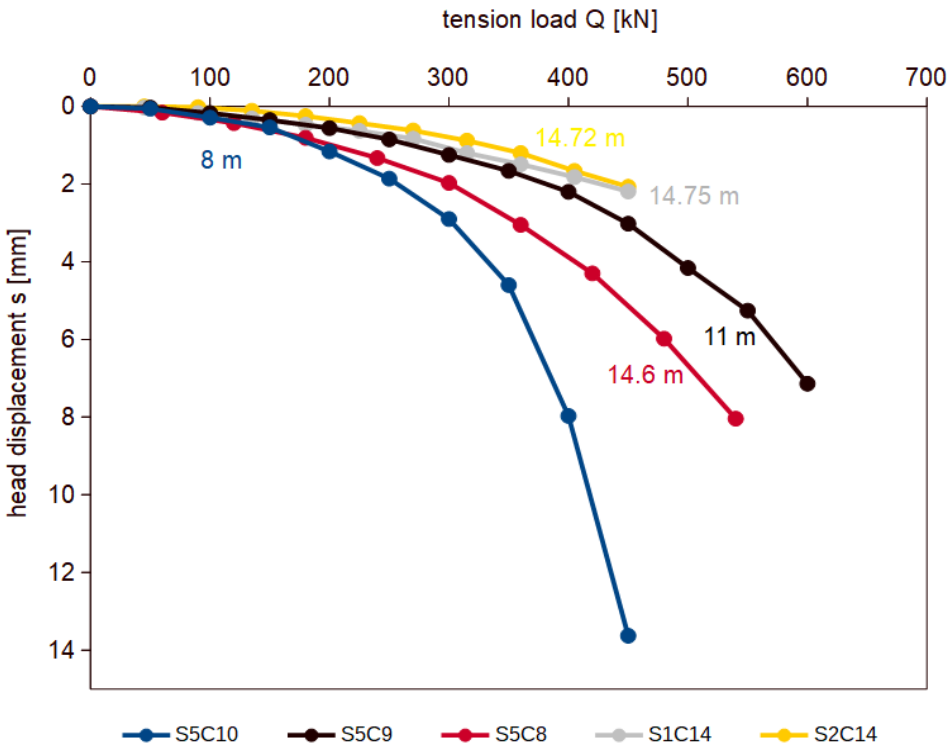

Figure 5.10. Influence of the pile length on the pull-out capacity - columns tested after 115 days

From Figures 5.9 and 5.10, a correlation between the length and load capacity of piles can be noticed. For columns tested after about 30 days, the diagrams, in the small displacement range, are similar. The 8 and 11 m long columns have similar load capacities, while the 14.6 m column, based on the bearing layer, and the 15.5 m column have significantly higher load capacities at higher displacements. A much bigger difference can be seen between the columns testes after approx.115 days. Here, there is a clear difference between the load capacities of the 8 meter and 11 meter columns. The 14.6 m columns have the highest load capacities, except for the S5C8 column, which deviates from the others.

5.3.4 Influence of previous compression on the bearing capacity of tension columns

Figure 5.11 shows four, 14.6-meter columns examined after about 115 days. Three of them were examined in the compression-tension scheme, and one was first pulled out and then pushed in. It can be seen by the shape of the graphs that the piles that were first pushed in have much higher pullout bearing capacities than the column that was subjected to tension. It is difficult, however, to compare the graphs clearly, as the piles after compression already have some residual stresses under the base and on the shaft, which cannot be directly estimated. Additional testing would be necessary to better quantify the effect compression on tension columns.

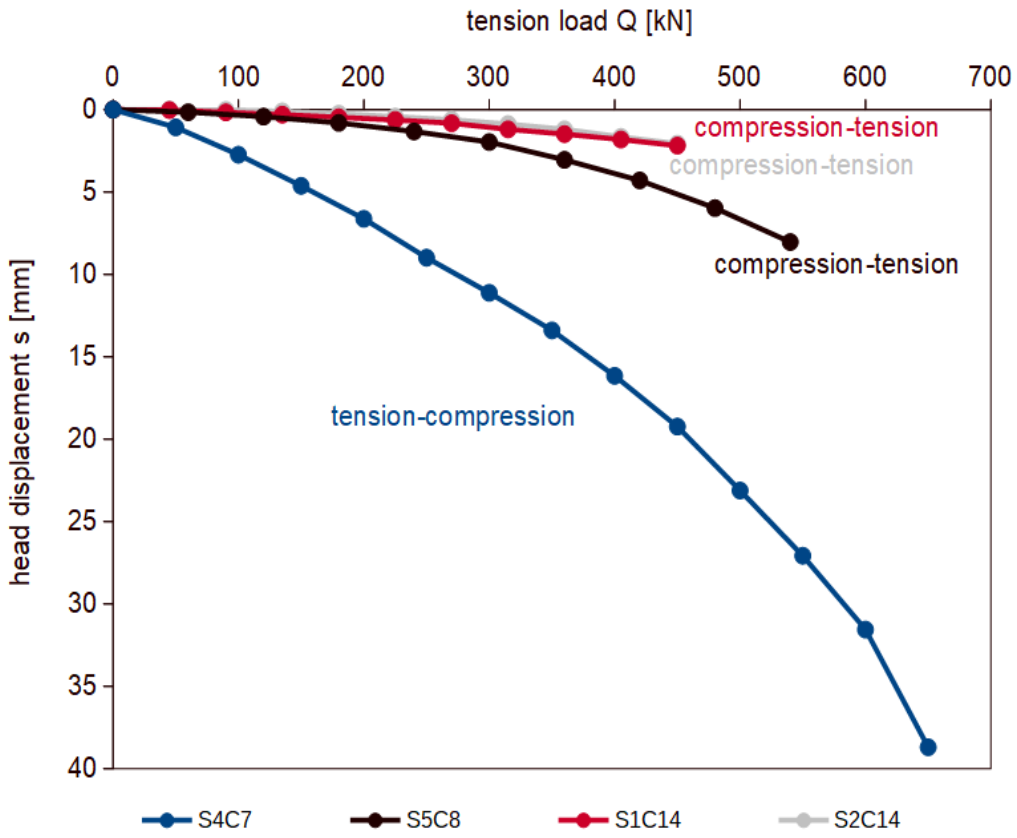

Figure 5.11. Influence of compression on the tension capacity

Chapter 6
Interface testing

6.1 Introduction

Shaft friction is the main part of the bearing capacity of axially loaded piles, in particular of tension piles. In order to design such piles correctly, it is important to appropriately estimate the friction between the pile and the soil.

During pile axial loading (as shown in Figure 6.1a) the load is transferred from the structure to soil through the contact zone which is normally called the interface. When pushing in (compression) or pulling out (tension), 3 zones are formed around the pile. The closest to the pile is a so-called thin shear zone with a width depending on the type of soil in which the pile is embedded. Further there is an intermediate zone in which simple shear occurs. The shear stress from the maximum value, decreases with increasing distance from the shaft until it reaches zero. Then the third, unaffected zone begins.

The width of the shear zone in sands was measured during model pull-out pile tests (Turner and Kulhawy, 1987) and during observations in the direct shear interface box (Desrues and Andò, 2015). It is about 10 times the mean grain size D_{50}. In granular soils significant volume changes take place in the shear zone. At the beginning of the shearing process, contractancy occurs, and then dilatancy or further contractancy proceeds, depending on the density of soil, grain size and shape, material roughness, level and stress history. The thickness of this zone and the tendency of the soil to dilate have a decisive influence on the shear stress in the soil-structure contact (Bałachowski, 2006; Doan and Lehane, 2018a).

In cohesive soils, shearing takes place practically at the interface between soil and structure, and the shear zone is negligible. Studies carried out by (Doan and Lehane, 2018a, 2018b) have shown that the shear zone reaches a width of approx. 0.3 mm when tested in CNL (Constant Normal Load) to 0.01 mm in CNS (Constant Normal Stiffness) studies at a stiffness of 1000 kPa/mm.

In the shear zone, the shear stress as well as pile displacement reach maximum values. Outside the shear zone, there is an intermediate zone of decreasing shear deformation. Whereas the distance from the shaft of the pile increases, the stress and displacement decreases. When the stresses and deformations reach zero, a zone without shear deformations can be distinguished, where the impact of the load on the surrounding soil is no longer observed (Engin, 2013; Konkol, 2017, 2015).

With deformations, there is a change in normal stress which has a direct effect on the amount of shaft friction. The greater the normal stress increase the greater the friction. The magnitude of the

increase in normal stress $\Delta\sigma_n$, depends primarily on the piling method, stress level, boundary conditions and pile aspect ratio (Lehane and White, 2005). In addition, $\Delta\sigma_n$ increases with the soil density and decreases with the pile diameter (Lehane and Jardine, 1994).

In order to better understand the mechanism of friction between the pile and the soil, laboratory tests have been performed in a direct/simple shear box to explore the parameters influencing friction eg. (Airey and Wood, 1987; Bjerrum and Landva, 1966).

Testing in a simple shear apparatus best reflects the soil behavior in the intermediate zone. In the simple shear test conditions, shear strain are imposed to the specimen, as shown in Figure 6.2a. During shearing, soil sample experiences a non-uniform shear stress distribution on the top and bottom faces. (Hanzawa et al., 2007)

Simple shear test is comparable to the direct shear test (Figure 6.2b). The essence of the test is to shear the sample placed in the two halves of a shear box, by pushing (or pulling) one part horizontally while the other remains fixed. A normal load is applied to the top of the specimen. This test allows to recognize the shearing behavior of soil and measure the values of the angle of internal friction of the soil and the maximum shear stress during shearing. In 1948, the modified direct shear device for interface tests was introduced in order to enable measurement of friction between the soil and construction materials (Hvorslev, 1960; Potyondy, 1961; Terzaghi and Peck, 1948). The modification consists in covering the lower half of the box with the tested construction material and the upper half with soil.

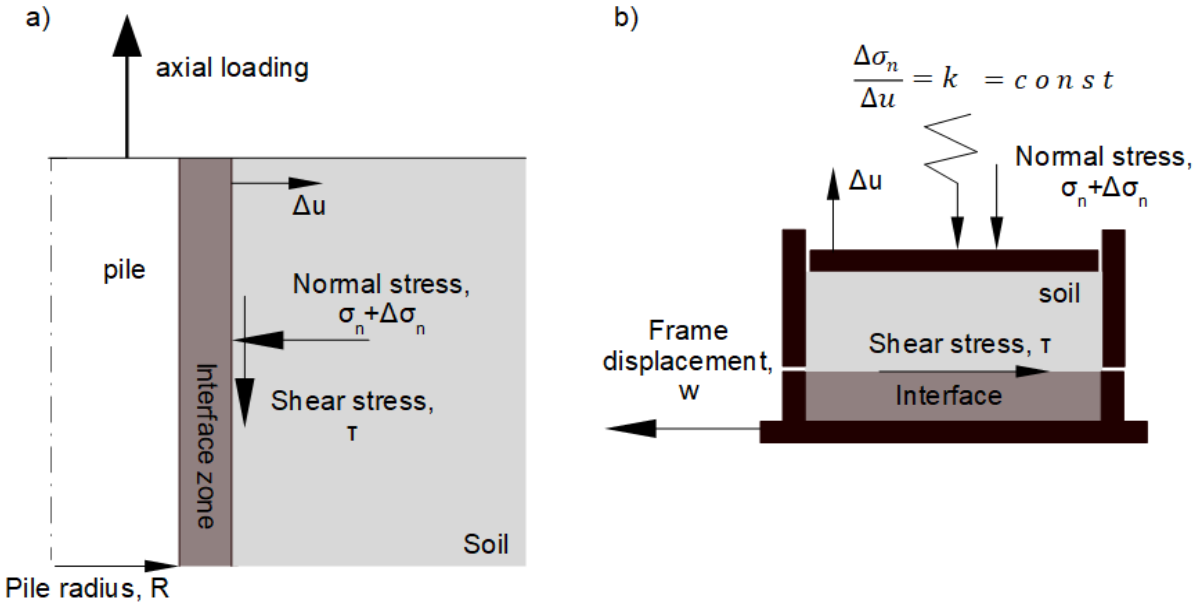

$$\frac{\Delta\sigma_n}{\Delta u} = \frac{2E_p}{R} = k$$

Figure 6.1. Analogy between a) the localized shear along a pile and b) a direct shear test with imposed stiffness

The main differences between direct and simple shear tests are related to the different mechanisms of failure. In simple shear test, failure can occur both along a number of horizontal and vertical planes connected to rotation, while in direct shear test, failure occurs along the forced horizontal plane.

In 1995, tests were carried out on rough steel interfaces, simultaneously in the simple shear and the direct shear apparatus at constant normal stress (CNL) (Fakharian and Evgin, 1995). At that time, equal values for maximum and residual shear stress were obtained. These results confirm that both methods can be equally used to determine the strength parameters of the interfaces.

In the direct shear or simple shear apparatus, the soil is subjected to similar conditions to those

existing within the pile, eg. (Randolph and Wroth, 1981). There are three possible shear paths (Pra-ai and Boulon, 2017). According to the definition of stiffness (Eq.6.1) the following conditions occur during these 3 types of tests:

- constant normal load (CNL): no increase in normal stress $\Delta\sigma_n$, stiffness $k = 0$;
- constant volume (CV): no increase in strain Δu, stiffness $k = \infty$;
- constant normal stiffness (CNS): increase in normal stress $\Delta\sigma_n$ proportional to the increase in strain Δu, stiffness $k = const$ and $k \neq 0$.

The constant normal load and constant volume can be considered as a boundary conditions that may occur during mobilization of friction along the pile shaft. Intermediate conditions, however, occur during tests under constant normal stiffness.

Initially used to determine frictional resistance at the pile shaft, CNL tests did not take into account the effects of volumetric changes that may occur during shearing. In order to take these into account and better reflect what is happening at the pile shaft, studies with constant normal stiffness were initiated (eg. (Ooi and Carter, 1987)). During the test, constant normal stiffness is assumed, which should correspond to the conditions occurring in-situ (e.g., those established by pressuremeter testing (see Eq.6.1)). When dilation or contraction occurs, the normal stress is automatically increased or decreased during shearing, thus providing a constant normal stiffness condition.

The validity of using CNS tests as a reflection of in-situ conditions was proven in 1986 when Boulon & Foray presented the analogy between shear mechanism on the pile shaft and the direct shear interface test with constant normal stiffness (Fig. 6.1.). They suggested that the normal stiffness applied to the shear box should be adjusted to the compressibility of the soil outside the shear zone (Boulon, M., & Foray, P., 1986). The same analogy can also be presented with a simple shear test (Fakharian and Vafaei, 2020).

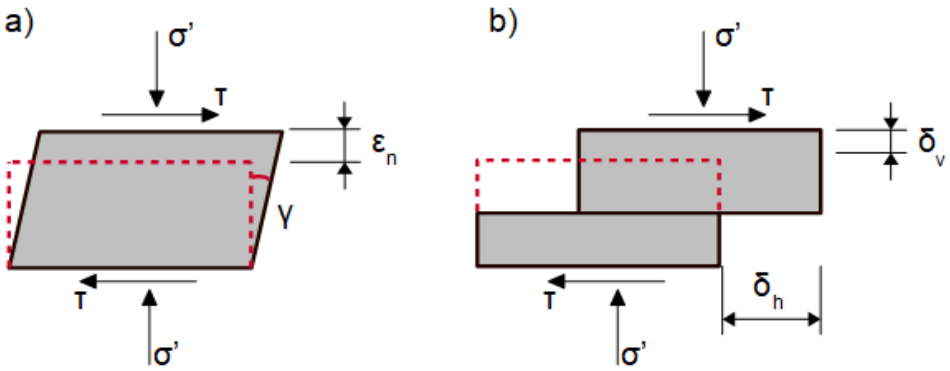

Figure 6.2 a) Simple shear vs. b) direct shear

During axial loading, shear stress τ are produced at the interface surrounded by soil mass which deforms u_1. A change in normal stress $\Delta\sigma_n$ on a cylindrical pile shaft of radius R, increases with the compaction of the surrounding soil. This behavior is analogous to the phenomenon occurring during CNS test. Volumetric changes during shearing (dilatancy or contractancy) cause a change of shear band thickness u_1, which in turn results in a change of stress $\Delta\sigma_n$.

It should also be noted that the behavior of interfaces depends not only on the stress change but also on the material type and roughness. Under the same test conditions and different roughness of the interfaces, the maximum and residual shear stress values are much higher for rough surfaces than for smooth ones. Additionally, rough concrete surface for sands dilates significantly while the smooth interface contracts (Fakharian and Evgin, 1996; Fakharian and Vafaei, 2020). Similar relations were observed for cohesive soils. The roughness of the concrete has an effect on the shaft friction not only in sands but also in clayey sands and clays. The shaft friction mobilized on the rough interface can be double that of the smooth one (Boukpeti and White, 2017; Doan and Lehane, 2018b). The same

dependence of shear strength on roughness was also confirmed for steel interfaces (Tsubakihara and Kishida, 1993; Uesugi et al., 1990). In the case of organic soils the dependence of strength on roughness has also been confirmed. Additionally, the highest interface friction angle was obtained between the organic soil and the concrete, and was higher than that of other construction materials (steel and wood) regardless of the shape of the soil particles. The lowest interface friction angles were observed for smooth steel. Shear strength decreases with increasing moisture of organic soil (Canakci et al., 2016).

6.2 Normal stiffness

During direct shear interface test with constant normal stiffness, volumetric changes of the soil induce a normal displacement in the surrounding soil and changes in the normal stress imposed on the pile shaft. Therefore, the stiffness of the surrounding soil k may be expressed as a ratio of these two variables and can also be related either to the pressuremeter modulus of the soil E_p (Wernick, 1978) or to the shear modulus of soil G (Tabucanon et al., 1995) (Equations 6.1 and 6.2):

$$k = \frac{\Delta\sigma_n}{\Delta u} = \frac{2E_p}{R} \tag{6.1}$$

$$k = \frac{4G}{d} \tag{6.2}$$

where: $\Delta\sigma_n$ – the increment of the normal stress imposed on the shaft [kPa], Δu – the increment of the normal displacement [mm], E_p - the pressuremeter modulus [kPa], R – the pile radius [mm], G – shear modulus of soil [kPa], d – pile diameter [mm]. Values of E_p and G moduli should be determined in the domaine of intermediate strains corresponding to the process of pile installation and loading.

In this thesis, shear modulus is based on constrained modulus from DMT, as it corresponds to the intermediate shear strain level of 0.1% (Marchetti et al., 2001). The shear modulus can be estimated using the dilatometer sounding results, see Equation 6.3 (Cox and Mayne, 2015).

$$G_{DMT} = \frac{M_{DMT}}{\frac{2(1-v)}{1-2v}} \tag{6.3}$$

where: M_{DMT} – constrained modulus from DMT [kPa], v – Poisson's ratio [-]. For the purpose of the estimation, the Poisson's ratio of 0.3 for fine soils and medium dense sand and 0.35 for dense sands can be used (Look, 2007).

In the classic test at constant normal stress, $k = 0$. In the test at constant normal stiffness the upper limit is related with lack of volumetric change ($k = \infty$). Since soil dilatation is limited by the surrounding soil mass, a significant increase in normal stress during shear can be observed. The greater normal stress increase, the more dense the soil is. In extreme cases, with no lateral deformation and the use of rough interface, even a 20 times increase of σ_n (for coarse sands) can be observed (Bałachowski, 2006).

6.3 Direct shear box tests

For the purpose of the research presented in this thesis, direct shear box tests were carried out on the interfaces between the soil and concrete. It was assumed that shear localized along a pile shaft is reflected in a direct shear test with imposed stiffness.

In order to test the soil samples taken from the field tests, the stiffness of the soil at particular

depths had to be determined. It was estimated on the basis of the results of field tests (after pile installation) presented in Chapter 4 and Equations 6.2 and 6.3. The results are summarized in Table 6.1.

Table. 6.1. Values of soil stiffness for analyzed soils.

Type of soil	σ_n	M_{DMT}	ν	G_{DMT}	k
	[kPa]	[kPa]	[-]	[kPa]	[kN/mm]
SM	18	90056	0.3	25730.36	300
ML/CL	336	15556	0.3	4444.58	44
OH	34	5960	0.3	1702.79	17
Pt/PH	33.5	2290	0.3	654.17	7
SM	53.5	67857	0.3	19387.66	226
SM	59	31791	0.3	9083.25	106
OL	35	-	-	-	-
OH	48	1541	0.3	440.35	4
SM	47.5	17819	0.3	5091.18	59
OH	54	2100	0.3	599.92	6
Pt	92.5	7667	0.3	2190.52	22
OH/Pt	73	3757	0.3	1073.44	11
SW	117	140054	0.35	32320.26	323
OH	108	5688	0.3	1625.27	16
SW	131	137412	0.35	31710.51	317
SW	144.5	148054	0.35	34166.39	342

As can be seen from Table 6.1, the normal stiffness values for cohesive soils are low and range from 4 (for normally consolidated organic soils) to 44 kN/mm (for slightly overconsolidated soils). Such low stiffness values are practically insignificant and can be successfully considered close to zero. The behavior of soil-concrete interface can be thus approximated with CNL tests ($k = 0$). For sands however, the stiffness increases with relative density and reaches over 200 kPa/mm for medium dense sands and over 300 kPa/mm for dense sands.

The influence of normal stress variation due to relatively high normal stiffness is presented in the CNS studies at different levels of initial normal stress (Fig. 6.3). The studies were carried out at the Grenoble Institute on dense Hostun sand and rough interface (Balachowski, 1995). The focus was on tests at normal stresses similar to those occurring in the analyzed testing site. It can be seen that more than 50% increase of normal stress during shearing can be observed at the normal stiffness of 400 kN/mm (Fig. 6.3a). The maximum shear stress values are similar from all tests and there is no clear correlation between the initial normal stress value and the shear strength (Fig. 6.3b). Figure 6.3c shows how the vertical deformations, and thus the stresses, change for different initial stress values.

The analyzed sands achieve stiffness of max. 340 kN/mm. Knowing that with a stiffness of 400 kN/mm the stress changes are approx. 40-50%, it can be assumed that with a lower stiffness the changes will be correspondingly lower. Additionally, on the basis of DMT probings presented in Chapter 4 (Fig. 4.3), it can be seen that the estimation of vertical drained constrained modulus M_{DMT} is burdened with an error, especially in the case of medium-dense sands, where the differences in values amount to approx. 50%. Therefore, the estimated stiffness is also affected by such level.

Taking into account the above observations and the fact that in the further part of this work, mainly piles with lengths up to 15.5 m (i.e. not embedded in sand layers with stiffness over 300 kN/mm) will be analyzed, it was decided to carry out all interface tests under constant normal stress. This simplified assumption will allow to extent the proposed approach in the future to the soil conditions with dense and very dense sand layers.

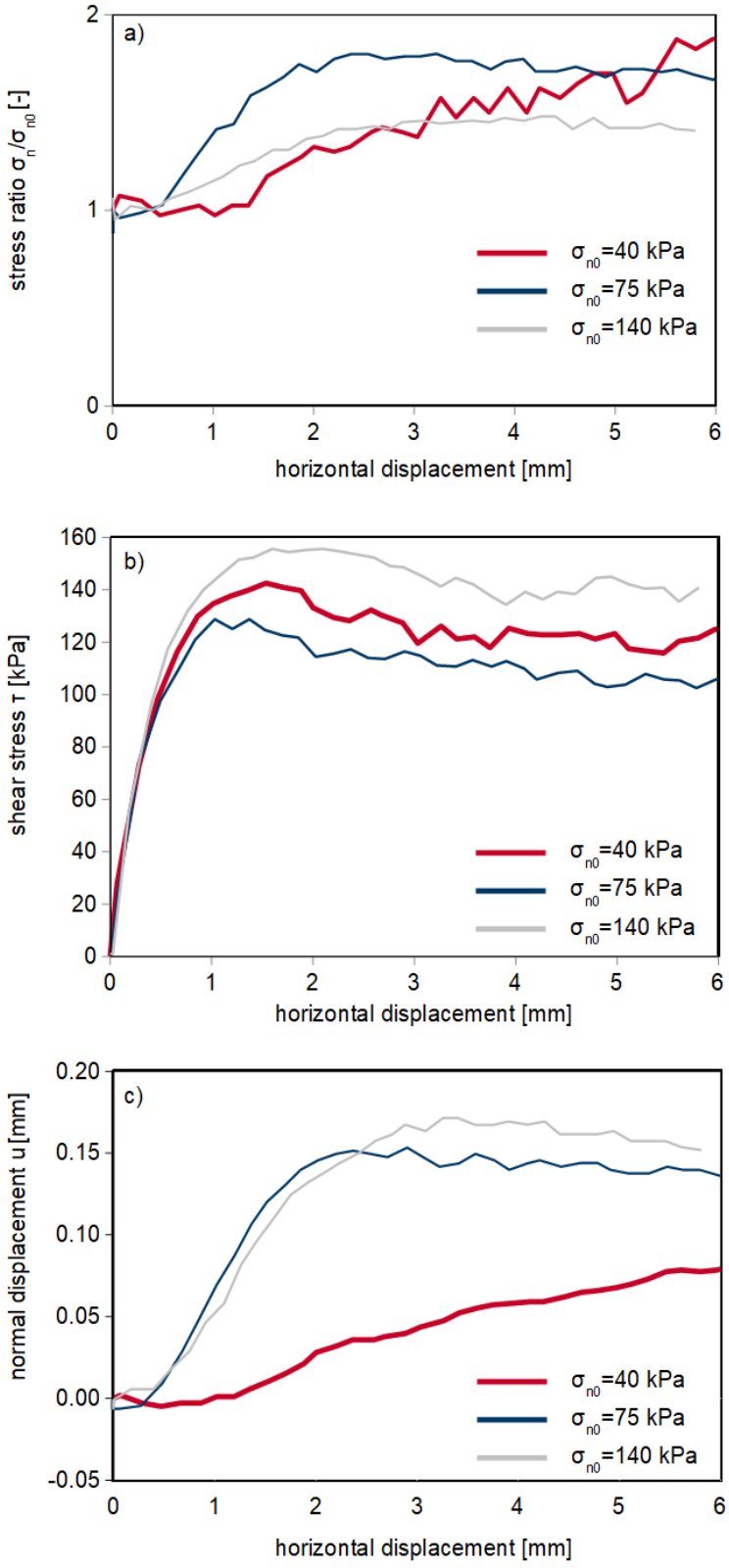

Figure 6.3. The direct shear interface test at CNS for dense Hostun sand-rough interface at k= 400 kN/mm, elaborated after, Bałachowski, 1995.

6.3.1 Testing program

Tests in the direct shear apparatus were carried out in 2017-2020, in the Geotechnical Investigation Laboratory, Department of Geotechnics, Geology and Marine Construction, Faculty of Civil Engineering and Environment at the Gdansk University of Technology. Samples taken directly during field tests were examined, as well as reconstructed ones (see subsection 6.3.4). All samples were tested according to ASTM D3080/D3080M (ASTM D3080, 2020) in 60x60 mm box.

Two series of tests were carried out at different shear rates in a direct shear apparatus. The following soil samples were tested in both measurement series:

- silt/clay (ML/CL);
- organic clay (OH);
- organic silt (OH);
- peat (Pt);
- medium dense sand (SM);
- dense sand (SW).

The first test series was made in direct shear apparatus with an analogue measurement system (Fig. 6.2a) allowing to set three shear speeds: 0.4, 1, and 2 mm/min. A series of one-way shearing of soil samples at 0.4 mm/min speed was performed. The dynamometer readings were made every 0.2 mm of the lower frame displacement, with an accuracy of 0.005 mm (accuracy of dial gauges). The shear stress were calculated using dynamometer calibration data. Measurements were carried out up to displacement of 7 mm, resulting in horizontal strain of 12%.

In the first series, tests were carried out at the normal stress values σ_n' presented in the Tables 6.2 (fine soils) and 6.3 (granular soils). These were preliminary, exploratory tests, at stress values possible to be obtained in an analogue apparatus. All samples were submerged in water during shearing.

Table 6.2. Normal stress values for cohesive soils in the first test series

Type of soil	*Smooth concrete*	*Rough concrete*
Silt/clay	*37 kPa*	*37 kPa*
Organic silt	*86 kPa*	*86 kPa*
Organic clay	*135 kPa*	*135 kPa*
	233 kPa	
	331 kPa	
Peat	*37 kPa*	*37 kPa*
	86 kPa	*86 kPa*
	135 kPa	*135 kPa*
	233 kPa	*233 kPa*
	331 kPa	*331 kPa*

Table 6.3 Normal stress values for non-cohesive soils in the first test series

Type of soil	*Smooth concrete*	*Rough concrete*
Medium dense sand	*37 kPa*	*37 kPa*
	60 kPa	*60 kPa*
	70 kPa	*70 kPa*
	86 kPa	*86 kPa*
	135 kPa	*135 kPa*
Dense sand	*100 kPa*	*100 kPa*
	150 kPa	*150 kPa*
	170 kPa	*170 kPa*

The second series of tests was performed in apparatus with a digital measurement system (Fig. 6.2b), which allows setting a shear rate between 0.00001 and 15 mm/min. It was therefore adjusted to the average pile pullout speed (see Chapter 5), which was 0.06 mm/min. The samples were sheared in both directions at the same speed. Thanks to the automatic data recording, in the initial range of displacements, the shear stress values were obtained every 0.007 mm of the frame displacement. As displacements increased, force readings were less frequent. The shearing was carried out to a deformation equal to 9 % of the horizontal dimension of the sample, i.e. to about 5 mm. All samples were submerged in water during shearing.

Photograph 6.2..a) analog direct shear apparatus b) digital direct shear apparatus

In the second series, fewer tests were carried out, but the level of the normal stresses acting on the laboratory specimen was adjusted to the level of the normal stress acting on the pile shaft in a given soil layer (see Chapter 4). All samples were sheared forward and backward. The same tests procedure was performed on smooth and rough concrete interface at the normal stress presented in Tables 6.4 (fine

soils) and 6.5 (granular soils). Some tests were repeated at the same stress level.

Table 6.4. Normal stress values for cohesive soils in the second test series

Type of soil	*Smooth concrete*	*Rough concrete*
Silt/clay	*35 kPa[(1)(2)]*	*35 kPa[(1)(2)]*
Organic silt	*48 kPa*	*48 kPa*
	54 kPa[(1)(2)]	*54 kPa[(1)]*
	73 kPa[(1)]	*73 kPa[(1)]*
	108 kPa	*108 kPa*
Organic clay	*34 kPa*	*34 kPa*
Peat	*34 kPa*	*34 kPa*
	73 kPa	*73 kPa*

[(1)]two samples tested during forward shearing
[(2)] two samples tested during backward shearing

Table 6.5 Normal stress values for non-cohesive soils in the second test series

Type of soil	*Smooth concrete*	*Rough concrete*
Medium dense sand	*48 kPa*	*48 kPa[(1)]*
	54 kPa	*54 kPa*
	59 kPa	*59 kPa*
Dense sand	*117 kPa*	*117 kPa*
	131 kPa	*131 kPa*
	144 kPa	*144 kPa*

[(1)]two samples tested during forward shearing

6.3.2 Interfaces preparation

Two types of concrete interfaces were prepared: smooth and rough (Photo 6.1). The square, 60x60 mm, steel forms were used for preparing the interfaces. In the bottom of the metal frame, steel plates with smooth or rough surface covered with an adhesive agent were placed. Then the forms were poured with concrete mortar (33 kPa strength) to about half of their height (5 mm) and then densified. On the leveled surface, the geomesh reinforcement was laid and the form was filled with concrete to the height of 10 mm, and densified again. Finished forms were secured with foil overlay and left for 7 days to bind. After that time, concrete tiles were squeezed out of the form and the steel plates were separated to obtain a smooth or rough surface. The tiles were left to bind completely for about 30 days.

Photograph 6.1. Smooth and rough interfaces

6.3.3 Sample preparation

Fine soil samples

The cohesive soil samples were taken from certain depths with the Piston Sampler ST:1 or as a block samples (see Chapter 4). Samples of silt/clay, peat and organic clay were cut out of intact soil blocks and placed directly in the direct shear box. They were then loaded to achieve the stress values shown in Tables 6.2 and 6.4. After loading, the consolidation process began, which lasted 24 hours, and then the samples were sheared.

In the case of organic silt, the preparation process was different due to the significant remolding of the samples taken. At first, the soil was remolded and soil slurry was made. Then the slurry was put into 60x60 mm boxes. The samples were flooded with water and then gradually loaded to a stress of 35 kPa (due to laboratory limitations). The samples were left to be consolidated for 1 month. After that time, the samples were immediately tested at a stress of 35 and 37 kPa. The remaining samples were additionally consolidated for 24 hours, in a direct shear box apparatus, to the values presented above and then sheared.

Granular soil samples

Sand samples have been prepared to represent the in-situ density conditions. Thus, the tests were divided for samples of medium dense sands ($\rho_d = 1.58\ g/cm^3$) and dense sands ($\rho_d = 1.71\ g/cm^3$) (see Chapter 4).

The interfaces were fitted into the lower half of the shear box. The upper frame was filled with moisture sand (w_c close to in-situ conditions) in two layers and densified. When the soil sample was prepared the box was submerged in waters to obtain full saturation of the sample. The samples were then consolidated to the stress at which they were sheared.

6.3.4 Direct shear tests results

Fine soils

Figures 6.3 and 6.4 show the forward shearing results on smooth and rough concrete respectively. The results from the first measurement series (at a shear rate of 0.4 mm/min) are marked in blue and the results from the second series (speed of 0.06 mm/min) are red.

The maximum values of shear resistance on smooth concrete were obtained at displacement of about 1 mm, and in the case of peat at displacement of 2 mm. The maximum shear stress values on rough interface were obtained at displacement around 1-2 mm.

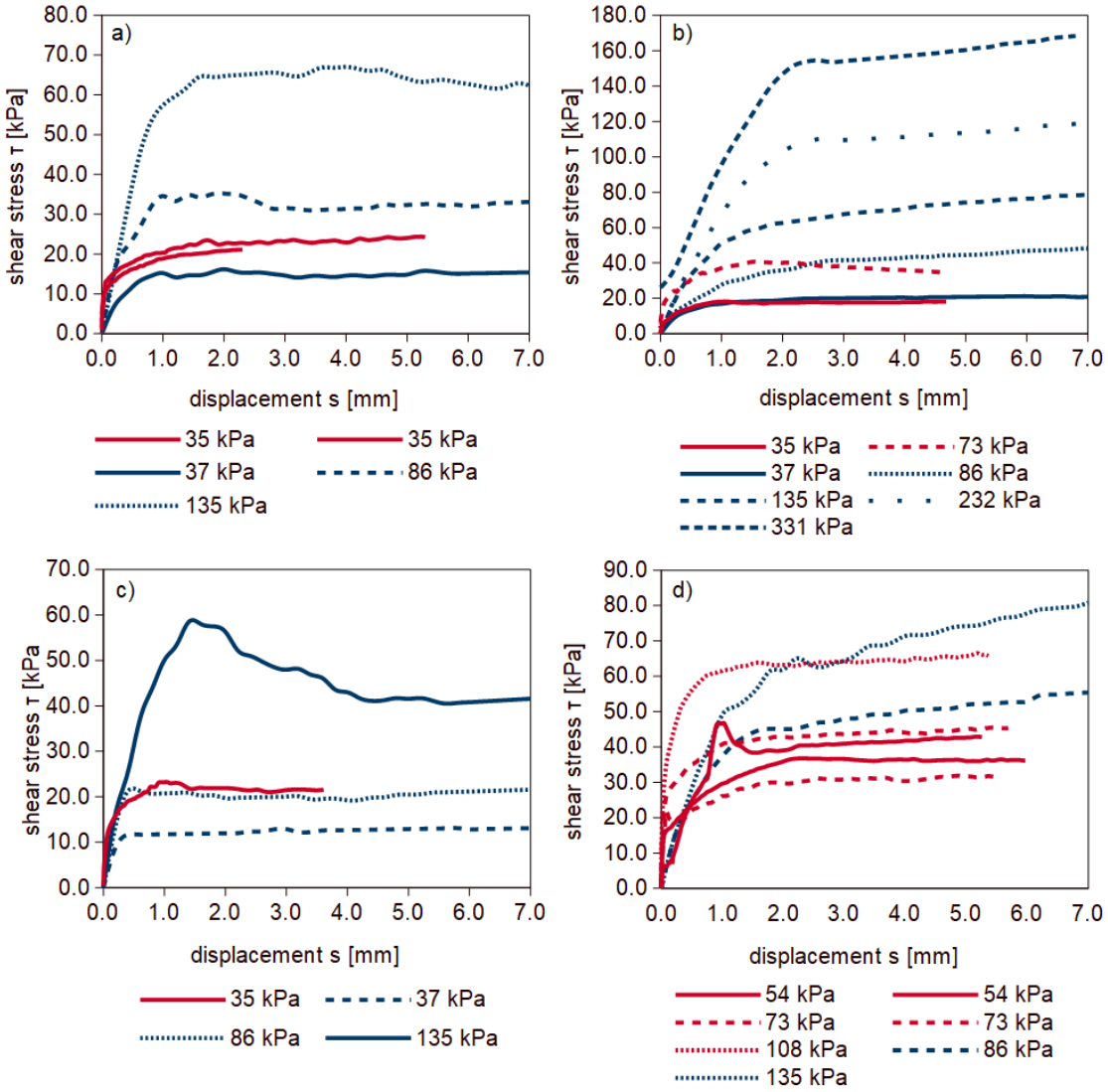

Figure 6.3. Shearing results of fine soils on smooth concrete a) silt/clay b) peat c) organic clay d) organic silt First series (shear rate: 0.4 mm/min) – blue; second series (0.06 mm/min) -red.

When analyzing the results, it is difficult to estimate the effect of the shear rate on the maximum shear strength values. In case of peat, the results from both series are similar. In the case of silt/clay samples and organic clay samples, the shear stress is higher at 35 kPa (first series: 0.4 mm/min) than at 37 kPa (second series: 0.06 mm/min). The differences in shear strength values are up to 10% and may be due to different test speeds or simply due to the scatter of test results.

Differences in results with such a small speed difference may disrupt the possible influence of speed on shear results. The results from both measurement series are practically the same. Therefore, in the remainder of this thesis, the division by shear rate will no longer be applied and all tests will be considered together.

Similar conclusions can be reached by analyzing the shear graphs on the rough interface (Fig.6.4). It can be seen that, for similar stress levels, the samples sheared at 0.06 mm/min (red) speed have reached slightly higher shear stress values than those sheared at 0.4 mm/min (blue). In the case of rough interfaces, the differences resulting from the spread of results may be even greater than for smooth concrete. Hence, as with smooth interfaces, the results from both series of measurements for rough concrete will be analyzed together.

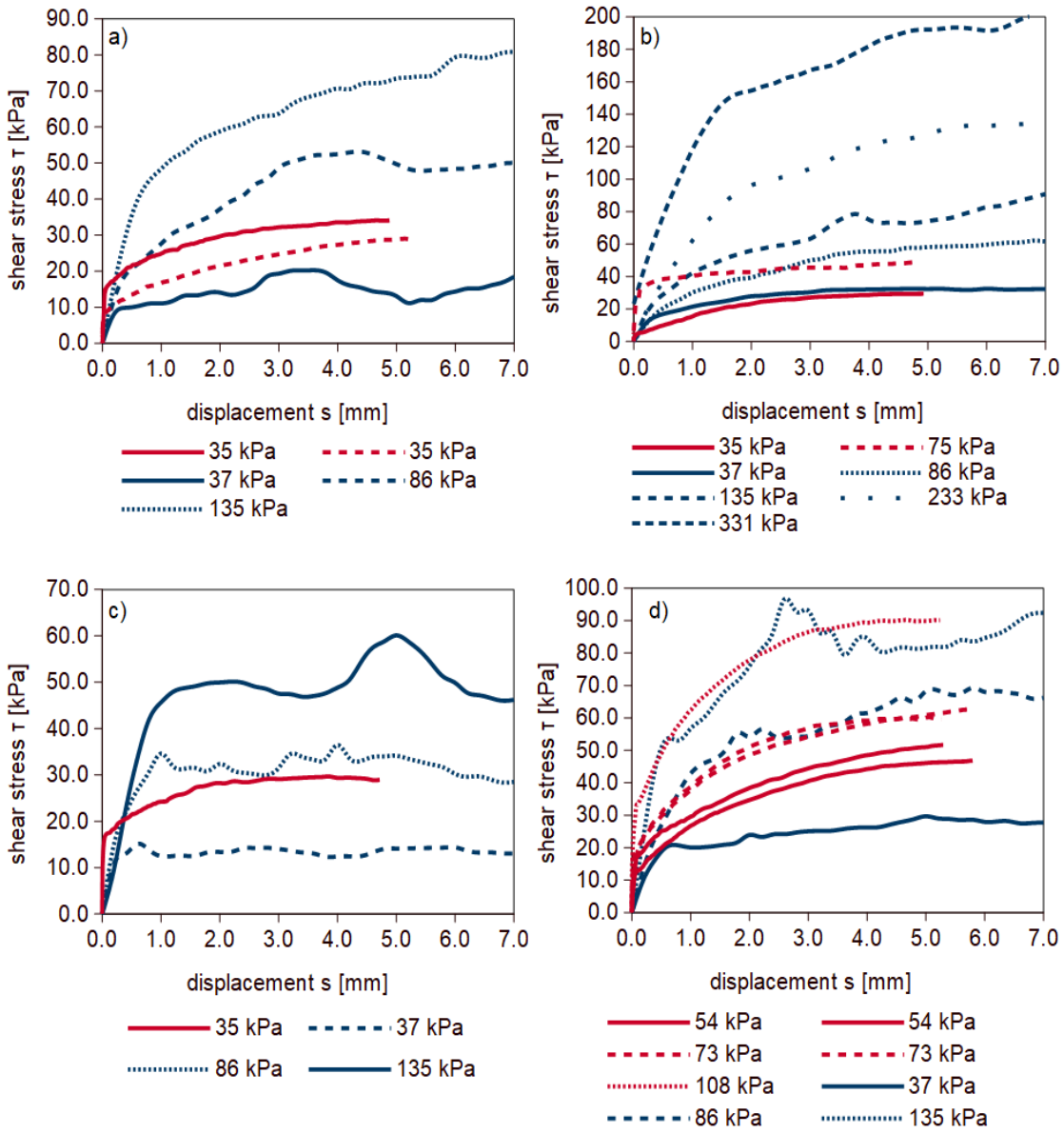

Figure 6.4. Shearing results of fine soils on rough concrete a) silt/clay b) peat c) organic clay d) organic silt First series (shear rate: 0.4 mm/min) – blue; second series (0.06 mm/min) - red.

Figures 6.5 and 6.6 show the results of backward shearing of fine soils on smooth and rough interfaces respectively. The values of maximum shear stress at a given level of normal stress for both smooth and rough concrete are similar to those obtained from initial shearing (grey graphs). Maximum shear stress values were obtained at displacement of 1 mm for smooth concrete interface and behind 1 mm for rough concrete interface.

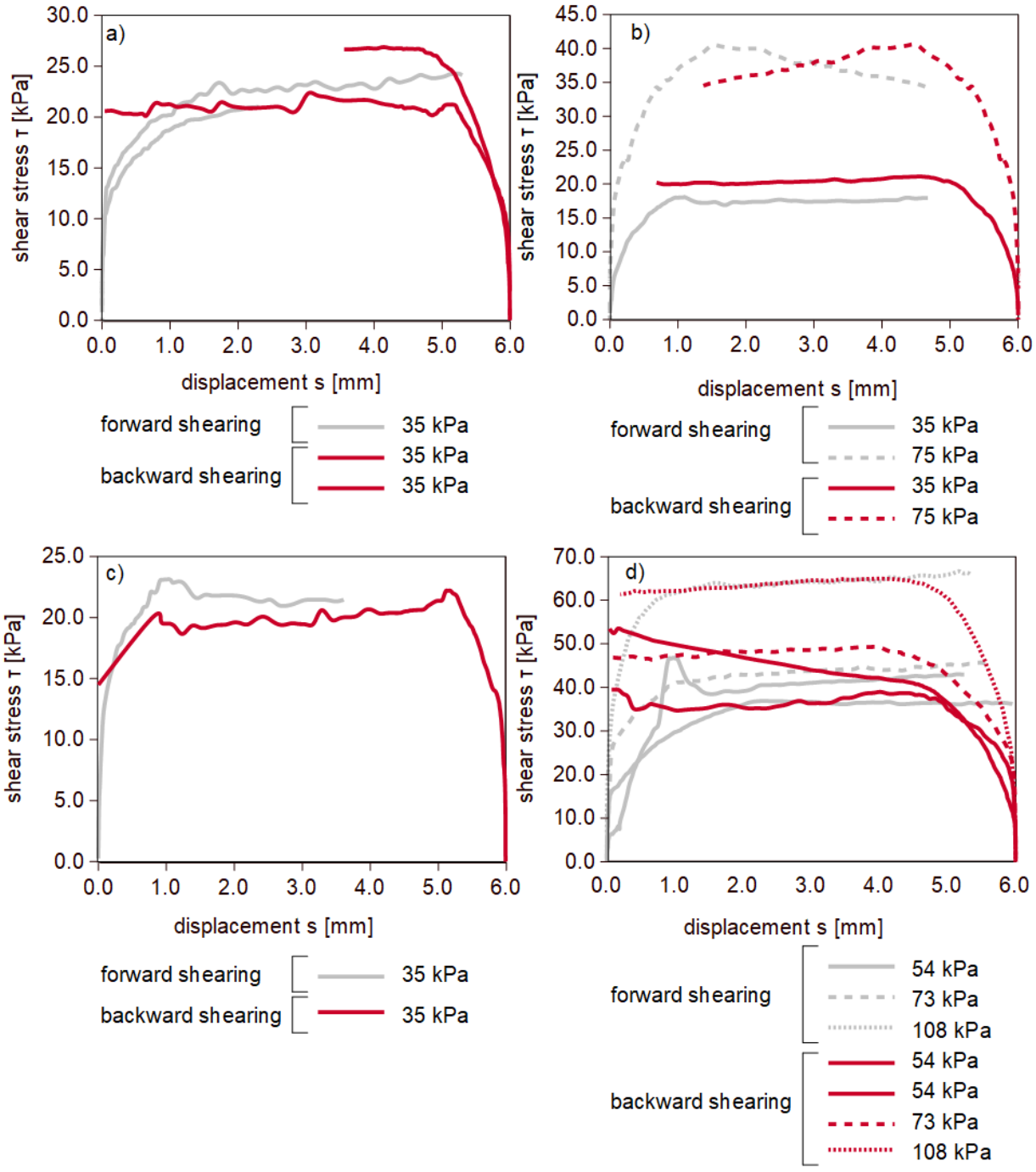

Figure 6.5. Results of backward shearing of fine soils on smooth concrete a) silt/clay b) peat c) organic clay d) organic silt

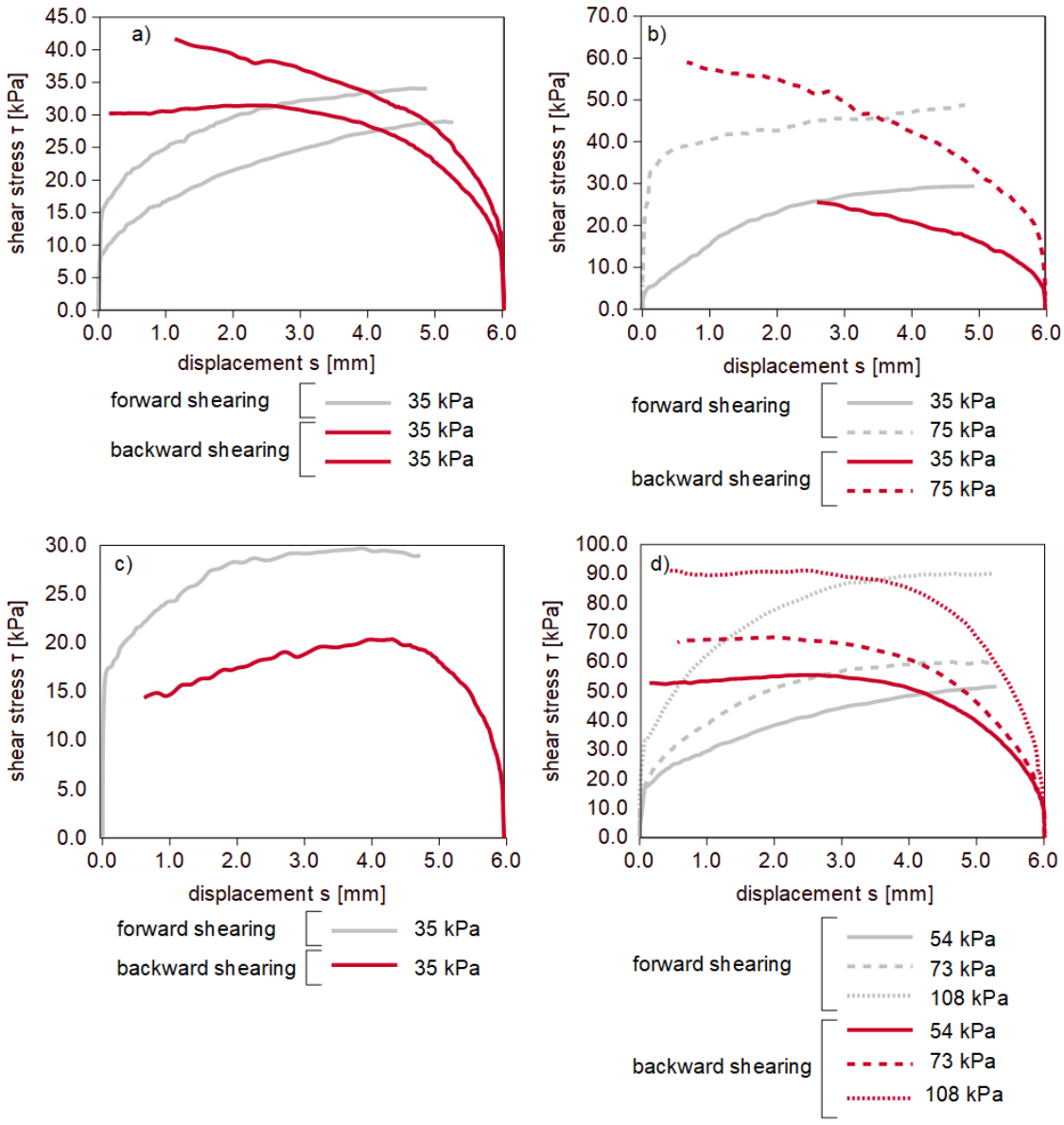

Figure 6.6. Results of fine soil backward shearing on rough concrete a) silt/clay b)peat c) organic clay d) organic silt

Granular soils

As in the case of fine soils, the results obtained for granular soil from the first and second series of tests for the same stress levels overlap each other. Figure 6.7 shows a clear increase in shear stress with an increase in normal stress for both medium and dense sands. The maximum shear stress values was mobilized at 1-2 mm displacements for medium sands, and at 0.5-1 mm for dense sands.

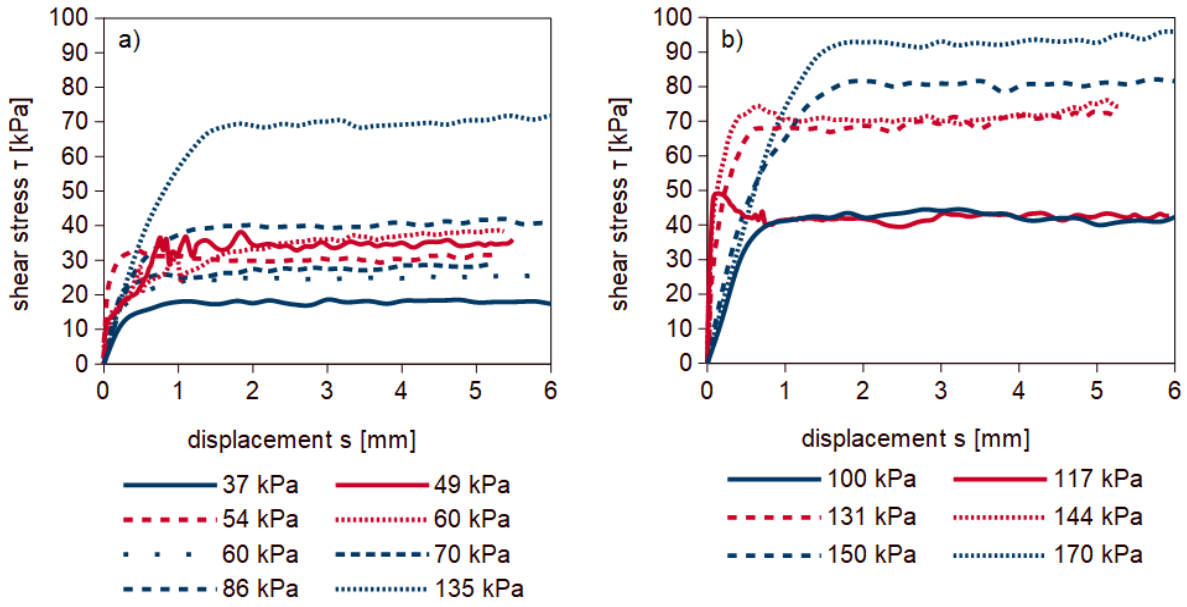

Figure 6.7. Direct shear test results of sands on smooth concrete a) medium dense sand b) dense sand First series (shear rate: 0.4 mm/min) – blue; second series (0.06 mm/min) -red.

In addition, Fig. 6.7 shows a dependence of shear stress on density in the normal stress range of 50-170 kPa. Higher density increases the maximum shear stress values. Backward shearing on smooth concrete (Fig.6.8) gives similar shear stress values as the forward shearing in medium dense sands. The maximum values have mobilized at 1 mm displacement. For dense sands the values of maximum shear stress from backward shearing are slightly higher than for forward shearing.

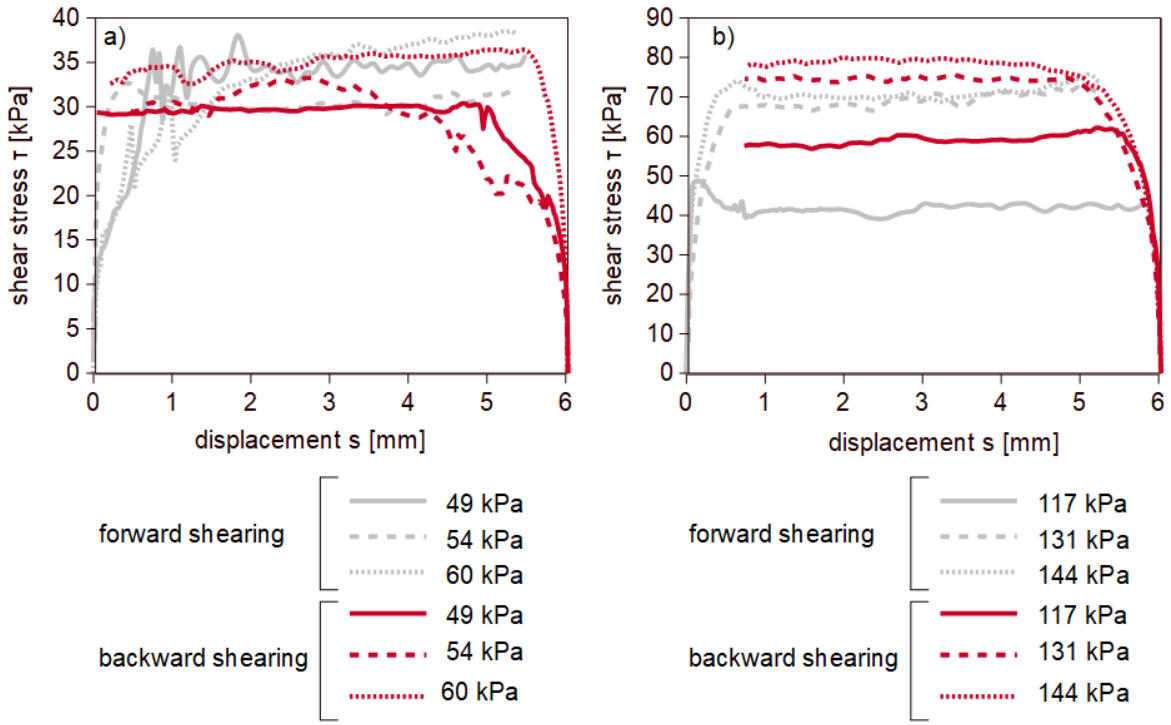

Figure 6.8.. Direct shear test results on smooth concrete in opposite direction a) medium dense sand b) dense sand

In the case of rough surface of concrete interface (Fig 6.9), maximum shear stress mobilization for medium dense sands took place at displacements from 1 to even 4 mm. Larger displacements were needed to mobilize shear stress at higher normal stress levels. In the case of dense sands, the maximum shear stress was mobilized at about 1-1.5 mm displacement.

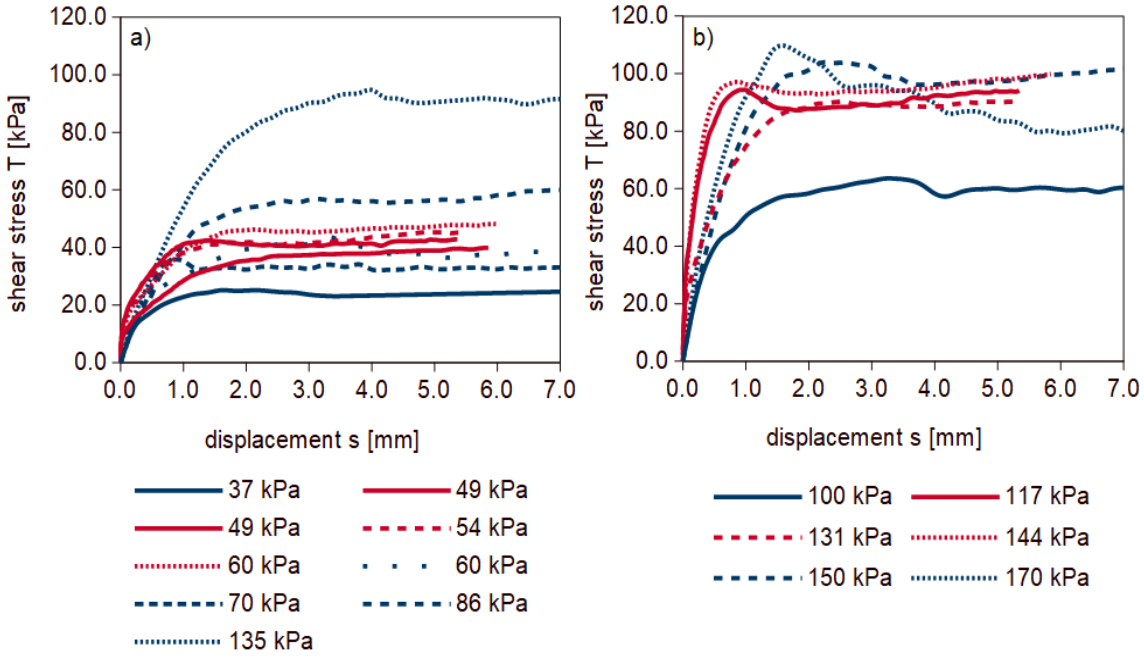

Figure 6.9. Direct shear results of sands on rough concrete a) medium dense sand b) dense sand First series (shear rate: 0.4 mm/min) – blue; second series (0.06 mm/min) -red.

A correlation between shear stress and density, in the normal stress range between 50 and 170 kPa (Fig.6.9.), exists similarly as in the case of smooth concrete. Additionally, from the initial part of the graph (these graphs are slightly steeper in the initial phase), it can be concluded that at low displacement values, dense sands exhibits higher shear stress values.

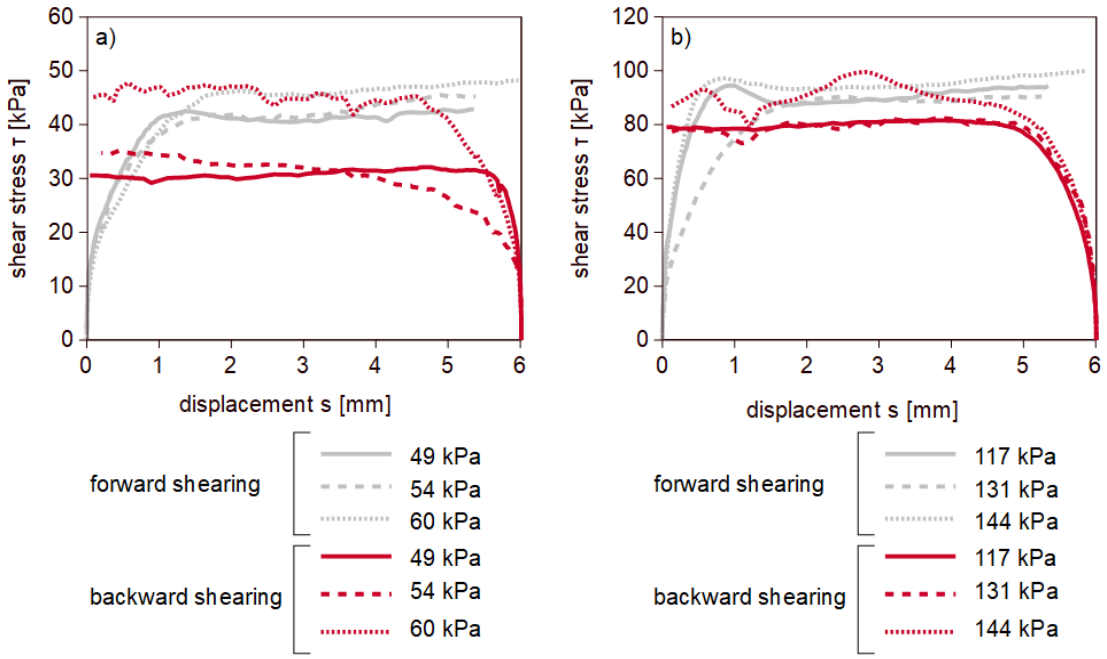

Figure 6.10. Direct shear test results on rough concrete in opposite direction a) medium dense sand b) dense sand

In the case of backward sands shearing on rough concrete, maximum shear stress was mobilized at 1 mm displacement, see Figure 6.10. In contrast to tests on smooth concrete, some backward shearing tests on rough concrete give lower shear stress values than forward shearing.

6.4 Conclusions

Below (Table 6.6), shear stresses, obtained from direct shear tests at normal stress corresponding to the normal stress acting on the pile shaft after installation (see Chapter 4), are listed.

Table 6.6. Maximum shear stress on smooth and rough interfaces from forward shearing.

Type of soil	σ_n*	Maximum shear stress [kPa]	
	[kPa]	Smooth concrete	Rough concrete
SM	18.0	-	-
ML/CL	33.6	23	30
OH	34.0	23	30
Pt/OH	33.5	23	29
SM	53.5	33	46
SM	59.0	39	48
OL	35.0	-	-
OH	48.0	32	-
SM	47.5	38	41
OH	54.0	41	48
Pt	92.5	-	-
OH/Pt	73.0	40	61
SW	117.0	49	94
OH	108.0	67	90
SW	131.0	73	90
SW	144.5	76	100

** in the middle of each layer*

Comparing the graphs for smooth and rough concrete (for forward shearing), it can be seen that testes for rough concrete interfaces resulted in higher shear stress values at the same normal stress level. In cohesive soils, the increase in shear stress ranges from 20% for clays to 50% for organic silts, while for sands, it is an increase from about 30% for medium sands to 90% for dense sands.

In the context of displacement piles, more recent studies (Tovar-Valencia et al., 2018a), (Doan and Lehane, 2018b) confirm that the roughness of the surface of the pile, both for sands and cohesive soils, has a significant impact on the friction mobilized at the pile shaft. As the roughness increases, the shear stress increases and can be practically twice as high as on smooth concrete piles. In addition, the roughness effect is more noticeable in dense sands.

Backward shearing for fine grained soils gives the same results as forward shearing. This fact is not surprising as the analyzed soils are normally consolidated.

For compacted sands sheared backward on smooth interface, shear stress is usually higher than from forward shearing. This is extraordinary. Some of these test were repeated and results are quite inconsistent. One can assume that for dense sands maximum shear stress are almost the same in terms of forward and backward shearing. For medium compacted sands, the results are inconclusive.

For sands sheared backward on rough interface, shear stresses are lower than from forward

shearing. The first shear is on the interface (the sand shears against the rough interface surface). The backward shearing occurs on the new surface (friction of the sand against the sand).

Chapter 7
Formulation of DMT method

7.1 Introduction

In order to create a method of displacement piles design using the results of dilatometer sounding, the model of transfer functions (also known as transfer curves or t-z curves) proposed by Frank & Zhao (Frank and Zhao, 1982), (Frank, 2017a) (see Chapter 3) was applied. This model is widely used in France because of its simplicity. Frank and Zhao proposed a direct relationship between the parameters k_t and k_q and the pressuremeter modulus E_p obtained from the MPM test (Menard Pressuremeter test) (Fig. 7.1).

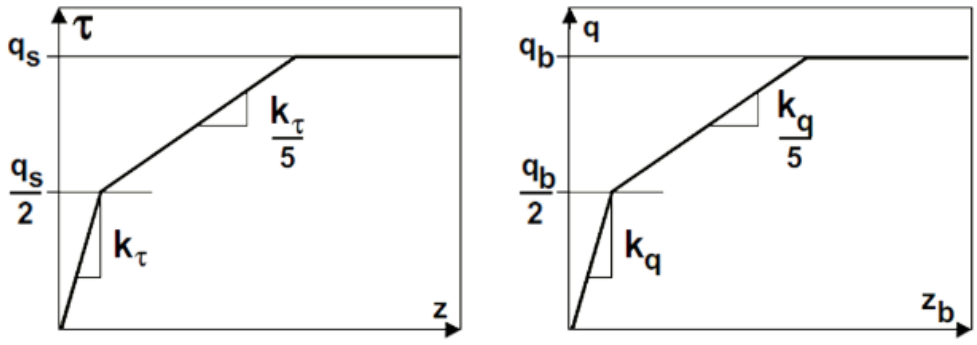

Figure 7.1. Model for t-z curves for MPM test results (Frank and Zhao, 1982)

Limit stresses q_s and q_b are, respectively, the unit shaft friction and base resistance derived from the MPM (or CPT) method and k_t and k_q are the initial slopes of the diagrams. The determination of k_t and k_q were described in more detail in Chapter 3, depending on the method used.

A similar approach has been used in the formulation of the DMT method for the purpose of this thesis. Friction at the pile shaft is expressed as a function of a dilatometer modulus M_{DMT} (Fig. 7.2). The characteristics of the mobilization of frictional resistance, necessary for the construction of transfer functions, were obtained on the basis of interface direct shear tests' results (see Chapter 6). The calibration of $q_b - z_b$ curves for base resistance mobilization is outside the scope of this thesis.

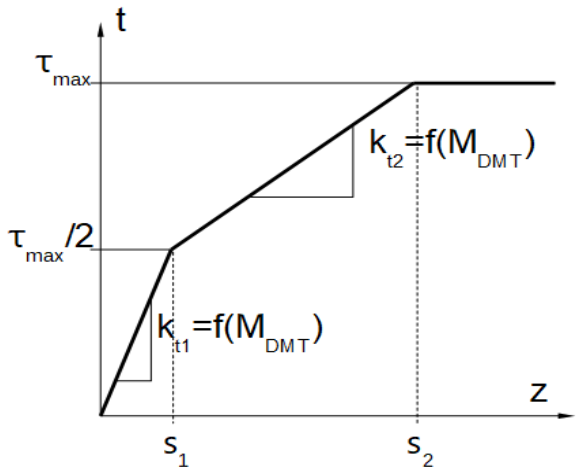

Figure 7.2. The concept of DMT model for unit shaft friction

In order to establish the t-z curves, following steps were made for each of the analyzed soil type:

- interface direct shear tests at CNL were performed for different soils and normal stress level;
- a curve was selected from the shear test apparatus for the normal stress corresponding to the horizontal stress acting on the pile shaft after installation;
- this curve was described as trilinear with inclinations of k_{t1} and k_{t2}, respectively;
- after matching the t-z curves to the friction mobilization from the direct shear apparatus, a relationships (see subsection 7.2 and 7.3) between shaft mobilization parameters k_{t1} and k_{t2} and M_{DMT} were created.

In order to avoid the difficulties of adjusting individual curves and for the purpose of generalization, the graphs were normalized with the maximum skin friction τ_{max}. Therefore, the graphs of $\tau/\tau_{max} - s$ (where s – displacement measured in the direct shear test [mm]) relation were obtained (see Figures 7.3, 7.5, 7.7, 7.11, 7.13, 7.17, 7.19, 7.21, 7.24, 7.26) . Consequently, the following notation was also introduced:

$$k_{t1} = \Delta\tau/\Delta s \tag{7.1}$$

$$k_{t1}^{*} = \frac{\Delta\tau}{\tau_{max}}/\Delta s \tag{7.2}$$

Hence the relationship 7.1 can be transformed to the following equation:

$$k_{t1} = k_{t1}^{*} \cdot \tau_{max} \tag{7.3}$$

The same applies to parameter k_{t2} (Equations 7.4-7.6).

$$k_{t2} = \Delta\tau/\Delta s \tag{7.4}$$

$$k_{t2}^{*} = \frac{\Delta\tau}{\tau_{max}}/\Delta s \tag{7.5}$$

$$k_{t2} = k_{t2}^{*} \cdot \tau_{max} \tag{7.6}$$

The dilatometer modulus for cohesive and non-cohesive soils was adopted on the basis of DMT probings carried out before the pile construction (see Chapter 4 for more details).

Tab. 7.1. Average values (AVG) and standard deviation (SD) of the dilatometer modulus adopted to create the transfer functions

Depth of soil layer [m]		Soil type	σ_n	M_{DMT} AVG	M_{DMT} SD
top	bottom		[kPa]	[MPa]	[MPa]
0.00	0.70	SM	18	-	-
0.70	1.80	ML/CL	336	15.6	4.1
1.80	2.70	OH	34	6.0	1.9
2.70	4.05	Pt/OH	33.5	2.3	0.6
4.05	5.55	SM	53.5	67.9	15.0
5.55	7.05		59	31.8	10.4
7.05	7.80	OL	35	-	-
7.80	10.20	OH	48	1.5	0.3
10.20	10.45	SM	47.5	17.8	7.6
10.45	12.15	OH	54	2.1	0.6
12.15	12.95	Pt	92.5	7.7	1.1
12.95	14.45	OH/Pt	73	3.8	1.2
14.45	15.70	SW	117	140.1	32.0
15.70	15.95	OH	108	5.7	1.6
15.95	17.50	SW	131	137.4	17.0
17.50	19.00		144.5	148.1	14.7

The bilinear functions were created according to the following procedure:

1) for the normalized shear stress $\tau/\tau_{max} = 0.5$, the displacement s_1 was determined and then the slope k_{t1}^* was calculated using the secant line;
2) for normalized shear stress $\tau/\tau_{max} = 1.0$, the displacement s_2 was determined and another secant between points (s_1, $\tau/\tau_{max} = 0.5$,) and (s_2; $\tau/\tau_{max} = 1.0$) was created;
3) the last part of the graph corresponds to the value $\tau/\tau_{max} = 1.0$.

The upper limit for the displacements s_1 is fixed as 1 mm, while for displacements s_2 the maximum value is 4 mm.

The above method was applied due to the preliminary character of this research, prepared on the basis of trial fields for specific soil conditions. In the case of having more tests for soils from different areas, it would be reasonable to operate on average values (with more curves available from direct shear test for particular soil type). This is one of the possibilities to continue and expand this model in future research.

7.2 Smooth concrete interface

7.2.1 Fine grained soils

Peat

On the basis of peat samples tested on smooth concrete, a scheme for creating transfer functions will be presented.

Figure 7.3 shows a diagram 6.2.b (Chapter 6) normalized with maximum shear stresses for

individual samples. For the test specimen at a normal stress of 35 kPa, the maximum shear stress was 18 kPa, and for the specimen sheared at $\sigma_n = 75\,kPa$, $\tau_{max} = 40\,kPa$. It can be seen that the mobilization of normalized shear stress in both diagrams is very similar. The slope of the first part of the graph is: $k_{t1}^* = \frac{\frac{\Delta\tau}{\tau_{max}}}{\Delta s} = \frac{0.5}{0.14} = 3.57$, while the second part of the graph is: $k_{t2}^* = \frac{0.5}{1.1-0.14} = 0.52$.

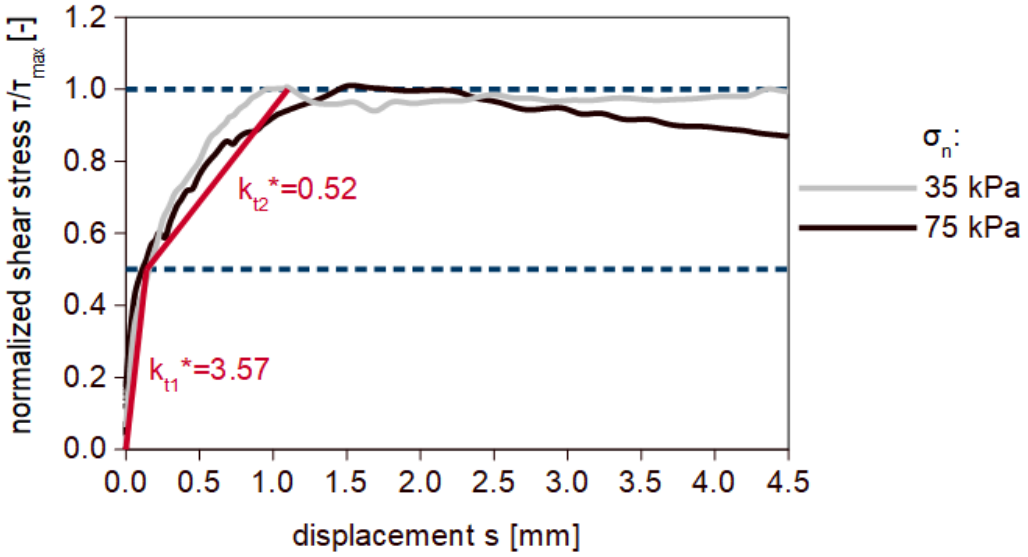

Figure 7.3. Normalized shear stress vs. displacement – peat (Pt) samples on smooth concrete

Figure 7.4 shows the relationship between the maximum shear stress τ_{max} and the normal stress σ_n, taking into account the results of both series of measurements (i.e. tests at 0.06 mm/min and 0.4 mm/min shear speed). On the basis of this graph the following relation (Eq. 7.7) was obtained for shearing peat on smooth concrete, with a coefficient of determination R^2 equal to 0.996.

$$\tau_{max} = 0.501 \cdot \sigma_n + 3.767 \tag{7.7}$$

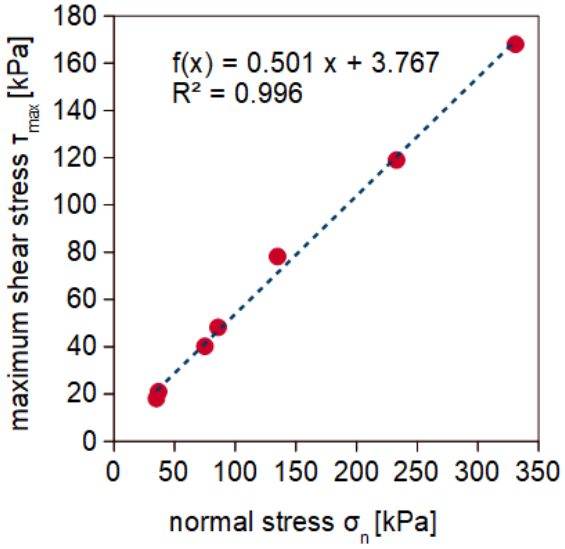

Figure 7.4. Maximum shear stress vs. normal stress – peat (Pt) samples on smooth concrete

Using the Equation (7.7), shear stresses are calculated for each normal stresses. The results are summarized with the results of maximum shear stresses obtained directly from the direct shear apparatus in Table 7.2.

Table 7.2. Maximum shear stress values for peat

τ_{max}	σ_n	τ_{max} (Eq.7.7)
[kPa]	[kPa]	[kPa]
18.1	35.0	21.3
40.2	75.0	41.3
21.0	37	22.2
48.2	86	46.7
78.2	135	71.2
119.0	233	120.2
168.0	331	169.3

The maximum error in determining τ_{max} is approx. 7 kPa.

Using the σ_n values for peat, presented in Table 7.1, and the τ_{max} (σ_n) relation (Equation 7.7) shear stresses for each depth level (horizontal stresses) were calculated. They are 20.52 and 50.02 kPa for depths 2.7-4.05 m and 12.15-12.95 m respectively. Then, using relations 7.3 and 7.6 values of k_{t1} and k_{t2} were determined equal to 73 and 10.7 for depth of 2.7-4.05 m as well as 179 and 26 for the second peat layer.

To create a general relationship between the slopes k_{t1}i k_{t2}, and M_{DMT}, it is necessary to create τ_{max} (σ_n) relations for all types of soils.

Organic clay and silt and silt/clay samples have been analyzed in the same way, so the following results will be discussed briefly.

Organic silt

The normalized diagrams for organic silt tested at normal stresses of 49, 54, 73 and 108 kPa are shown in Figure 7.5. As in the case of peat, the diagrams mostly overlap. k_{t1}^* is 1.67, while k_{t2}^* is 0.42.

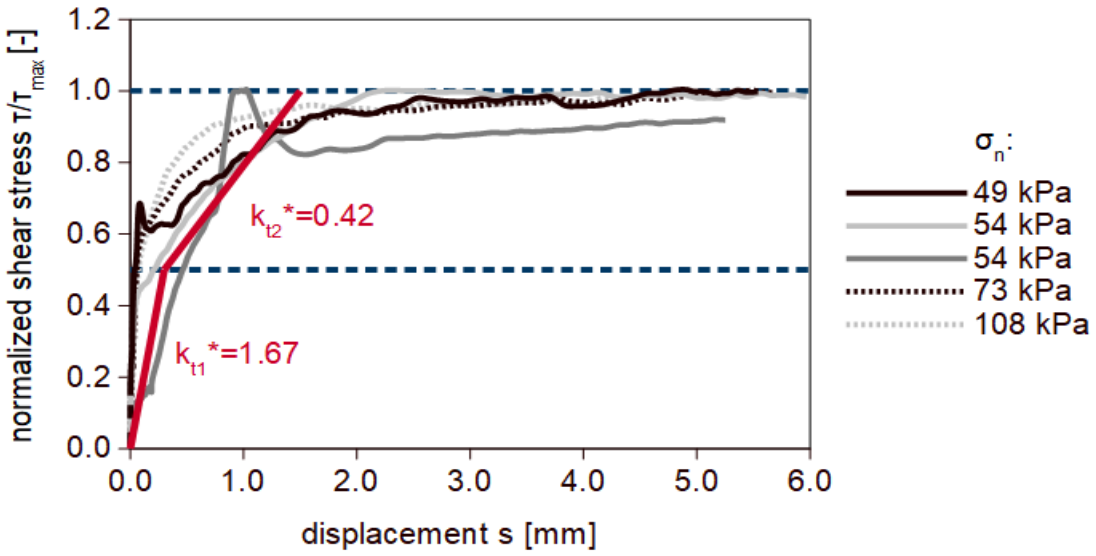

Figure 7.5. Normalized shear stress vs. displacement – Organic silt (OH) samples on smooth concrete

From Figure 7.6 the failure envelope for organic silt is described with the following relation (Eq. 7.8), with the coefficient of determination equal to 0.991:

$$\tau_{max} = 0.606 \cdot \sigma_n + 3.219 \tag{7.8}$$

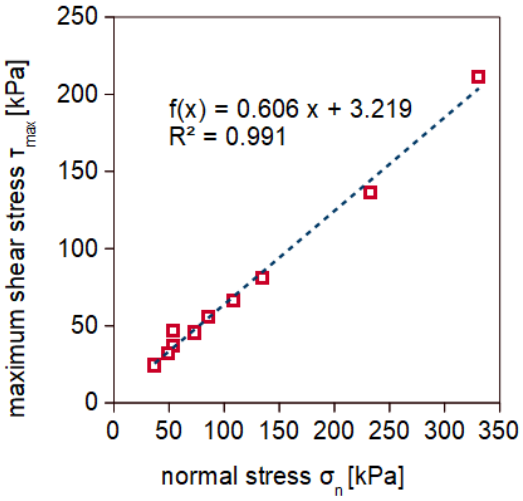

Figure 7.6. Maximum shear stress vs. normal stress – Organic silt (OH) samples on smooth concrete

The results of maximum shear stress are summarized in Table 7.3 below.

Table 7.3. Maximum shear stress values for organic silt.

τ_{max}	σ_n	τ_{max} (Eq.7.8)
[kPa]	[kPa]	[kPa]
36.8	54.0	36.2
46.7	54.0	36.2
45.6	73.0	47.8
31.8	49.0	33.1
66.5	108.0	69.1
24.4	37.0	25.6
55.4	86.0	55.6
80.8	135.0	85.5
136.0	233.0	145.3
210.9	331.0	205.1

The maximum error in determining τ_{max} is approx. 10 kPa.

Organic clay + Silt/Clay

The charts of organic clay and clay were analyzed altogether because the shear stress mobilization curves for these soils are similar (Figure 7.7). The slope k_{t1}^* is 10.00, while k_{t2}^* 0.43.

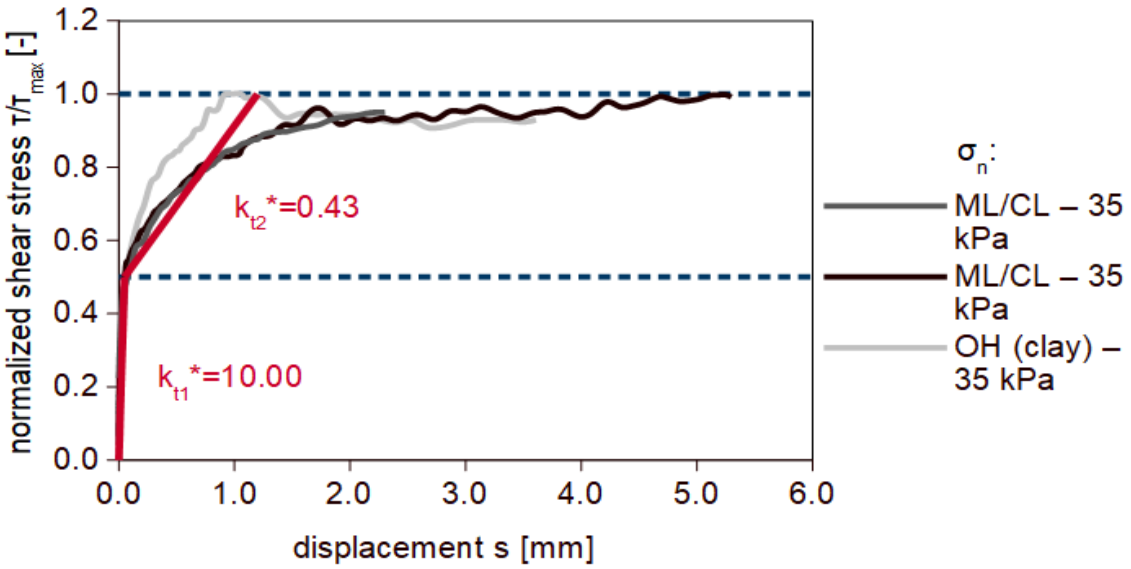

Figure 7.7. Normalized shear stress vs. displacement – Organic clay (OH) and Silt/Clay (ML/CL) samples on smooth concrete

From Figure 7.8 the failure envelope for organic clay– smooth concrete interface is described by following formula with coefficient of determination equal to 0.972:

$$\tau_{max} = 0.249 \cdot \sigma_n + 6.551 \qquad (7.9)$$

whereas from Figure 7.9 the failure envelope for silt/clay (Eq. 7.10) was obtained with the coefficient of determination equal to 0.985:

$$\tau_{max} = 0.419 \cdot \sigma_n + 4.159 \qquad (7.10)$$

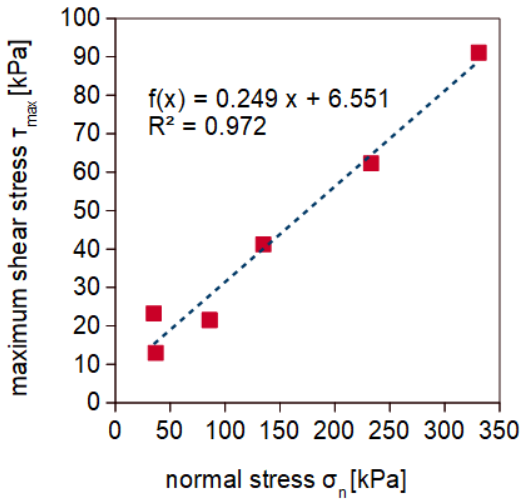

Figure 7.8.. Maximum shear stress vs. normal stress – Organic clay (OH) samples on smooth concrete

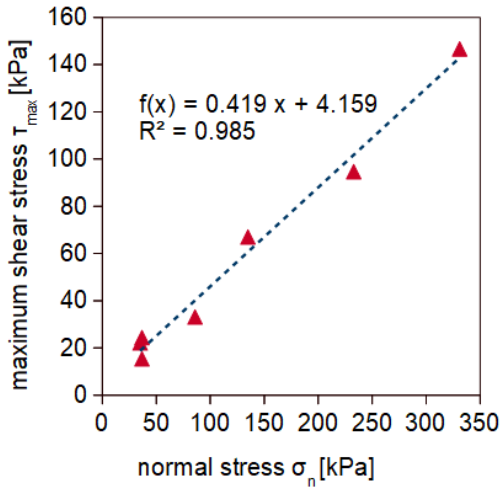

Figure 7.9. Maximum shear stress vs. normal stress – Silt/Clay (ML/CL) samples on smooth concrete

The results of maximum shear stress are summarized in Table 7.4 below.

Table 7.4.. Maximum shear stress values for organic clay and silt/clay.

	τ_{max}	σ_n	τ_{max} (Eq.7.9, 7.10)
	[kPa]	[kPa]	[kPa]
Organic clay	23.4	35.0	15.3
	13.0	37.0	15.7
	21.55	86.0	28.0
	41.2	135.0	40.3
	62.3	233.0	64.8
	91.1	331.0	89.3
Silt/Clay	22.2	35,0	18.9
	24.4	37.0	19.6
	15.4	37.0	19.6
	33.1	86.0	40.2
	67.0	135.0	60.8
	94.7	233.0	102.0
	146.7	331.0	143.2

The maximum error in determining τ_{max} for organic clay and silt/clay is approx. 8 kPa.

7.2.2 Granular soils

Non-cohesive soils were analyzed in the same way as cohesive ones. One type of sand of different relative density was tested (see Chapter 4). On this basis, it was distinguished: medium-dense sands and dense sands.

Medium dense sand

In Figure 7.11, graphs of medium-dense sand tested at normal stresses of 49, 54 and 60 kPa are presented. The slope coefficient of the first part of the graph is 2.50 and of the second part of the graph is 0.39. The graph of sample tested at 54 kPa slightly differs from the others, which may have resulted from the sand grains interlocking during shearing.

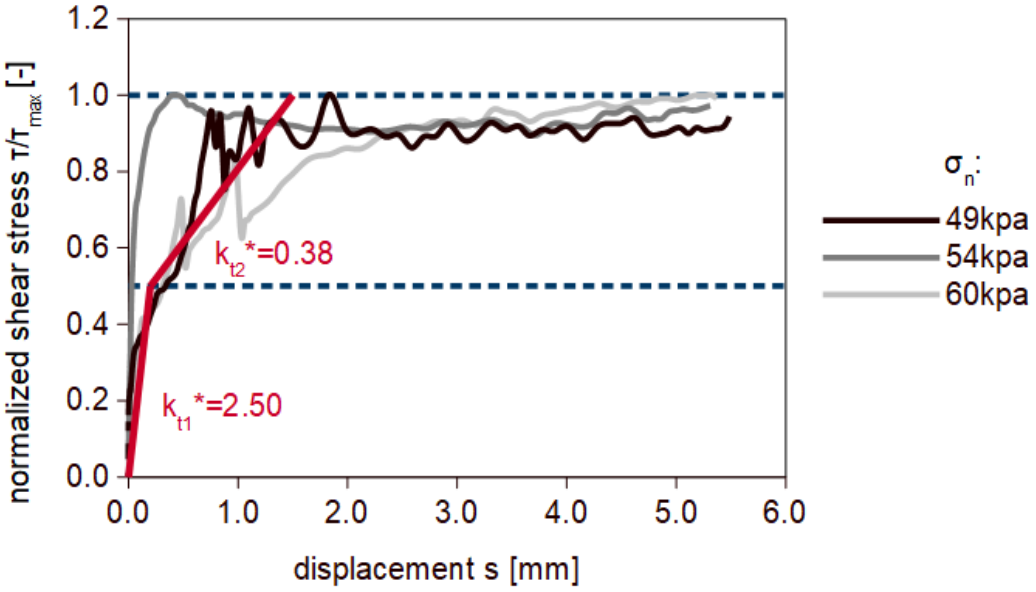

Figure 7.11. Normalized shear stress vs. displacement – Medium dense sand (SM) samples on smooth concrete

From Figure 7.12 the following relation (Eq. 7.11) was obtained for medium-dense sand, with the coefficient of determination equal to 0.980:

$$\tau_{max} = 0.551 \cdot \sigma_n - 0.947 \tag{7.11}$$

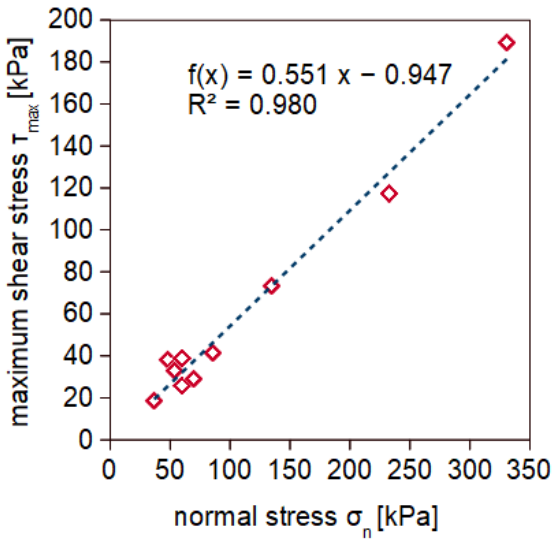

Figure 7.12. Maximum shear stress vs. normal stress – Medium dense sand (SM) samples on smooth concrete

The results of maximum shear stress are summarized in Table 7.5 below.

Table 7.5. Maximum shear stress values for medium dense sand.

τ_{max}	σ_n	τ_{max} *(Eq.7.11)*
[kPa]	*[kPa]*	*[kPa]*
38.2	*48.0*	*25.5*
32.8	*54.0*	*28.8*
38.6	*60.0*	*32.1*
25.7	*60.0*	*32.1*
29.0	*70.0*	*37.6*
18.5	*37.0*	*19.3*
41.6	*86.0*	*46.2*
73.4	*135.0*	*73.2*
117.3	*233.0*	*127.1*
189.4	*331.0*	*181.1*

The maximum error in determining τ_{max} for medium dense sands is approx. 13 kPa.

Dense sand

In Figure 7.13, normalized graphs of dense sand tested at stresses of 117, 131 and 144 kPa are presented. The inclination of the first part of the graph is 5.0 and that of the second part is 1.0. Determination of the slope k_{t1}^{*} is hampered in this case because the shear strength has already mobilized at small displacements and it is difficult to separate the first part of the graph.

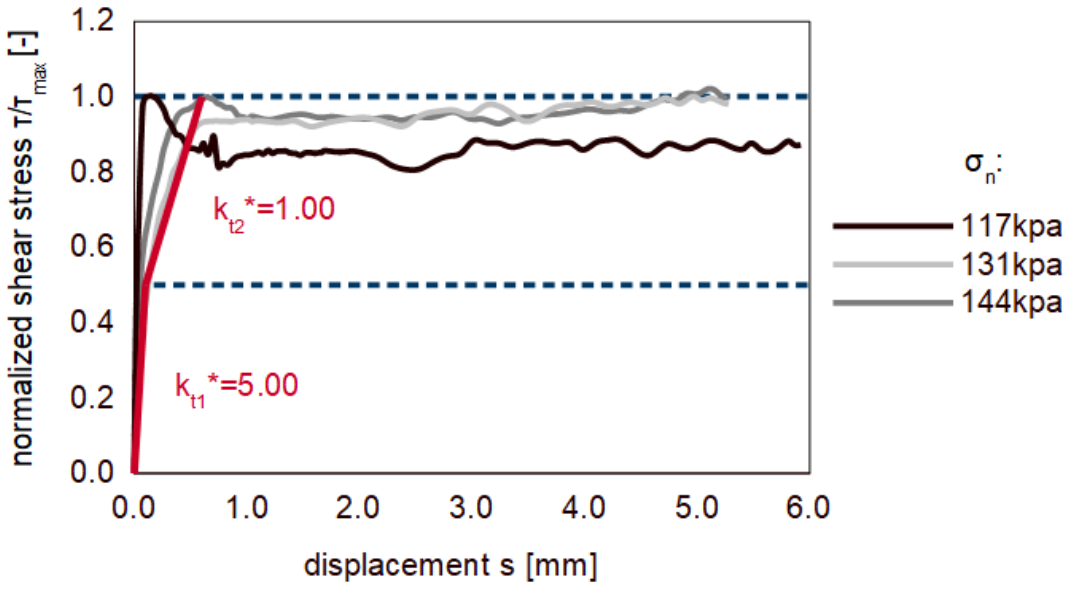

Figure 7.13. Normalized shear stress vs. displacement – Dense sand (SW) samples on smooth concrete

From Figure 7.14 the following relation (Eq. 7.12) was obtained for dense sand, with a 0.990 coefficient of determination:

$$\tau_{max} = 0.530 \cdot \sigma_n \tag{7.12}$$

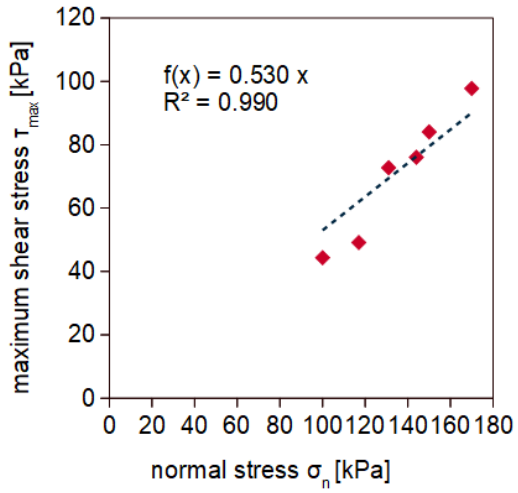

Figure 7.14. Maximum shear stress vs. normal stress – Dense sand (SW) samples on smooth concrete

Due to a bias created during testing, it was necessary to force the graph to pass through the origin. The results of maximum shear stress are summarized in Table 7.6 below .

Table 7.6. Maximum shear stress values for dense sand.

τ_{max}	σ_n	τ_{max} *(Eq.7.12)*
[kPa]	*[kPa]*	*[kPa]*
49.1	*117.0*	*62.0*
72.7	*131.0*	*69.4*
76.0	*144.0*	*76.3*
44.3	*100.0*	*53.0*
84.1	*150.0*	*79.5*
97.8	*170.0*	*90.1*

The maximum error in determining τ_{max} for dense sands is approx. 12 kPa.

7.3 Rough concrete interface

An analogous analysis as in smooth interface case was conducted for on rough concrete interface. The results for fine-grained soils will be presented first, and then, the results for coarse ones will be shown.

7.3.1 Fine grained soils

Peat

Figure 7.15 shows normalized shear stress diagram for specimens tested at a normal stress of 35 and 75 kPa. When tested at 75 kPa, the frame of the apparatus was jammed at the initial displacement and this diagram is different from the 35 kPa diagram, which should be considered as correct in this case. The slope k_{t1}^* is 0.5, and k_{t2}^* 0.2.

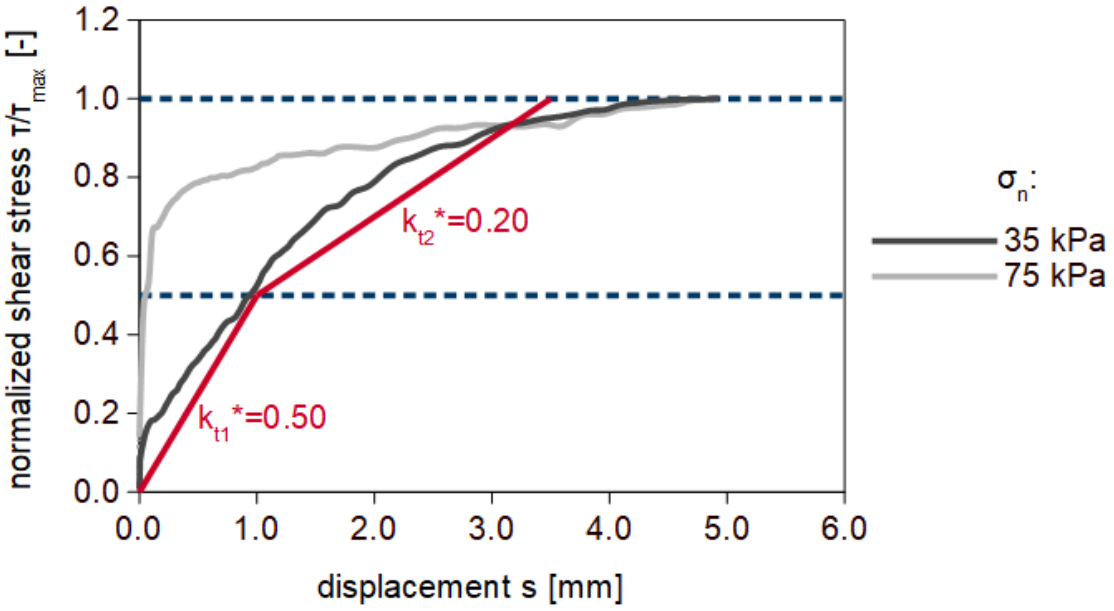

Figure 7.15. Normalized shear stress vs. displacement – peat (Pt) samples on rough concrete

On the basis of Figure 7.16 the following relation (Eq. 7.13) was obtained for shearing peat on rough concrete with a coefficient of determination equal to 0.996. The gradient of the line is in this case very close to the result obtained on smooth concrete, which was 0.501.

$$.\tau_{max} = 0.565 \cdot \sigma_n + 10.509 \tag{7.13}$$

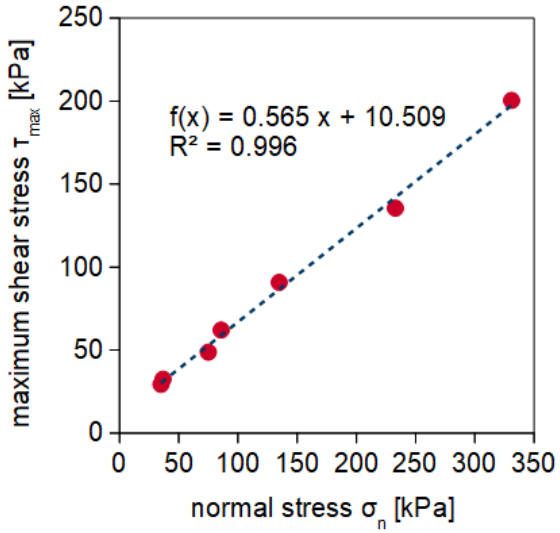

Figure 7.16. Maximum shear stress vs. normal stress – peat (Pt) samples on rough concrete

Table 7.7 summarizes the results of maximum shear stresses obtained directly from the shear box apparatus test and those obtained from relation 7.13.

Table 7.7. Maximum shear stress values for peat on rough concrete

τ_{max}	σ_n	τ_{max} *(Eq.7.13)*
[kPa]	*[kPa]*	*[kPa]*
29.4	*35.0*	*30.1*
48.8	*75.0*	*52.5*
32.5	*36.8*	*31.1*
62.1	*85.8*	*58.6*
90.8	*134.8*	*86.0*
135.5	*232.9*	*140.9*
200.4	*331.0*	*195.9*

The maximum error in determining τ_{max} for peats is approx. 5 kPa.

Organic silt

Figure 7.17 shows normalized diagrams for organic silt tested at stresses 54, 73 and 108 kPa. The slope k_{t1}^* is 1.00, whereas k_{t2}^* is 0.14.

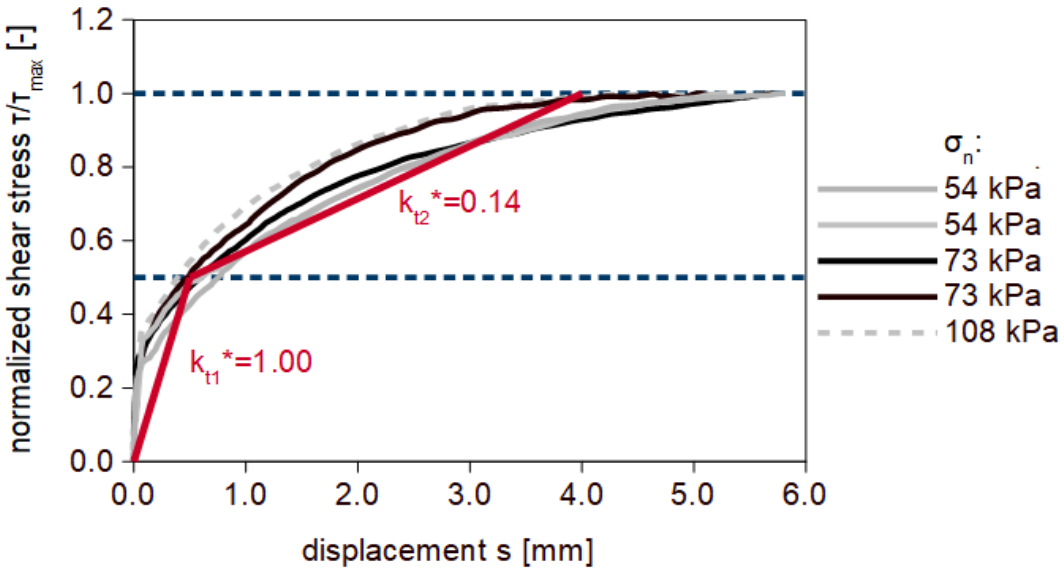

Figure 7.17. Normalized shear stress vs. displacement – Organic silt (OH) samples on rough concrete

From Figure 7.18 the following relation (Eq. 7.14) was obtained for organic silt, with a coefficient of determination equal to 0.962. In this case the inclination of the failure envelope is also similar to that of smooth concrete, which is 0.61.

$$\tau_{max} = 0.681 \cdot \sigma_n + 10.598 \tag{7.14}$$

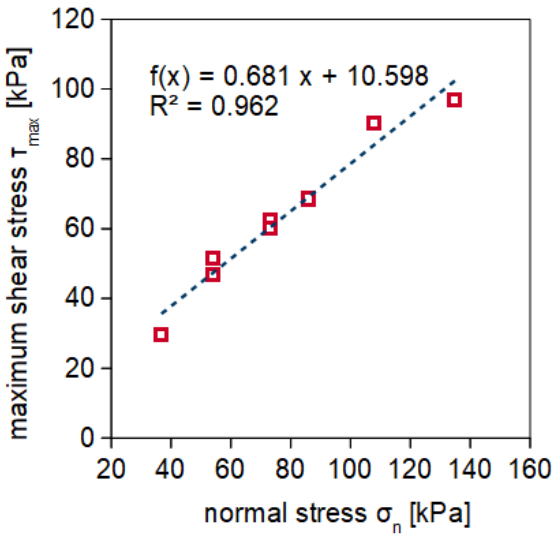

Figure 7.18. Maximum shear stress vs. normal stress – Organic silt (OH) samples on rough concrete

The results of maximum shear stress for organic silt samples are summarized in Table 7.8 below.

Table 7.8. Maximum shear stress values for organic silt.

τ_{max}	σ_n	τ_{max} *(Eq.7.14)*
[kPa]	*[kPa]*	*[kPa]*
46.8	*54.0*	*47.3*
51.6	*54.0*	*47.3*
62.6	*73.0*	*60.2*
60.2	*73.0*	*60.2*
90.2	*108.0*	*84.0*
29.7	*36.8*	*35.6*
68.5	*85.8*	*69.0*
96.7	*134.8*	*102.3*

The maximum error in determining τ_{max} is approx. 6 kPa.

Organic clay + Silt/Clay

The charts of organic clay and silt/clay have been again analyzed together because the shaft mobilization of for these soils is similar (Figure 7.19). The slope k_{t1}^{*} is 10.00, and k_{t2}^{*} is 0.14.

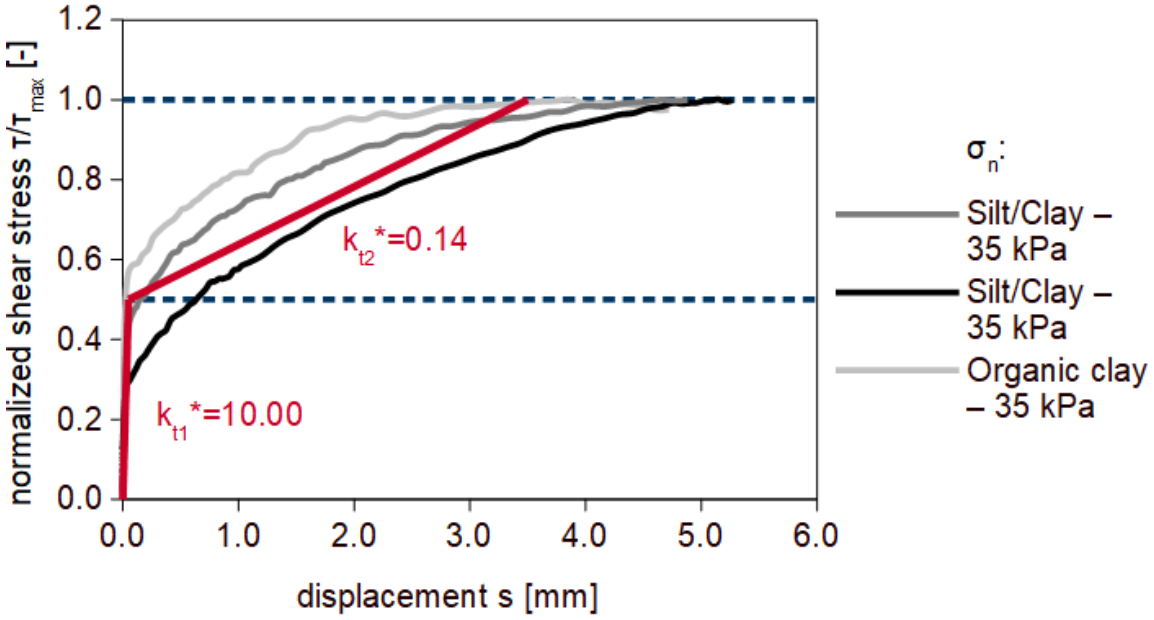

Figure 7.19. Normalized shear stress vs. displacement – Organic clay (OH) and Silt/Clay (ML/CL) samples on rough concrete

From Figure 7.20, the following relation (Eq. 7.15) was obtained for organic clay, with the coefficient of determination equal to 0.867:

$$\tau_{max} = 0.374 \cdot \sigma_n + 7.751 \tag{7.15}$$

while from Figure 7.21 the relation for silt/clay (eq. 7.16) was obtained with the coefficient of determination equal to 0.953:

$$\tau_{max} = 0.605 \cdot \sigma_n - 0.178 \tag{7.16}$$

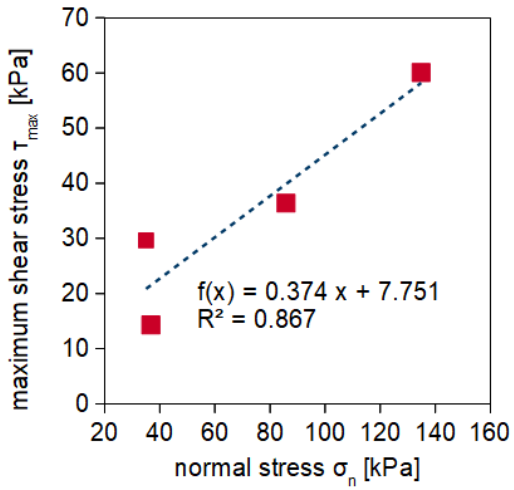

Figure 7.20. Maximum shear stress vs. normal stress – Organic clay (OH) samples on rough concrete

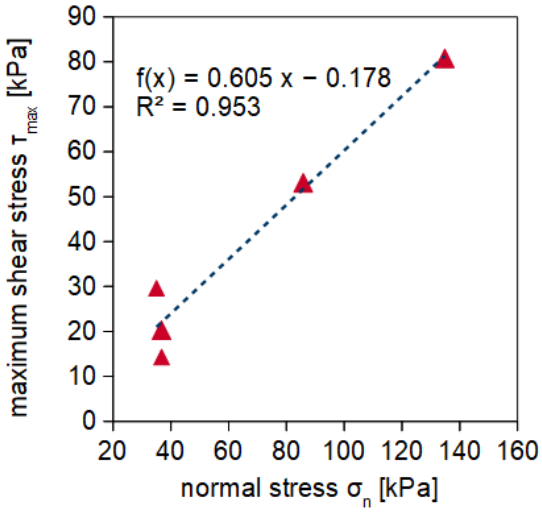

Figure 7.21.. Maximum shear stress vs. normal stress – Silt/Clay (ML/CL) samples on rough concrete

Table 7.9 below shows the results of maximum shear stress obtained directly from the direct shear test and using Equations 7.15 and 7.16.

Table 7.9. Maximum shear stress values for organic clay and silt/clay.

	τ_{max}	σ_n	τ_{max} *(Eq.7.15, 7.16)*
	[kPa]	*[kPa]*	*[kPa]*
Organic clay	*29.6*	*35.0*	*20.7*
	14.3	*36.8*	*21.4*
	36.4	*85.8*	*39.5*
	60.1	*134.8*	*57.6*
Silt/Clay	*29.6*	*35.0*	*20.8*
	14.3	*36.8*	*21.9*
	20.3	*36.8*	*21.9*
	53.1	*85.8*	*51.3*
	80.8	*134.8*	*80.7*

The maximum error in determining τ_{max} is approx. 9 kPa.

7.3.2 Granular soils

Medium dense sand

In Figure 7.22, graphs of medium-dense sand tested at stresses 49, 54 and 60 kPa are presented. The slope of the first part of the graph is 1.67 and of the second part is 0.29.

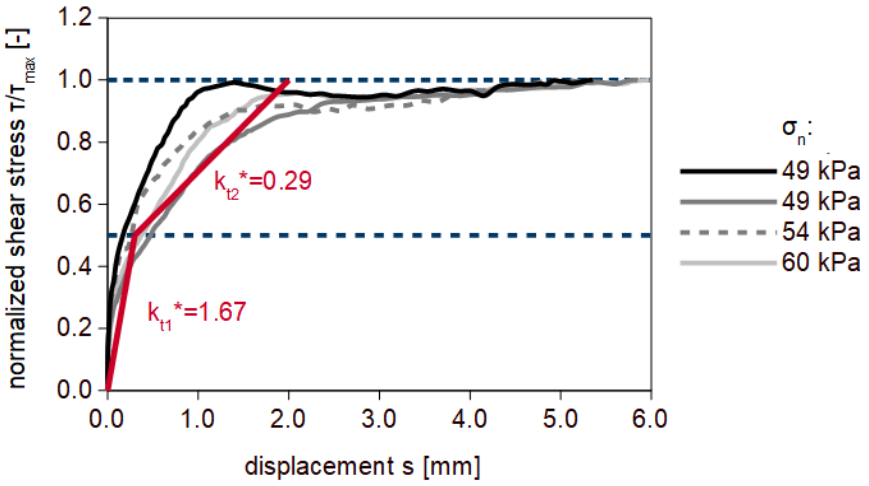

Figure 7.22. Normalized shear stress vs. displacement – Medium dense sand (SM) samples on rough concrete

From Figure 7.23 the following failure envelope (Eq. 7.17) was obtained for medium-dense sand, with the coefficient of determination equal to 0.990:

$$\tau_{max} = 0.720 \cdot \sigma_n + 0.658 \tag{7.17}$$

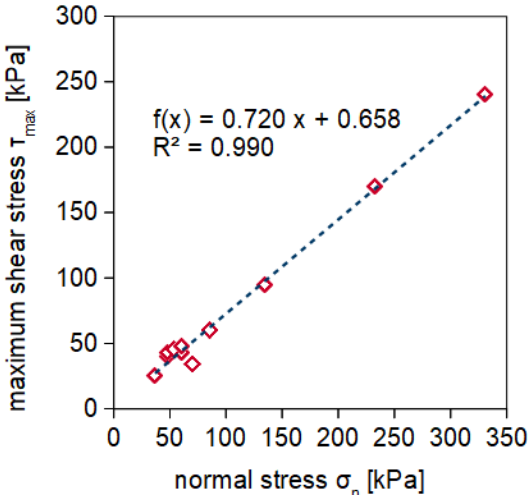

Figure 7.23. Maximum shear stress vs. normal stress – Medium dense sand (SM) samples on rough concrete

Table 7.10 below shows the results of maximum shear stress measured in interface shear box tests and calculated using Eq. 7.17.

Table 7.10. Maximum shear stress values for medium dense sand.

τ_{max}	σ_n	τ_{max} *(Eq.7.17)*
[kPa]	*[kPa]*	*[kPa]*
39.8	*48.0*	*35.2*
42.8	*48.0*	*35.2*
45.5	*54.0*	*39.5*
48.2	*60.0*	*43.9*
43.3	*60.0*	*43.9*
33.9	*70.0*	*51.1*
25.2	*36.8*	*27.1*
60.0	*85.8*	*62.4*
94.7	*134.8*	*97.7*
170.1	*232.9*	*168.3*
240.2	*331.0*	*239.0*

The maximum error in determining τ_{max} for medium dense sands is approx. 17 kPa.

Dense sand

In Figure 7.24, graphs for dense sand tested at stresses of 117, 131 and 144 kPa are presented. The slope of the first part of the graph is 2.00 and of the second part is 0.53.

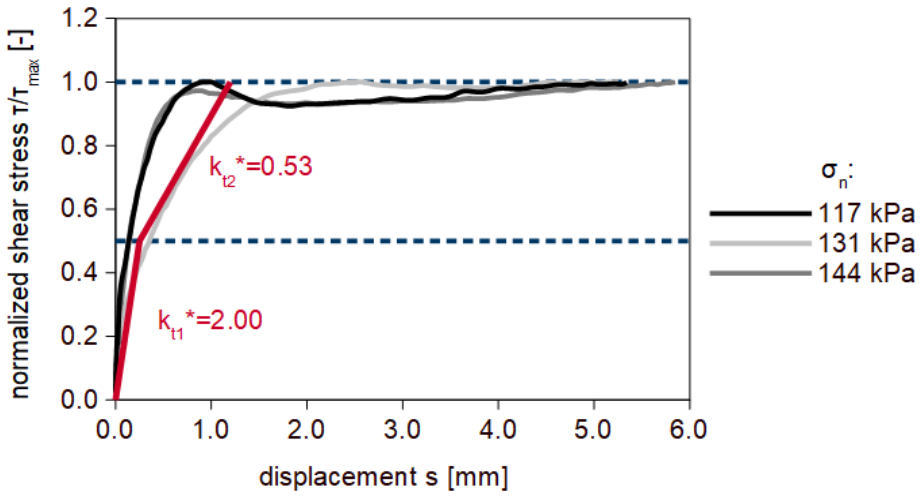

Figure 7.24. Normalized shear stress vs. displacement – Dense sand (SW) samples on rough concrete

The relation between τ_{max} and σ_n is presented in Figure 7.25. The failure envelope is described with Equation 7.18 with a coefficient of determination 0.995:

$$\tau_{max} = 0.689 \cdot \sigma_n \tag{7.18}$$

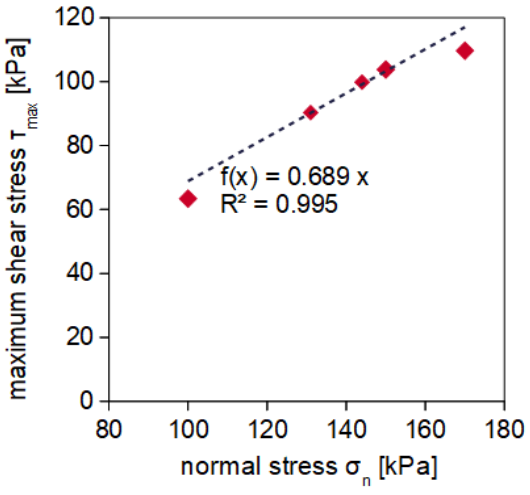

Figure 7.25. Maximum shear stress vs. normal stress – Dense sand (SW) samples on smooth concrete

Due to a bias created during testing, it was necessary to force the graph to pass through the origin. Table 7.11 below shows the results of maximum shear stress measured in interface shear box and calculated using eq. 7.15.

Table 7.11. Maximum shear stress values for dense sand.

τ_{max}	σ_n	τ_{max} *(Eq.7.18)*
[kPa]	*[kPa]*	*[kPa]*
94.4	*117.0*	*80.6*
90.3	*131.0*	*90.3*
99.9	*144.0*	*99.2*
63.4	*100.0*	*68.9*
103.8	*150.0*	*103.4*
109.7	*170.0*	*117.1*

The maximum error in determining τ_{max} is approx. 14 kPa.

7.4 Construction of $k_t - M_{DMT}$ functions

After analyzing all graphs presented in this subsections 7.2 and 7.3, a summary of all data concerning smooth and rough interfaces was prepared. The columns of Tables 7.12. and 7.13 show the following data:

- depth ranges of soil layers;
- type of soil;
- average dilatometer modulus (as an average of eight probings performed before columns installation) and standard deviation of the measurement (see Chapter 4);
- horizontal stress acting in the middle of a given soil layer in-situ before columns installation (see Chapter 4);
- coefficients k_{t1}^* and k_{t2}^*;
- τ_{max} calculated for a given normal stress σ_n (AVG) using equations 7.7-7.18;
- coefficients k_{t1} and k_{t2} calculated with equations 7.3 and 7.6.

Table 7.12. Summary of slopes k_{t1} and k_{t2} obtained for particular soils tested on smooth concrete

Depth of soil layer [m]		Soil type	M_{DMT} AVG	M_{DMT} SD	σ_n AVG	k_{t1}*	k_{t2}*	τ_{max}	k_{t1}	k_{t2}
top	bottom		[kPa]	[kPa]	[kPa]	[-]	[-]	[kPa]	[-]	[-]
0.00	0.70	SM	90056	13451	18.0	-	-	-	-	-
0.70	1.80	ML/CL	15556	4063	36.0	10.00	0.44	19.28	192.80	8.39
1.80	2.70	OH	5960	1903	34.0	10.00	0.44	15.05	150.50	6.55
2.70	4.05	Pt/OH	2290	589	33.5	3.57	0.52	20.52	73.26	10.67
4.05	5.55	SM	67857	14995	53.5	2.50	0.39	28.48	71.19	10.96
5.55	7.05	SM	31791	10416	59.0	2.50	0.39	31.50	78.75	12.13
7.05	7.80	OL	-	-	35.0	-	-	-	-	-
7.80	10.20	OH	1541	304	48.0	1.67	0.42	32.50	54.28	13.55
10.20	10.45	SM	17819	0	47.5	2.50	0.39	25.18	62.94	9.69
10.45	12.15	OH	2100	605	54.0	1.67	0.42	36.16	60.39	15.08
12.15	12.95	Pt	7667	1110	92.5	3.57	0.52	50.02	178.57	26.01
12.95	14.45	Pt/OH	3757	1182	73.0	1.67	0.42	47.75	79.74	19.91
14.45	15.70	SW	140054	31990	117.0	5.00	1.00	62.01	310.05	62.01
15.70	15.95	OH	5688	1614	108.0	1.67	0.42	69.10	115.40	28.81
15.95	17.50	SW	137412	16990	131.0	5.00	1.00	69.43	347.15	69.43
17.50	19.00	SW	148054	14692	144.0	5.00	1.00	76.32	381.60	76.32

Then, on the basis of the above data, the relations between coefficients k_{t1} and k_{t2}, and the dilatometer modulus M_{DMT} are presented in Figures 7.26 and 7.27, respectively.

For fine grained soils, the relation to the k_{t1} coefficient is very satisfactory with the coefficient of determination of 0.9353. In case of slope k_{t2}, the points corresponding to clayey soils do not match the trend. The relationship between k_{t2} and M_{DMT} was based in this case only on the results for peat and organic silt, obtaining a coefficient of determination 0.7476.

In case of non-cohesive soils, both dependencies between coefficients k_{t1} and k_{t2}, and the dilatometer modulus M_{DMT} are satisfactory with high coefficient of determination .

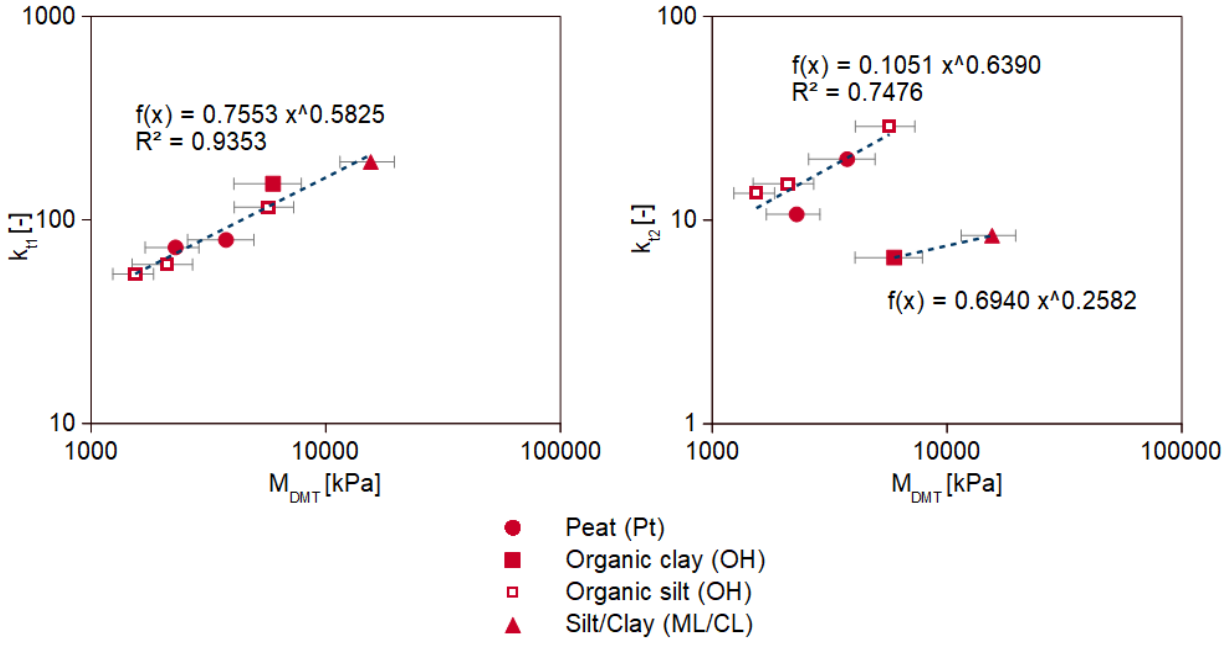

Figure 7.26. Relationship between coefficients k_{t1} and k_{t2} and dilatometer modulus M_{DMT} for fine soils on smooth concrete.

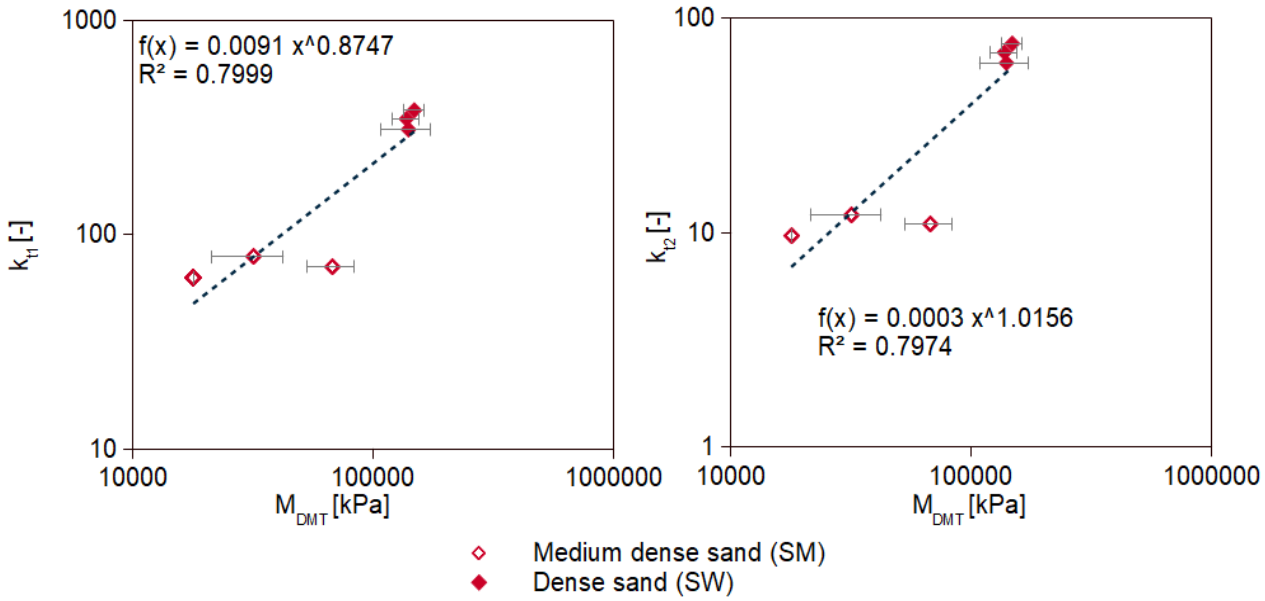

Figure 7.27. Relationship between coefficients k_{t1} and k_{t2} and dilatometer modulus M_{DMT} for non-cohesive soils on smooth concrete.

The results of analysis on rough concrete for all soil layers are summarized in Table 7.13.

Table 7.13. Summary of slopes k_{t1} and k_{t2} obtained for particular soils tested on rough concrete

Depth of soil layer [m]		Soil type	M_{DMT} AVG	M_{DMT} SD	σ_n AVG	k_{t1}*	k_{t2}*	τ_{max}	k_{t1}	k_{t2}
top	bottom		[kPa]	[kPa	[kPa]	[-]	[-]	[kPa]	[-]	[-]
0.00	0.70	SM	90056	13451	18.0	-	-	-	-	-
0.70	1.80	ML/CL	15556	4063	36.0	10.0	0.17	21.42	214.20	3.64
1.80	2.70	OH	5960	1903	34.0	10.0	0.17	20.33	203.30	3.46
2.70	4.05	Pt/OH	2290	589	33.5	0.5	0.20	29.27	14.64	5.85
4.05	5.55	SM	67857	14995	53.5	1.7	0.29	39.18	65.43	11.36
5.55	7.05	SM	31791	10416	59.0	1.7	0.29	43.14	72.04	12.51
7.05	7.80	OL	-	-	35.0					
7.80	10.20	OH	1541	304	48.0	1.0	0.14	43.24	43.24	6.18
10.20	10.45	SM	17819	0	47.5	1.7	0.29	34.86	58.22	10.11
10.45	12.15	OH	2100	605	54.0	1.0	0.14	47.32	47.32	6.76
12.15	12.95	Pt	7667	1110	92.5	0.5	0.20	62.31	31.16	12.46
12.95	14.45	Pt/OH	3757	1182	73.0	1.0	0.14	60.24	60.24	8.61
14.45	15.70	SW	140054	31990	117.0	2.0	0.53	80.73	161.46	42.79
15.70	15.95	OH	5688	1614	108.0	1.0	0.14	84.04	84.04	12.01
15.95	17.50	SW	137412	16990	131.0	2.0	0.53	90.39	180.78	47.91
17.50	19.00	SW	148054	14692	144.0	2.0	0.53	99.36	198.72	52.66

On the basis of the above data, the relations between coefficients k_{t1}, k_{t2} and the dilatometer modulus M_{DMT} for rough concrete interface, presented in Figures 7.28 and 7.29, were determined.

For cohesive soils, the relation to the k_{t1} coefficient is satisfactory with the coefficient of determination 0. 6526 whereas in case of k_{t2} only dependence based on organic silt and peat was used, which gives quite high coefficient of determination, over 0.87. The data for organic clay and silt/clay give practically the same results.

In case of non-cohesive soils, both dependencies are satisfactory, with high coefficient of determination 0.80 as in case of dependencies for smooth concrete interface.

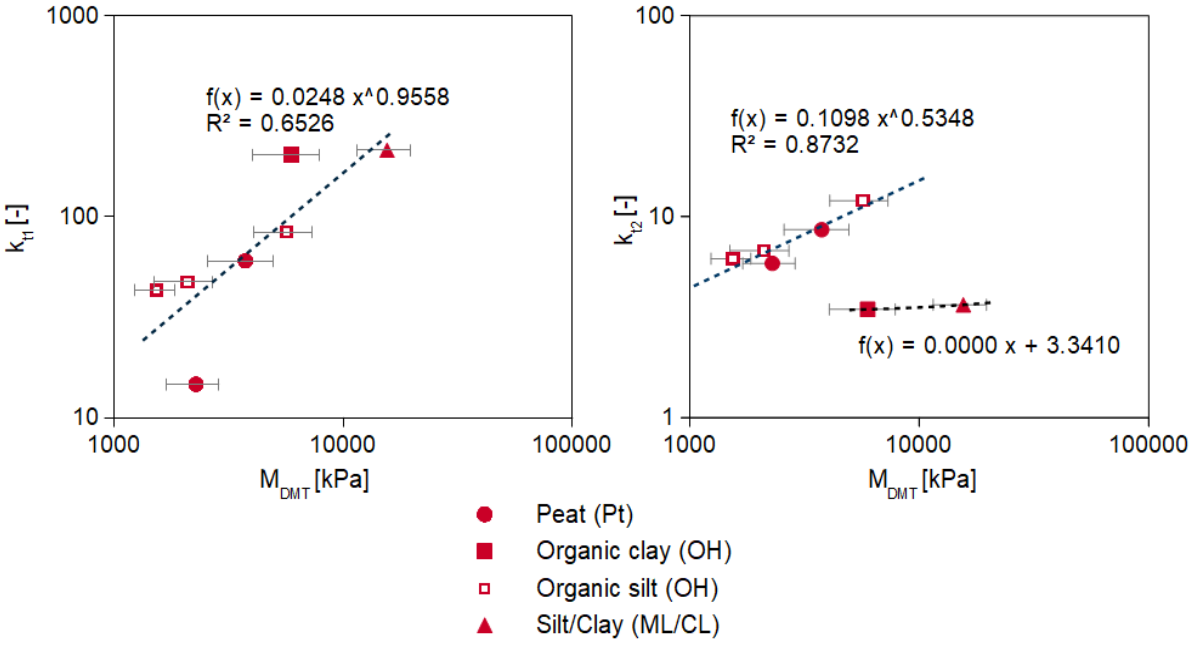

Fig. 7.28. Relationship between coefficients k_{t1} and k_{t2} and dilatometer modulus M_{DMT} for fine grained soils on rough concrete.

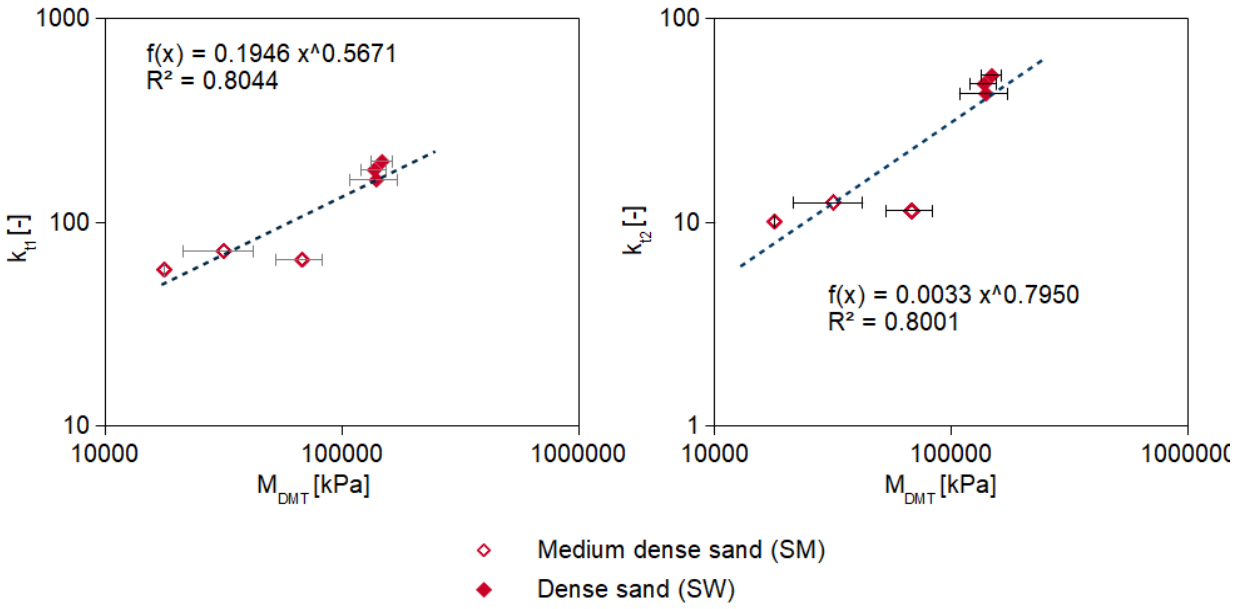

Figure 7.29. Relationship between coefficients k_{t1} and k_{t2} and dilatometer modulus M_{DMT} for non-cohesive soils on rough concrete.

All relations, for both cohesive and cohesionless soils, smooth and rough interfaces are described with power functions (Table 7.14). The equations are analogous for both interfaces.

Table 7.14. Comparison of the relationships between the slope of the t-z curve and the DMT modulus.

	Fine grained soils		*Granular soils*	
Smooth concrete	$k_{t1} = 0.7553 \cdot (M_{DMT})^{0.5825}$	*(7.19)*	$k_{t1} = 0.0091 \cdot (M_{DMT})^{0.8747}$	*(7.21)*
	$k_{t2} = 0.1051 \cdot (M_{DMT})^{0.6390}$	*(7.20)*	$k_{t2} = 0.0003 \cdot (M_{DMT})^{1.0156}$	*(7.22)*
Rough concrete	$k_{t1} = 0.0248 \cdot (M_{DMT})^{0.9558}$	*(7.23)*	$k_{t1} = 0.1946 \cdot (M_{DMT})^{0.5671}$	*(7.25)*
	$k_{t2} = 0.1098 \cdot (M_{DMT})^{0.5348}$	*(7.24)*	$k_{t2} = 0.0033 \cdot (M_{DMT})^{0.7950}$	*(7.26)*

7.5 Relation between t_{max} and DMT soundings parameters

To construct the t-z function (Fig. 7.2) the maximum shear stress at the interface in the particular soil layer have to be known. In order to enable the estimation of t_{max} for soils at different depths, at different levels of horizontal stress (without the necessity to perform tests in the direct shear apparatus each time), the relations between the already calculated t_{max} values for smooth and rough concrete (see Table 7.12 and 7.13) and the parameters measured directly in DMT probing were established.

The relations between t_{max} and different DMT sounding parameters were evaluated ($p_0, p_1, I_D, E_D, K_D, \sigma'_n, M_{DMT}$). The most promising relation was obtained for p_0 (the pressure applied to the soil at the start of the expansion). From theoretical point of view it is quite inconvenient. p_0 reflects initial horizontal stresses in the soil. For analyzed case, the horizontal stresses in soft soil before and after installations are quite the same. For sands, they are not. This is the disadvantage of using DMT determination of t_{max}. However, the aim of this thesis is to design pile based entirely on DMT soundings before pile installation. Consequently, for preliminary character of DMT method, the $t_{max} - p_0$

characteristics will be used for further evaluation.

The relations between the maximum shear stress τ_{max} obtained from the transfer functions (Eq. 7.7-7.18) and the pressure applied to the soil at the start of the expansion of the DMT membrane p_0 has been developed. The p_0 was measured and averaged in the given soil layers from all dilatometer probings made before the installation of piles. These values are presented in Table 7.15.

Table 7.15. Summary of p_0 and t_{max} values for particular soils

Depth of soil layer [m]		Soil type	p_0	t_{max}	
				smooth concrete	rough concrete
top	bottom		[kPa]	[kPa	[kPa]
0.00	0.70	SM	-	-	-
0.70	1.80	ML/CL	228	19.28	21.42
1.80	2.70	OH	151	15.05	20.33
2.70	4.05	Pt/OH	145	20.52	29.27
4.05	5.55	SM	324	34.72	39.18
5.55	7.05	SM	244	38.79	43.14
7.05	7.80	OL	-	-	-
7.80	10.20	OH	254	32.5	43.24
10.20	10.45	SM	260	30.28	34.86
10.45	12.15	OH	295	36.16	47.32
12.15	12.95	Pt	500	50.02	62.31
12.95	14.45	Pt/OH	372	47.75	60.24
14.45	15.70	SW	966	62.01	80.73
15.70	15.95	OH	407	69.10	84.04
15.95	17.50	SW	960	69.43	90.39
17.50	19.00	SW	1013	76.32	99.36

The relationships between p_o and τ_{max} for smooth and rough concrete interfaces are shown in Figures 7.30 and 7.31 respectively. These correlations are common to all soils presented in this research on the analyzed testing site.

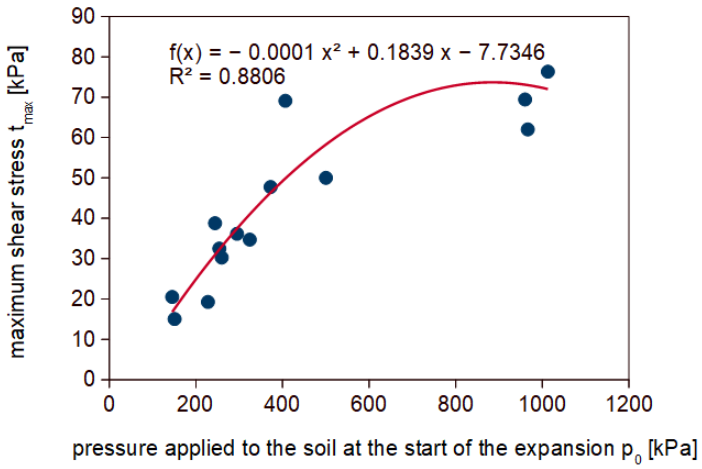

Figure 7.30. Relationship between p_0 and t_{max} for smooth interface

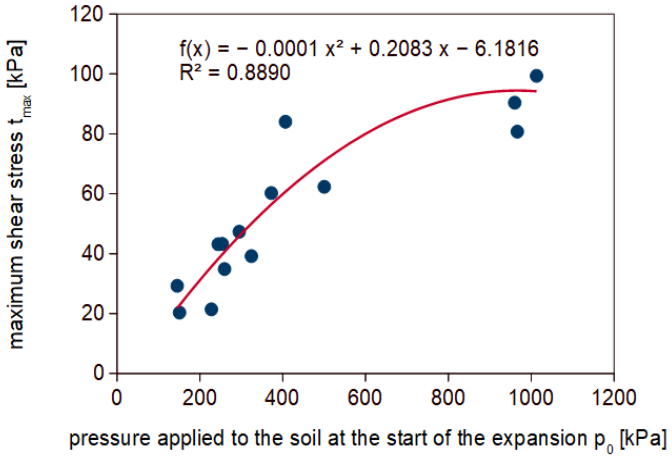

Figure 7.31. Relationship between p_0 and t_{max} for rough interface

7.6 Transfer curves for backward shearing

As a supplementary analysis, the results for the reverse shearing were also developed in a similar way. However, this is not the main purpose of this PhD thesis, and therefore only the final correlations between the parameters k_{t1} and k_{t2} and M_{DMT} are presented (Fig. 7.32 -7.35)

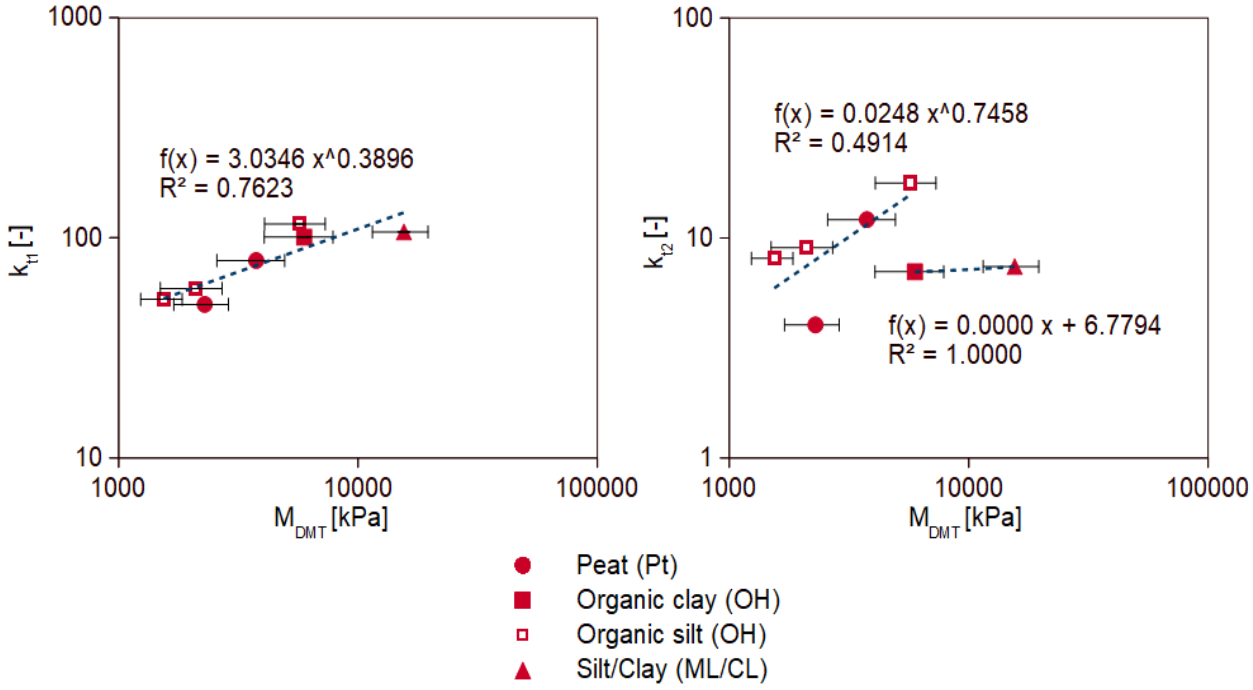

Figure 7.32. Relationship between coefficients k_{t1} and k_{t2} and dilatometer modulus M_{DMT} for fine grained soils on smooth concrete.

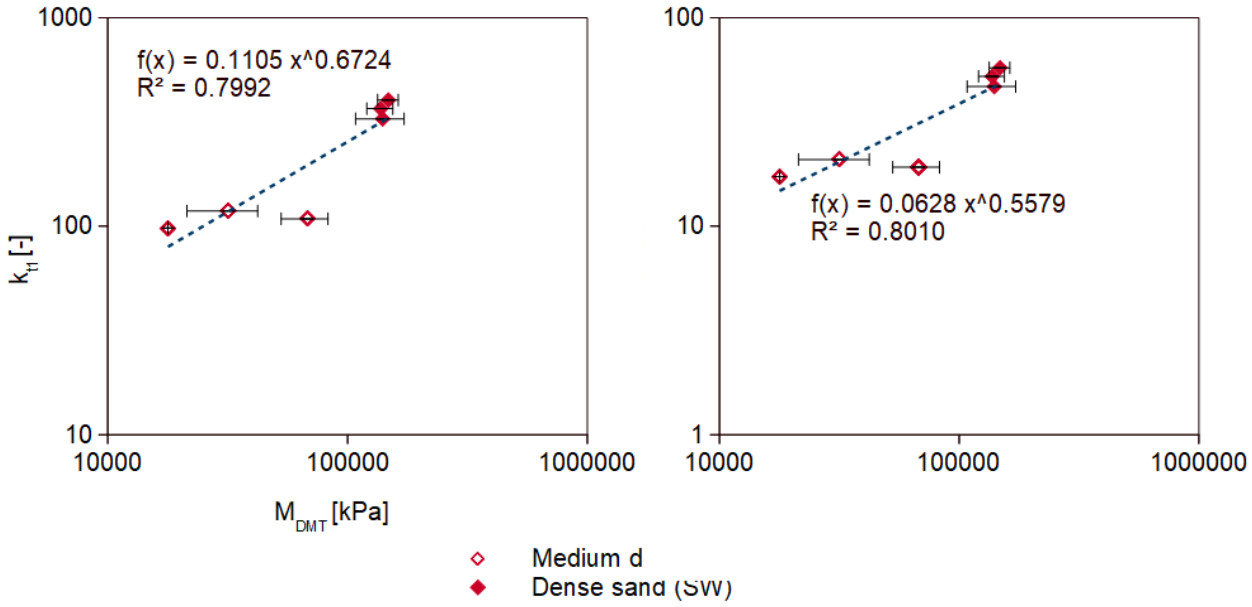

Figure 7.33. Relationship between coefficients k_{t1} and k_{t2} and dilatometer modulus M_{DMT} for non-cohesive soils on smooth concrete.

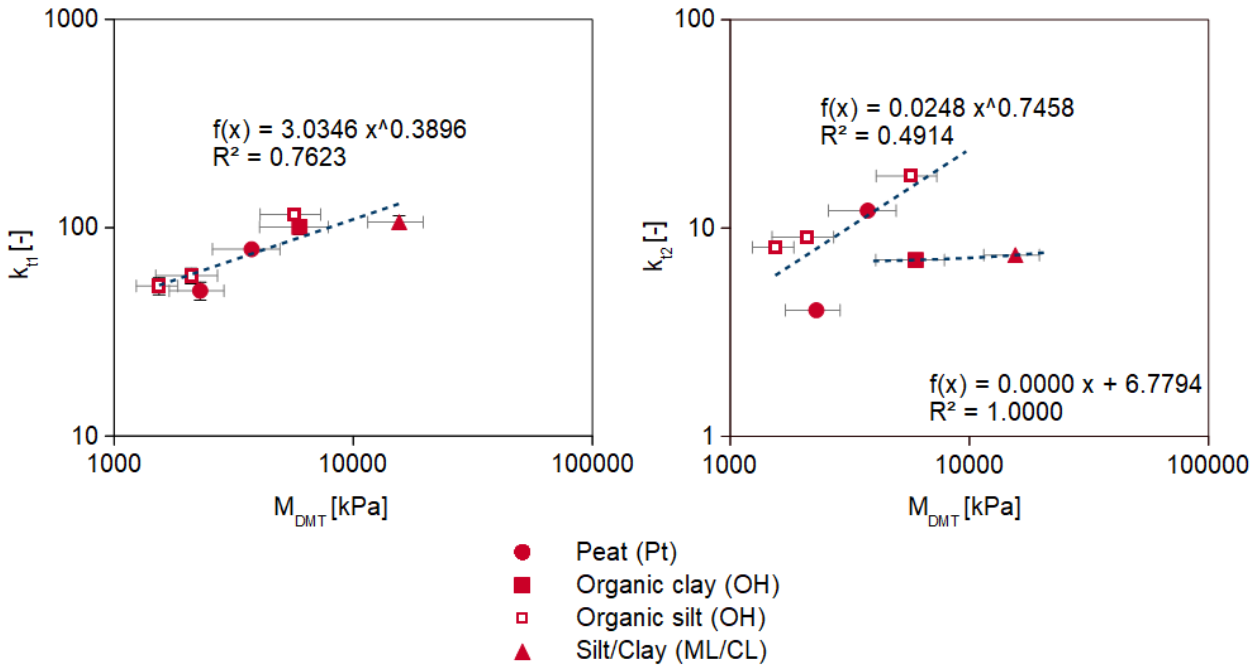

Figure 7.34. Relationship between coefficients k_{t1} and k_{t2} and dilatometer modulus M_{DMT} for fine grained soils on rough concrete.

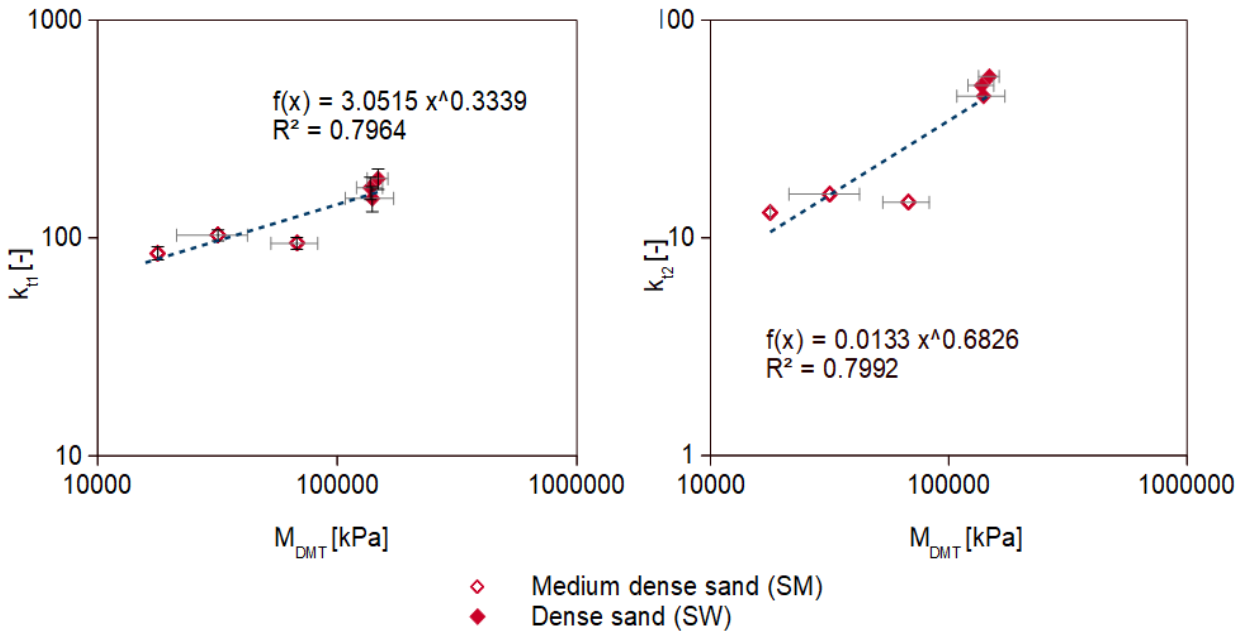

Figure 7.35. Relationship between coefficients k_{t1} and k_{t2} and dilatometer modulus M_{DMT} for non-cohesive soils on rough concrete.

Again all relations, are described with power functions (Table 7.16) and the resulting equations are similar to those from forward shearing.

Table 7.16. Comparison of the relationships between the slope of the t-z curve and the DMT modulus for reverse shearing

	Fine grained soils		*Granular soils*	
Smooth concrete	$k_{t1} = 3.0346 \cdot (M_{DMT})^{0.3896}$	(7.27)	$k_{t1} = 0.1105 \cdot (M_{DMT})^{0.6724}$	(7.29)
	$k_{t2} = 0.0248 \cdot (M_{DMT})^{0.7458}$	(7.28)	$k_{t2} = 0.0628 \cdot (M_{DMT})^{0.5579}$	(7.30)
Rough concrete	$k_{t1} = 3.0346 \cdot (M_{DMT})^{0.3896}$	(7.31)	$k_{t1} = 3.0515 \cdot (M_{DMT})^{0.3339}$	(7.33)
	$k_{t2} = 0.0248 \cdot (M_{DMT})^{0.7458}$	(7.32)	$k_{t2} = 0.0133 \cdot (M_{DMT})^{0.6826}$	(7.34)

In the case of tests on smooth concrete, for most of soil, higher values of the slope k_{t1} for backward shearing can be observed, while values of k_{t2} are then lower. For rough concrete, both k_{t1} and k_{t2} have higher values for backward shearing.

The relations between the maximum shear stress τ_{max} obtained from the transfer functions and parameter p_0 measured in dilatometer probing in given soil layers and averaged from all probings made before the pile installation, were again developed. These relationships for smooth and rough concrete are presented in Figures 7.36 and 7.37 respectively.

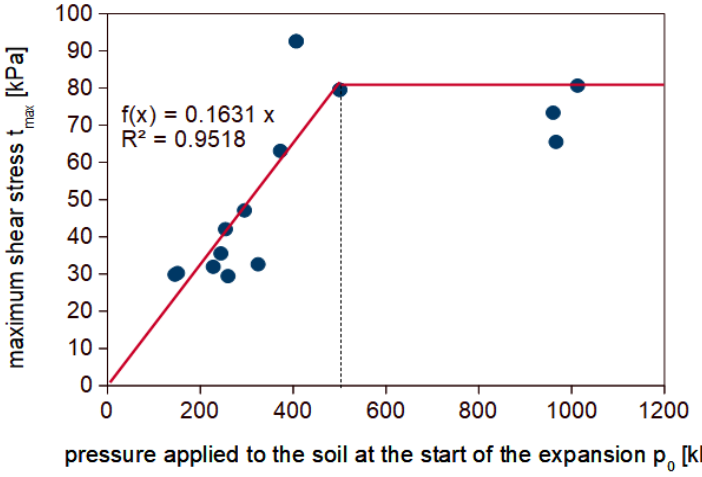

Figure 7.36. Relationship between p_0 and t_{max} from reverse shearing for smooth concrete

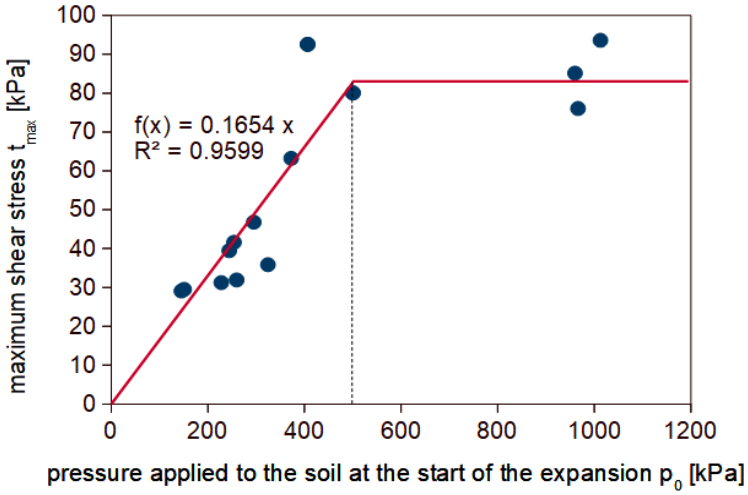

Figure 7.37. Relationship between p_0 and t_{max} from reverse shearing for rough concrete

Chapter 8
Verification of the proposed method

In order to verify the method presented in Chapter 7, the results of tests that have been carried out on the testing field in Jazowa, were used (see Chapter 5). The results of dilatometer probings prior to the installation of piles and the results of static test loads were used.

Out of 27 tested columns, 8 were used for verification. Those 8 piles underwent significant displacement during the test loads (see Chapter 5). The remaining columns exhibits 2 mm displacements, which gives an incomplete picture of the column load-settlement characteristics.

A dilatometer test performed closest to the column axis was assigned to each column under analysis. The piling plan with investigated columns and DMT tests selected for analysis is shown in Fig. 8.1. The characteristics of the selected columns are shown in Table 8.1.

Table 8.1. Characteristics of the analyzed columns

Testing site	*Column number*	*Column designation*	*Column length*	*The nearest DMT sounding*		*Maximum displacement from the SLT*
[-]	*[-]*	*[-]*	*[m]*	*Testing site*	*Column*	*[mm]*
5	*10*	*S5C10*	*8.0*	*5*	*10*	*13.62*
5	*13*	*S5C13*	*11.0*	*5*	*10*	*32.44*
4	*8*	*S4C8*	*11.0*	*4*	*8*	*11.78*
5	*9*	*S5C9*	*11.0*	*5*	*10*	*7.14*
4	*3*	*S4C3*	*14.6*	*4*	*3*	*5.26*
4	*4*	*S4C4*	*14.6*	*4*	*3*	*10.94*
5	*8*	*S5C8*	*14.6*	*2*	*23*	*8.04*
5	*3*	*S5C3*	*15.5*	*5*	*4*	*6.44*

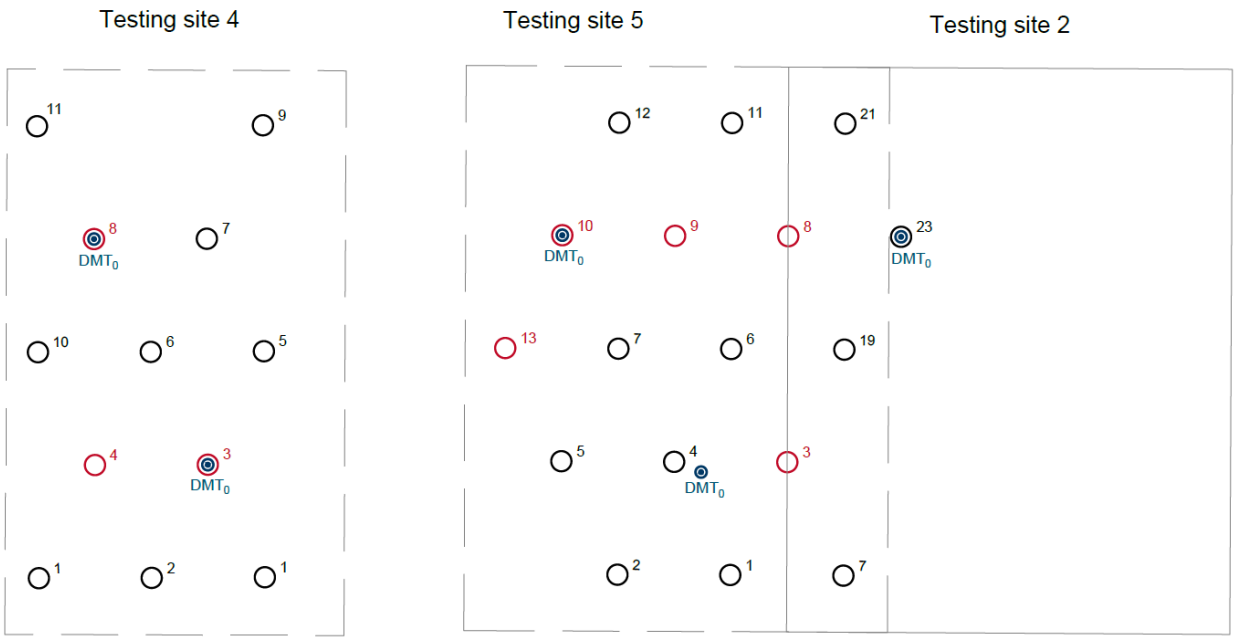

Figure. 8.1. Distribution of the analyzed columns and DMT probings

8.1 Calculation method

The calculations were performed in spreadsheet. In order to verify the proposed method, dilatometer probing results were used. Using the parameters measured directly in the dilatometer probings, in accordance with the formulas presented in Chapter 4, the following parameters were determined:

- E_D – dilatometer modulus;
- I_D – material index;
- K_D – horizontal stress index.

Using the above parameters, vertical drained constrained modulus M_{DMT} was determined using Equation 4.5.

In order to determine the maximum pile skin friction at the interface τ_{max} in each soil layer, the dependencies using parameter p_0 from dilatometer soundings were used (Fig. 7.30-7.31).

Then, using functions 7.16-7.23, the values of slopes k_{t1} and k_{t2} for fine grained and granular soils, were determined.

Knowing the values of k_{t1} and k_{t2} and τ_{max}, the values of s_1 and s_2 displacements (see Fig. 7.2), at which the slope changes, were determined. In this way, for each depth of DMT sounding (i.e. every 0.20 m) the transformation curve can be determined.

The t-z curves show the full mobilization of the pile shaft resistance depending on the current displacement. In order to estimate the bearing capacity of the pile, it is necessary to know the displacements of the pile at particular depths when applying successive load steps.

The simplified assumption of linear extension of pile due to applied tension load was considered in the analysis (Fig.8.2). The following assumptions were made in the calculation of proper deformation of pile due to tension load:

- the pile has the same shape and diameter (section) with depth;
- the concrete is homogeneous and its modulus is the same with depth;

— the tension force is decreasing linearly with depth; there is no tension at the pile base.

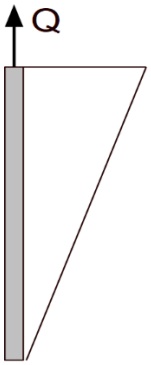

Figure 8.2. Simplified assumption of linear decrease of the tension force with depth in the calculation of pile extension

Using the above assumptions, of head displacement and linear distribution of friction, the next steps in the calculation are:

— displacement s in the middle of each calculation layer was estimated for a certain load step;
— the values of unit skin friction τ, corresponding to the designated displacement, was obtained from the transfer curves;
— pile skin friction multiplied by the area of the shaft A in a given layer returns the load capacity F of a given pile section.

Repeating the above steps consecutively along the whole length of the pile, the total capacity of the pile shaft of a given length was calculated.

Based on the results of DMT soundings presented in Chapter 4, it can be seen that the values of the M_{DMT} modulus for fine grained soils do not exceed 15 000 kPa. Due to that, it was assumed that transfer functions for cohesive soils will be applied when $M_{DMT} < 15\,000\ kPa$. In other cases, functions for granular soils is used.

Below, table 8.2 presents an example of the calculations of column S5C10 with a length of 8 m for the head displacement of 4 mm and rough concrete interface.

The calculations presented in this chapter were carried out separately using the functions for smooth and rough concrete (Chapter 7) and according to the column type: floating columns and columns with base resting on the bearing layer.

Table 8.2. Calculations for column S5C10

Depth	p_0	E_D	I_D	K_D	$R_{M.0}$	R_M	M_{DMT}	s	τ_{max}	k_{t1}	k_{t2}	s_1	s_2	τ	A	F
[m]	[kPa]	[MPa]	[-]	[-]	[-]	[-]	[kPa]	[mm]	[kPa]	[-]	[-]	[mm]	[mm]	[kPa]	[m^2]	[kN]
0.3	27	32.7	34.93	5.3	5.29	1.95	63718	3.85	23.7	969	41	0.012	0.304	23.7	0.4	9.0
0.5	474	58.8	3.58	40.3	0.59	3.82	224590	3.75	56.5	3231	80	0.009	0.362	56.5	0.3	14.2
0.7	474	58.8	3.58	40.3	0.59	3.82	224590	3.65	56.5	3231	80	0.009	0.362	56.5	0.3	14.2
0.9	211	61	8.33	13.5	1.30	2.78	169832	3.55	37.2	2473	69	0.008	0.278	37.2	0.3	9.4
1.1	148	63.2	12.29	7.6	1.89	2.26	142935	3.45	32.6	2098	63	0.008	0.268	32.6	0.3	8.2
1.3	185	7.1	1.11	8	0.22	2.28	16179	3.35	35.3	261	20	0.068	0.970	35.3	0.3	8.9
1.5	107	12.9	3.48	4	0.57	1.70	21983	3.25	29.6	350	23	0.042	0.684	29.6	0.3	7.4
1.7	156	6.4	1.18	5.2	0.23	1.85	11869	3.15	33.2	194	17	0.085	1.087	33.2	0.3	8.3
1.9	158	4.9	0.91	5	0.19	1.80	8837	3.05	33.3	147	14	0.114	1.291	33.3	0.3	8.4
2.1	187	5.6	0.89	5.6	0.18	1.92	10733	2.95	35.5	177	16	0.100	1.229	35.5	0.3	8.9
2.3	216	6.7	0.93	6.2	0.19	2.02	13536	2.85	37.6	220	18	0.085	1.142	37.6	0.3	9.4
2.5	141	2.7	0.59	3.8	0.14	1.51	4072	2.75	32.1	70	9	0.229	1.945	32.1	0.3	8.1
2.7	217	6	0.84	5.7	0.18	1.93	11596	2.65	37.7	190	16	0.099	1.249	30.9	0.3	7.8
2.9	141	3.1	0.69	3.4	0.15	1.40	4342	2.55	32.1	74	10	0.216	1.873	32.1	0.3	8.1
3.1	161	2.7	0.53	3.8	0.13	1.51	4072	2.45	24.8	70	9	0.177	1.500	24.8	0.3	6.2
3.3	172	2.4	0.44	3.9	0.12	1.53	3684	2.35	26.7	64	9	0.210	1.715	26.7	0.3	6.7
3.5	162	2.4	0.47	3.5	0.12	1.42	3418	2.25	24.9	59	9	0.211	1.674	24.9	0.3	6.3
3.7	192	2.4	0.40	4	0.11	1.56	3746	2.15	30.1	65	9	0.233	1.917	30.1	0.3	7.6
3.9	182	2.4	0.43	3.7	0.11	1.48	3554	2.05	28.4	61	9	0.231	1.864	28.4	0.3	7.1

Depth	p_0	E_D	I_D	K_D	$R_{M.0}$	R_M	M_{DMT}	s	τ_{max}	k_{t1}	k_{t2}	s_1	s_2	τ	A	F
[m]	[kPa]	[MPa]	[-]	[-]	[-]	[-]	[kPa]	[mm]	[kPa]	[-]	[-]	[mm]	[mm]	[kPa]	[m²]	[kN]
4.1	101	10.0	3.72	1.7	0.61	0.96	9609	1.95	13.8	159	15	0.044	0.511	13.8	0.3	3.5
4.3	164	22.8	4.75	3	0.76	1.45	33157	1.85	25.3	71	13	0.177	1.154	25.3	0.3	6.4
4.5	552	38.8	2.13	11	0.37	2.59	100501	1.75	78.3	134	31	0.293	1.545	78.3	0.3	19.7
4.7	563	45.4	2.45	10.7	0.42	2.56	116408	1.65	79.4	145	35	0.273	1.403	79.4	0.3	20.0
4.9	536	35.9	2.05	9.7	0.36	2.47	88733	1.55	76.7	125	28	0.308	1.663	73.5	0.3	18.5
5.1	240	25.3	3.53	3.8	0.58	1.66	41987	1.45	38.1	81	16	0.234	1.451	38.0	0.3	9.6
5.3	314	22.8	2.36	5	0.40	1.87	42614	1.35	49.4	82	16	0.300	1.861	41.3	0.3	10.4
5.5	314	22.8	2.37	4.8	0.41	1.83	41778	1.25	49.4	81	16	0.304	1.890	39.4	0.3	9.9
5.7	293	23.5	2.67	4.3	0.45	1.75	41097	1.15	46.3	80	15	0.287	1.793	36.4	0.3	9.1
5.9	393	23.5	1.93	5.8	0.34	1.99	46739	1.05	60.2	87	17	0.348	2.118	42.1	0.3	10.6
6.1	229	18.8	2.91	3	0.49	1.45	27207	0.95	36.3	64	11	0.285	1.923	25.5	0.3	6.4
6.3	429	18.8	1.41	6	0.26	2.00	37664	0.85	64.8	77	14	0.423	2.682	38.5	0.3	9.7
6.5	356	21.3	1.99	4.7	0.35	1.79	38223	0.75	55.3	77	15	0.358	2.264	33.3	0.3	8.4
6.7	398	19.9	1.64	5.2	0.30	1.87	37294	0.65	60.9	76	14	0.400	2.540	34.0	0.3	8.5
6.9	303	16.2	1.86	3.6	0.33	1.54	24895	0.55	47.8	61	10	0.394	2.709	25.5	0.3	6.4
7.1	169	11.8	2.95	1.6	0.49	0.90	10647	0.45	26.2	175	16	0.075	0.911	19.0	0.3	4.8
7.3	205	14.4	2.76	2.1	0.46	1.12	16129	0.35	32.3	261	20	0.062	0.889	21.8	0.3	5.5
7.5	197	5.6	1.16	1.9	0.22	0.86	4807	0.25	31.0	82	10	0.189	1.703	16.1	0.3	4.0
7.7	201	3.1	0.63	1.9	0.14	0.85	2635	0.15	31.6	46	7	0.343	2.477	6.9	0.3	1.7
7.9	232	2.0	0.34	2.2	0.10	0.95	1896	0.05	36.8	34	6	0.546	3.502	1.7	0.3	0.4

8.2 Floating columns

Floating columns are those that have not reached the level of the bearing strata (Chapter 5). One column 8 m long and three 11 m long columns were used for the analysis. All characteristics of floating columns including, lengths, maximum loads and displacements, extrapolated bearing capacity are listed in Table 8.3.

Table 8.3. Characteristics of the floating columns

Column designation	*Column length*	*Maximum displacement from the SLT*	*Maximum load from the SLT*	*Bearing capacity from Chin's method*
[-]	*[m]*	*[mm]*	*[kN]*	*[kN]*
S5C10	*8*	*13.62*	*450*	*510*
S4C8	*11*	*11.78*	*600*	*748*
S5C13	*11*	*32.44*	*650*	*706*
S5C9	*11*	*7.14*	*600*	*699*

The dead weight of the column was estimated as 24.13 kN and 33.18 kN for column 8 and 11 m respectively, assuming a concrete volume weight of 24 kN/m^3. In addition, the buoyancy of water below the groundwater table (located at a depth of 1.7 m) was considered. For 8-meter column it was a force of about 7.77 kN, and for column 11 m, 11.46 kN.

The results of the static test load (tension load – head displacement curves) for analyzed floating columns are shown in Figure 8.3. This diagram also shows the theoretical curves and the maximum load capacity obtained with the Chin's method (see Chapter 5).

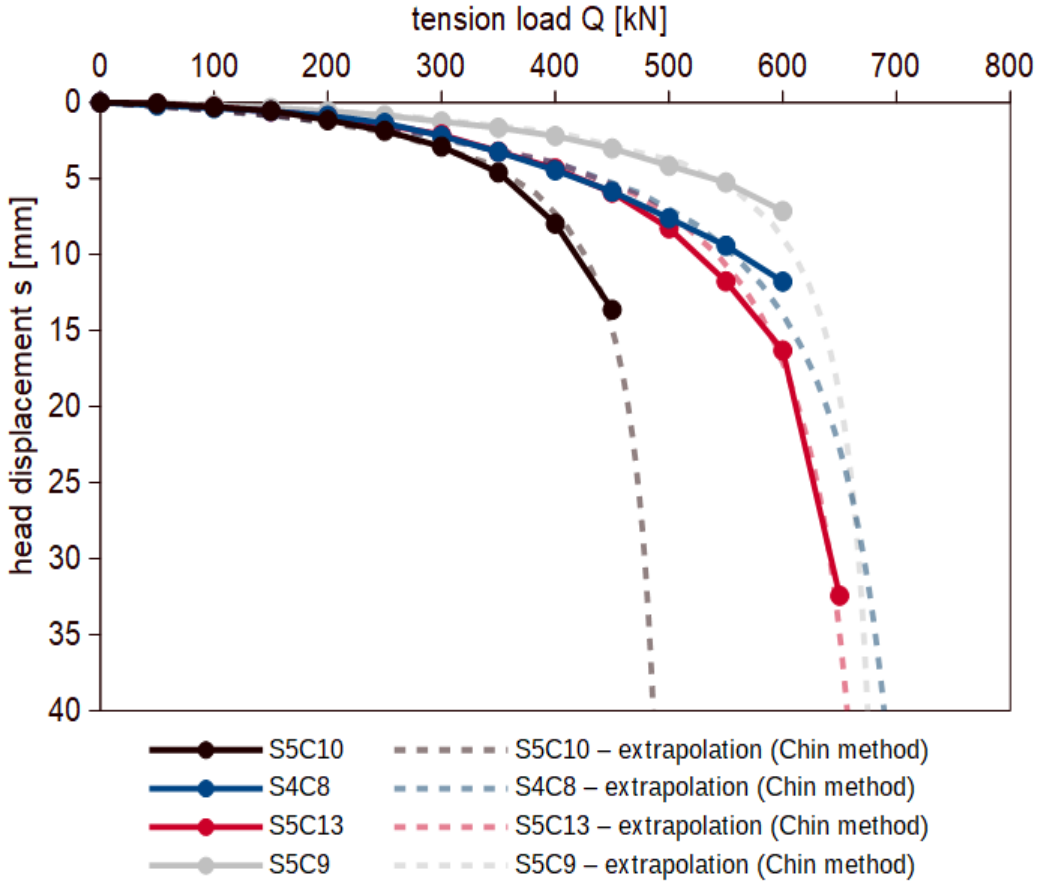

Figure 8.3. Tension load – head displacement curves and extrapolated load capacity of all floating columns

On the basis of the DMT probing results, performed in the axis of the column before its installation, the load capacity of columns was estimated using the algorithm set out in subsection 8.1. The pile's S5C10 capacity and calculated load-settlement curves obtained with the function for smooth and rough concrete are shown in the Figure. 8.4.

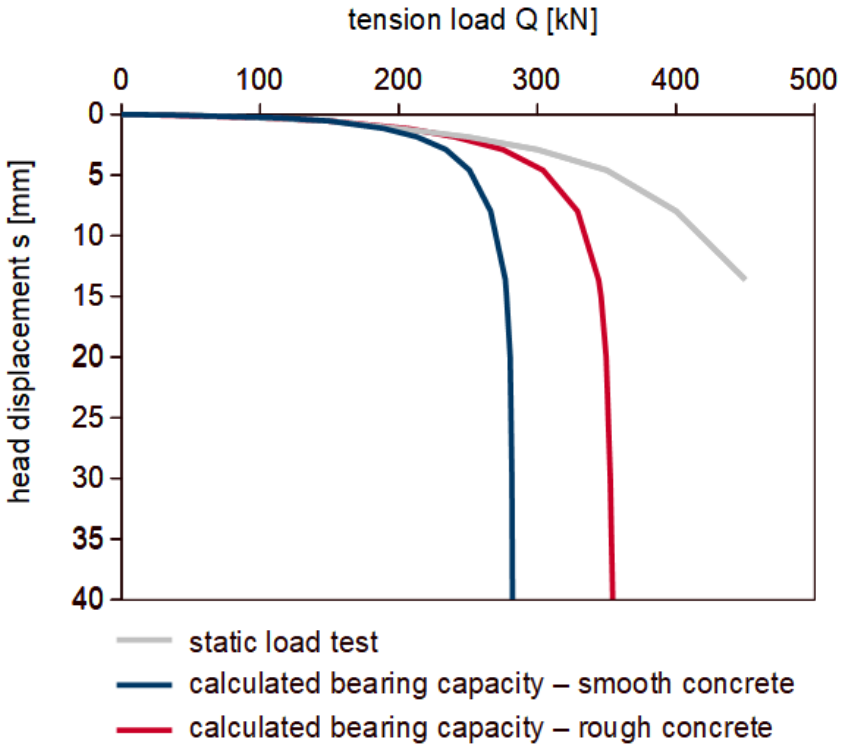

Figure 8.4. Results of DMT method for column S5C10 compared to the static load test results

As can be seen from the above graph, the $Q - s$ curves obtained from the proposed method coincide with the test load results in the initial settlement range (up to approx. 3 mm displacement) and then overestimate the load settlement value by approx. 20% for rough concrete and by 35% for smooth concrete. This is a quite satisfactory result, leaving the designer on the safe side, giving a safety stock. Furthermore, as expected, the settlements for rough concrete interface are lower than for smooth concrete interface. Better approximation of settlement should be achieved using the results of CNS interface shear tests.

The following Figures (8.5-8.7) show the corresponding results for columns S5C3, S4C8 and S5C9, respectively.

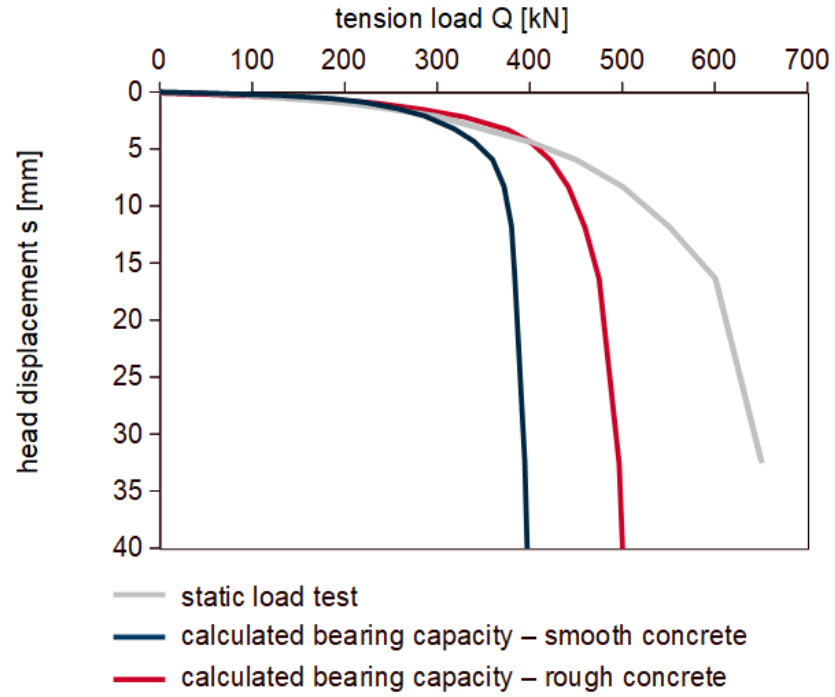

Figure 8.5. Results for the S5C13 column

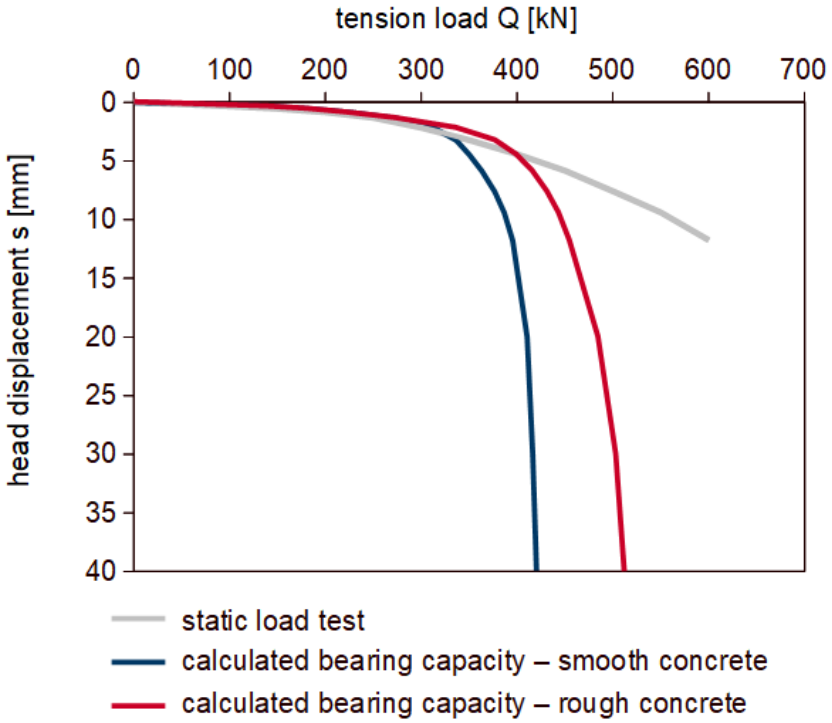

Figure 8.6. Results for the S4C8 column

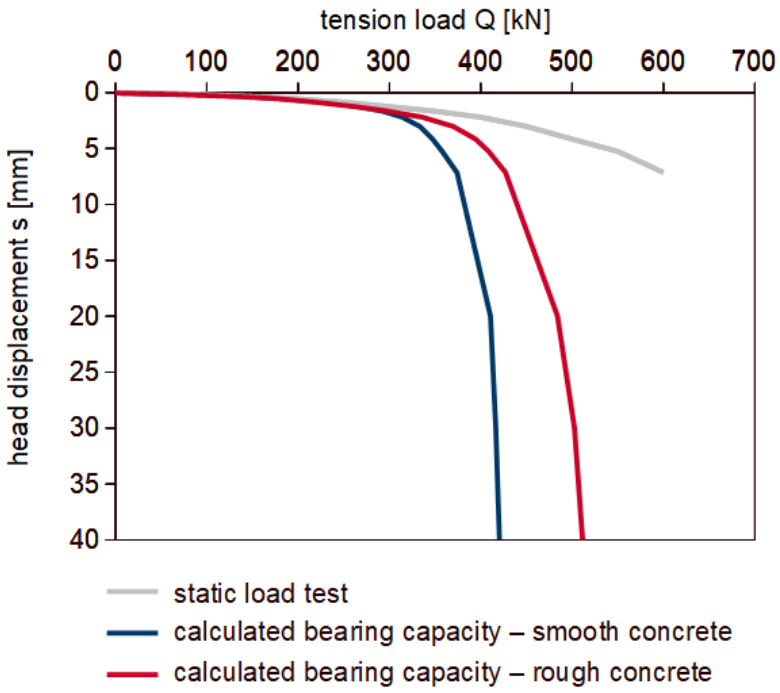

Figure 8.7. Results for the S5C9 column

All these results are similar to those obtained for an 8-meter column, i.e. they coincide with the static load test results only in the initial settlement range, up to approx. 3mm, and then overestimate the settlement by approx. 15-20% - rough concrete and 30-35% - smooth concrete at small settlement range.

8.3 Columns based on bearing soil layer

Columns based on the bearing soil layer have a shaft made in layers of soft soils, while the base is based on the bearing soil but not significantly embedded in it (Chapter 5). Three 14.6-meter-long columns were used for the analysis (see Table 8.4). These columns were subjected to tension and then compression load. The dead weight of the column was 44.03 kN and the buoyancy of the column in water was 15.90 kN.

Table 8.4. Characteristics of the columns based on bearing layer

Column designation	*Column length*	*Maximum displacement from the SLT*	*Maximum load from the SLT*	*Bearing capacity from Chin's method*
[-]	*[m]*	*[mm]*	*[kN]*	*[kN]*
S4C3	*14.6*	*5.26*	*480*	*694*
S4C4	*14.6*	*10.94*	*600*	*746*
S5C8	*14.6*	*8.04*	*540*	*714*

The results of the static test load as well as theoretical curves obtained with Chin's method for columns based on the bearing layer are shown in Figure 8.8.

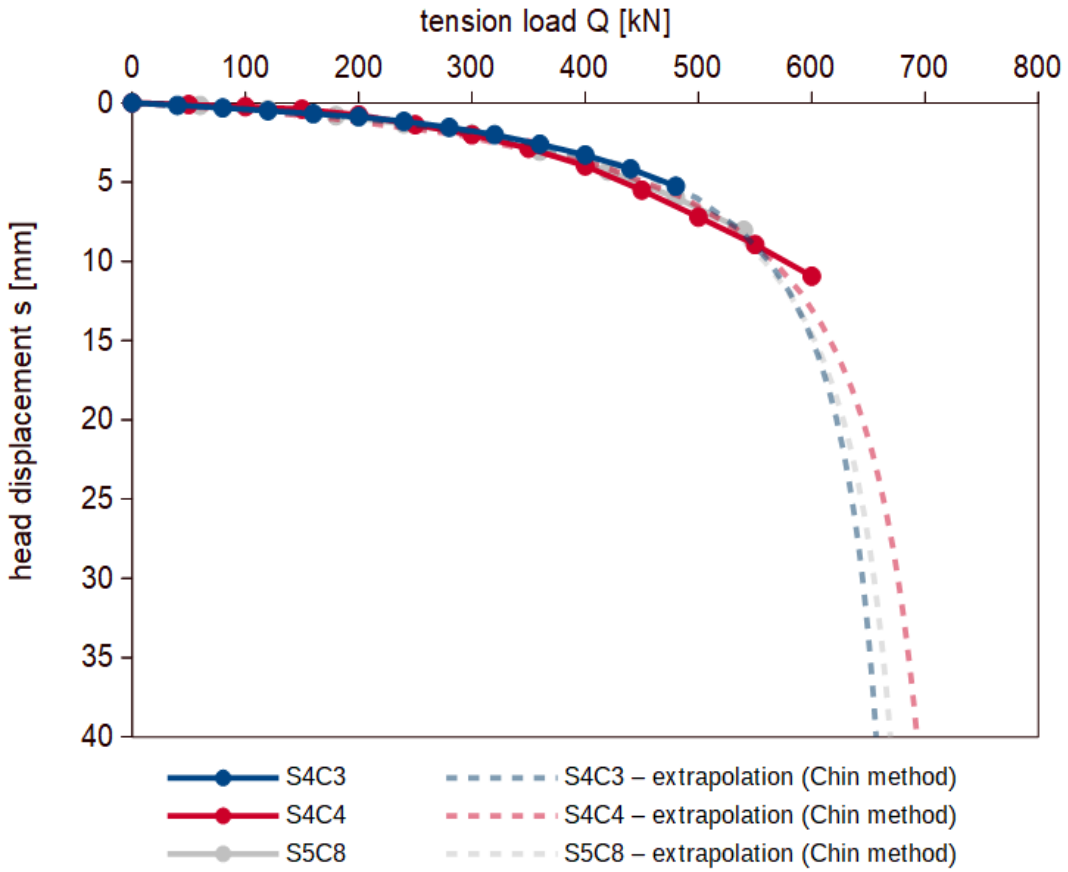

Figure 8.8. Tension load – head displacement curves and extrapolated load capacity of columns based on the bearing layer

During the static load tests, the columns obtained quite low displacement values, which gives an incomplete column characteristics. The displacements were accordingly: 5.26, 10.94 and 8.04 mm for S4C3, S4C4 and S5C8 columns, respectively. A very good agreement between these three curves is observed in the initial range of displacements,. The results of load tests and bearing capacity estimated using the proposed transfer functions are shown in Figures 8.9-8.11.

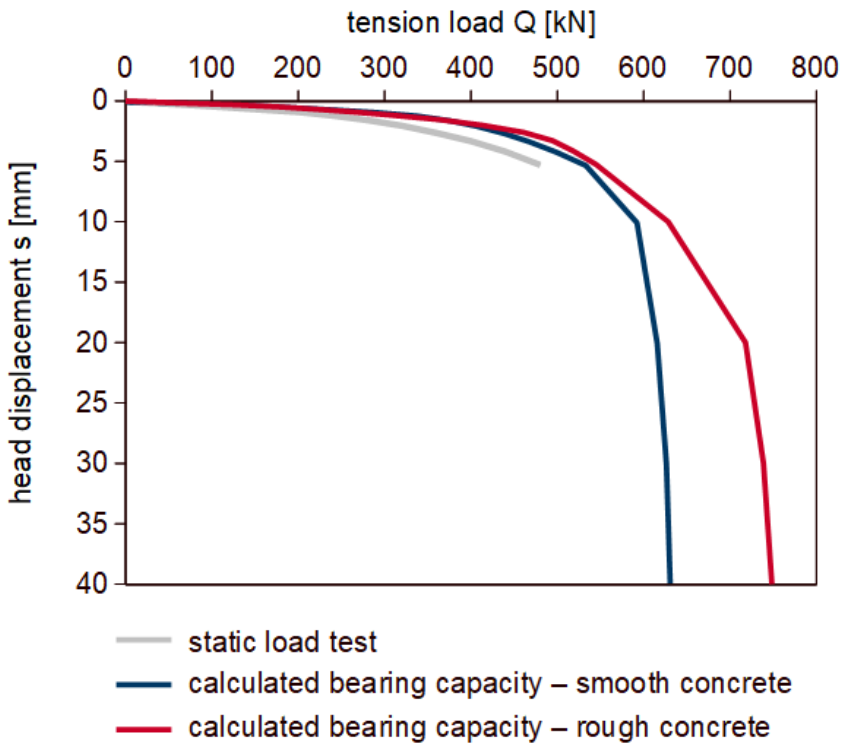

Figure 8.9. Results for the S4C3 column

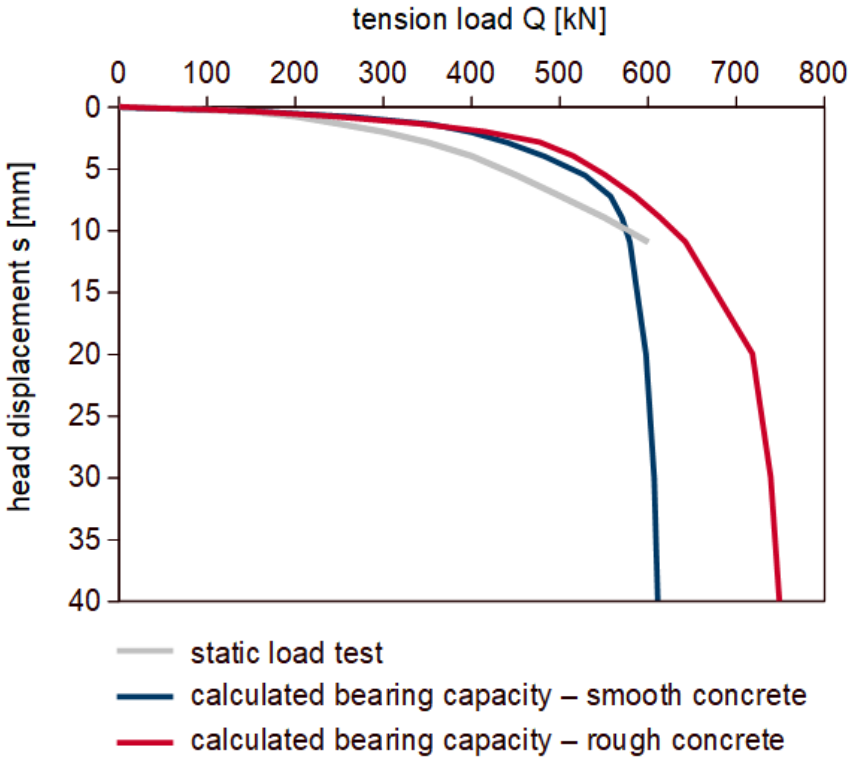

Figure 8.10. Results for the S4C4 column

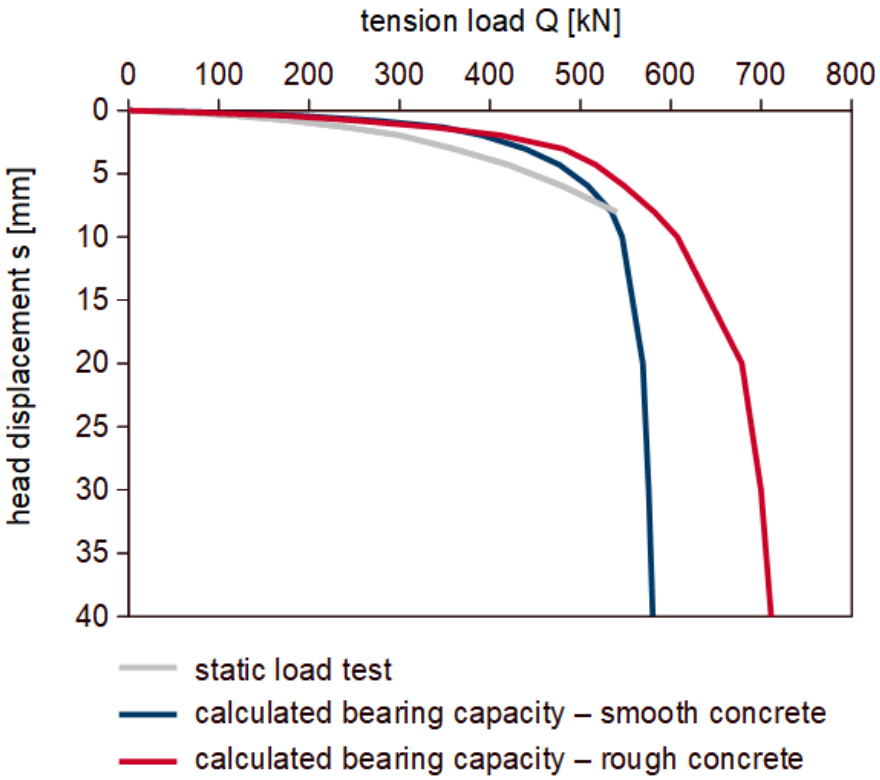

Figure 8.11. Results for the S5C8 column

In the case of columns based on the bearing soil layer, the proposed functions underestimate the settlement obtained from the static load tests in the initial range of displacement. It could be related to the presence of large thickness of soft soils in this profile.

8.4 Additional analysis for compression-tension column

As a part of the additional analysis, one compression-tension column was examined. The 15.5-meter-column (S5C3), was selected, embedded for about 1m in the bearing soil layer. When pulling out with a force of 650kN, it obtained a displacement of 6.44mm. The results from the static test load are presented in Figure 8.12 as well as theoretical curves obtained with Chin's method.

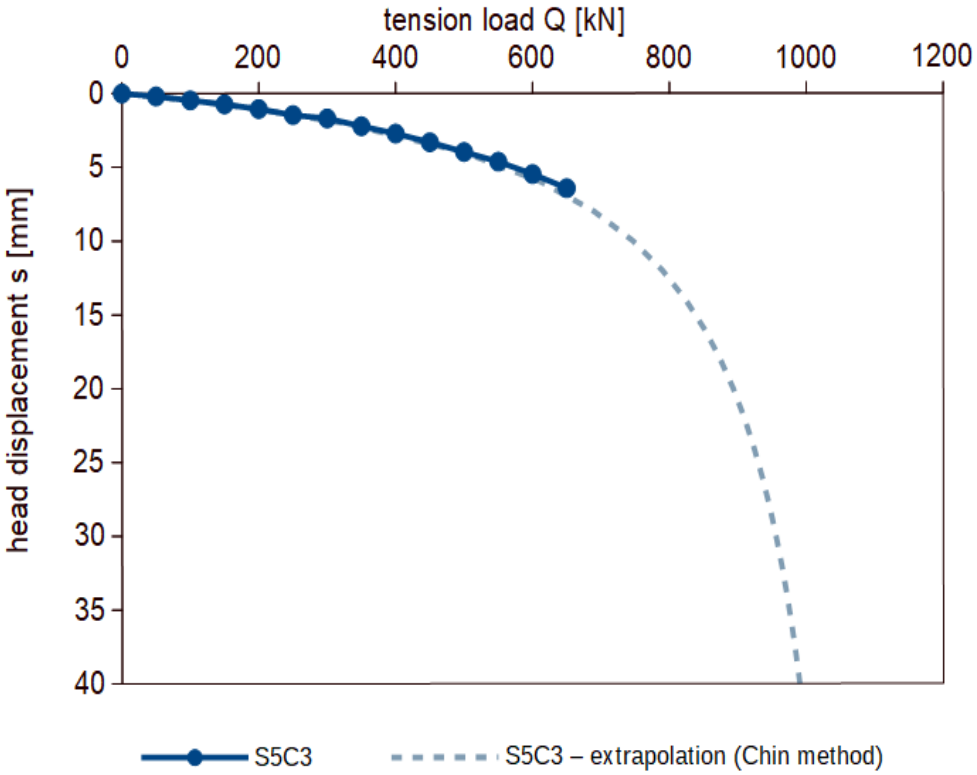

Figure 8.12. Results from the pull-out test for the S5C3 column

In order to estimate the bearing capacity of this column, transfer functions developed from backward shearing were used (Eq. 7.16-7.23) as well as relations between the maximum pile skin friction τ_{max} and parameter p_0 (Fig. 7.36 – 7.37).

The results of the static load test and the estimated capacity are shown in Figure 8.13. In addition, for comparison, the same column is analyzed using the functions from forward shearing.

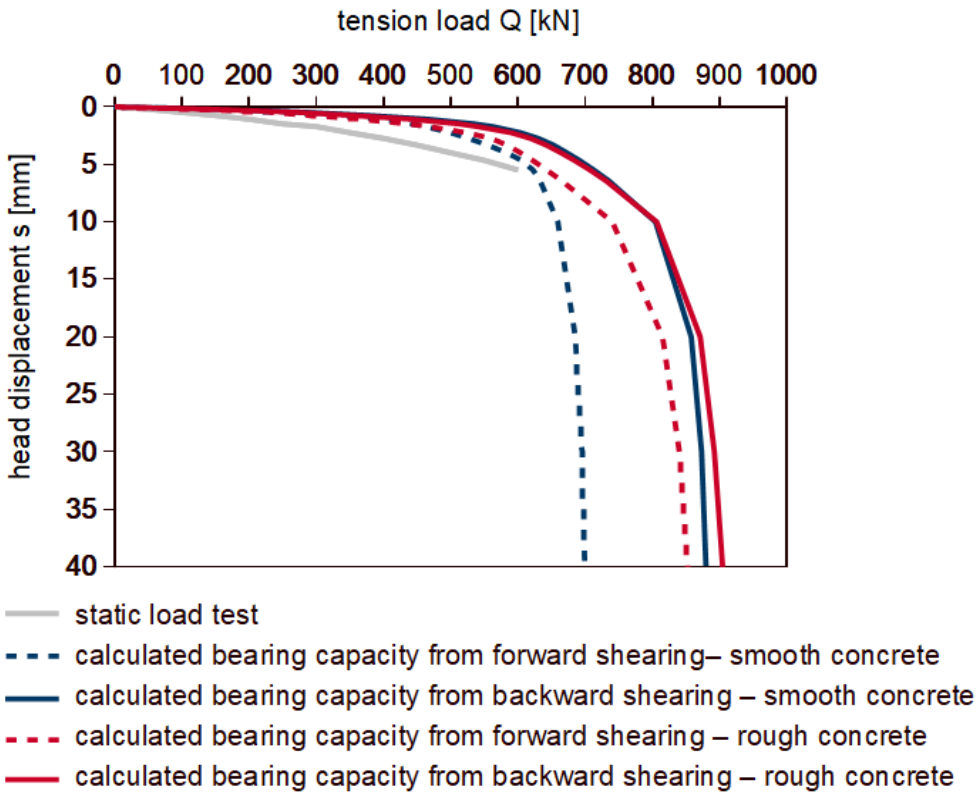

Figure 8.14. Results for the S5C3 column

As can be seen from Figure 8.14, the capacity estimated using the proposed functions is greater than that expected from the load test. For the initial shearing functions, it is clear that the bearing capacity for rough concrete is higher than for smooth concrete. For reverse shearing, the difference is negligible. In addition, the resistances obtained for reverse shearing are slightly higher than those for initial shearing, which indicates a slight increase in soil strength during repeated shearing in the opposite direction. Similar conclusions could be reached by analyzing and comparing the results for pull-out and push-in-pull-out columns (see Chapter 5). An additional aspect, that affects the discrepancy in results for previously pushed-in columns, are the residual stresses (also under the base) after the pressed pile is relieved. So in the initial phase of pullout the actual friction is lower, then this effect disappears with higher pullout displacements.

Summarizing the above analysis, the proposed method is quite suitable for floating columns (in this case columns 8 and 11m) and columns based on the bearing layer. In the case columns embedded in the bearing layer, there are factors related to the base effect that are not included in this thesis and may affect the accuracy of results.

Chapter 9
Pile capacity based on direct methods

9.1 Introduction

This chapter presents calculations of pile bearing capacity using methods presented in Chapter 2. As this dissertation focuses on floating columns with lengths of 8, 11 and 14.6 m, each method was used to estimate bearing capacity of 3 columns with exactly these lengths. Then, the obtained results were compared with the results obtained by the author's method based on the results of DMT sounding, presented in Chapter 7. The calculations were performed on the basis of averaged measurements obtained from CPT sounding on test plots (before pile installation). These data are presented and discussed further in Chapter 2. Below, Fig.9.1 recalls the q_t, f_s and u_2 measurements used in the selected calculation methods. All calculations were performed on the characteristic values so that they can be compared with the results of the author's newly developed method. Calculations were performed up to the depth of 14.6 m (the longest pile analyzed) with 0.02 m resolution of CPT measurements.

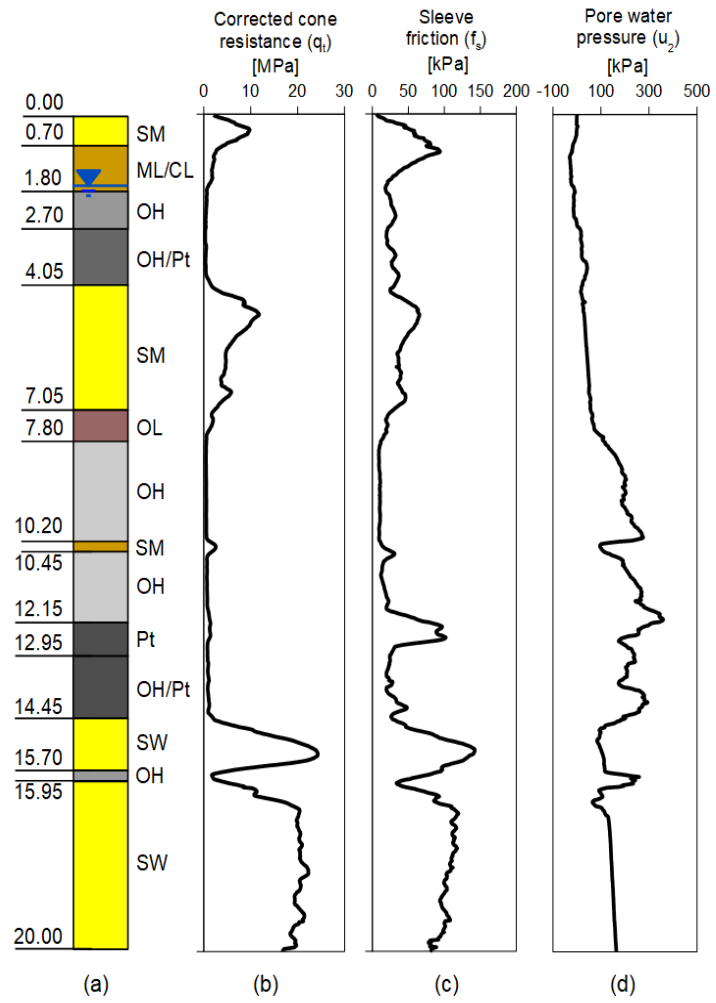

Figure 9.1. Soil profile (a), and CPTU sounding results (b)-(d) for Jazowa testing site.

9.2 LCPC method

The CMC columns can be classified as Category IA piles (see Table 2.1). Based on the cone resistance measurements q_t and Table 2.1, appropriate α values were selected for each soil type and are shown in red in Figure 9.2.a.

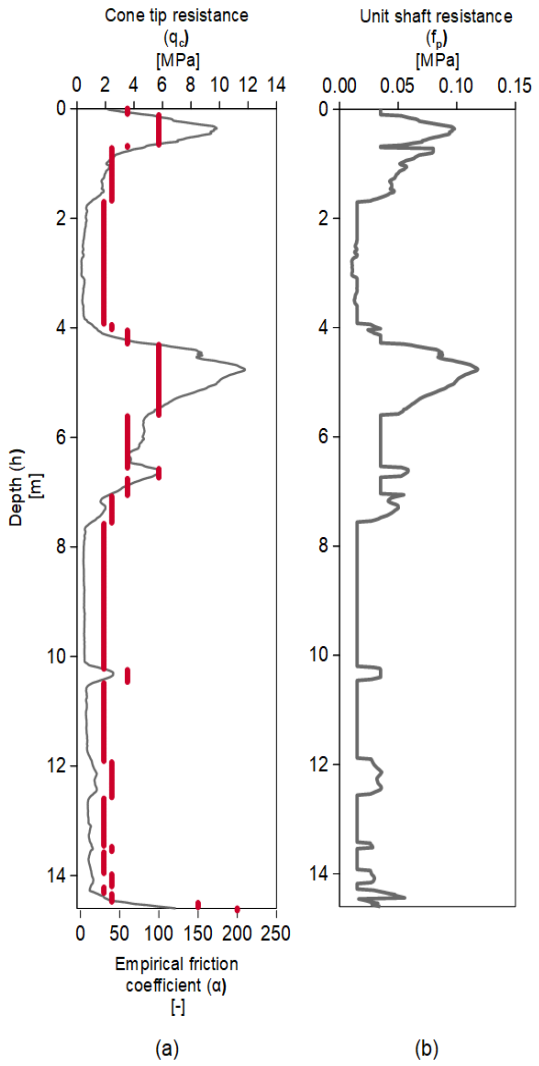

Figure 9.2. Values of a) empirical coefficients α for calculating the limit skin friction for analyzed cone tip resistance q_t b) values of unit shaft resistance f_p

Then, using Equation 2.1, the unit shaft resistance f_p was determined for each depth and the maximum values were assigned based on Table 2.1. The final f_p values are shown in Fig.9.2b.

The total shaft bearing capacity is the sum of the product of the resistance f_p and the area of the shaft (e.g. Equation 2.4). The characteristic values of bearing capacity of piles of different lengths according to the LCPC method are summarized in Table 9.1.

Table 9.1. Calculated shaft resistance according to the LCPC method

Pile length	*Calculated shaft resistance*
[m]	*[kN]*
8	*423*
11	*485*
14.6	*580*

9.3 CPT 2012

The CMC columns, according to Table 2.2, are attributed to pile class C3 and category 7. In the French AFNOR standard, soil layers are subdivided according to the European Soil Classification System (ESCS) (BS EN ISO 14688-2-2004 + A1-2013). The previously used USCS subdivision has been converted to ESCS and is summarized in Table 9.2, below.

Table 9.2. Soil type according to USCS and ESCS

Soil type according to Unified Soil Classification System (USCS)	*Soil type according to European Soil Classification System (ESCS)*
siSa	*Intermediate soil*
ML/CL	*Clays & Silts*
OH	
OH/Pt	
Pt	
SM	*Sands & Gravels*
SW	

The pile shaft resistance has been calculated using the procedure described in Chapter 2. The empirical coefficient α is equal to 1.15, 0.95 and 1.45 for intermediate soils, soft soils and sand layers, respectively (Table 2.3). The maximum pile unit shaft resistance is equal to 130 kPa for intermediate and soft soils, while it corresponds to 200 kPa for sands (Table 2.4).

The f_{sol} has been determined according to the equation (2.3). The soil-type parameters a, b and c are distinguished in Table 9.3 below.

Table 9.1. Soil-type parameters adopted for calculations

	Soil-type parameter		
Soil type	*a*	*b*	*c*
Intermediate soil	*0.0015*	*0.1*	*0.25*
Clays & Silts	*0.0018*	*0.1*	*0.4*
Sands & Gravels	*0.0012*	*0.1*	*0.15*

Then, the unit pile shaft capacity have been calculated and then, the total pile resistance in tension has been obtained according to Eq. 2.4. The results are presented in Table 9.3.

Table 9.3. Calculated shaft resistance according to the CPT 2012 method

Pile length	*Calculated shaft resistance*
[m]	*[kN]*
8	*589*
11	*671*
14.6	*820*

9.4 Togliani method

In order to determine the side resistance in Togliani's method, the friction ratio (Eq. 2.8) was first determined, and then, depending on the values obtained, coefficient k_1 was estimated using equations 2.9-2.11. Graphs of these two coefficients are shown in Fig. 9.3 a and b, respectively.

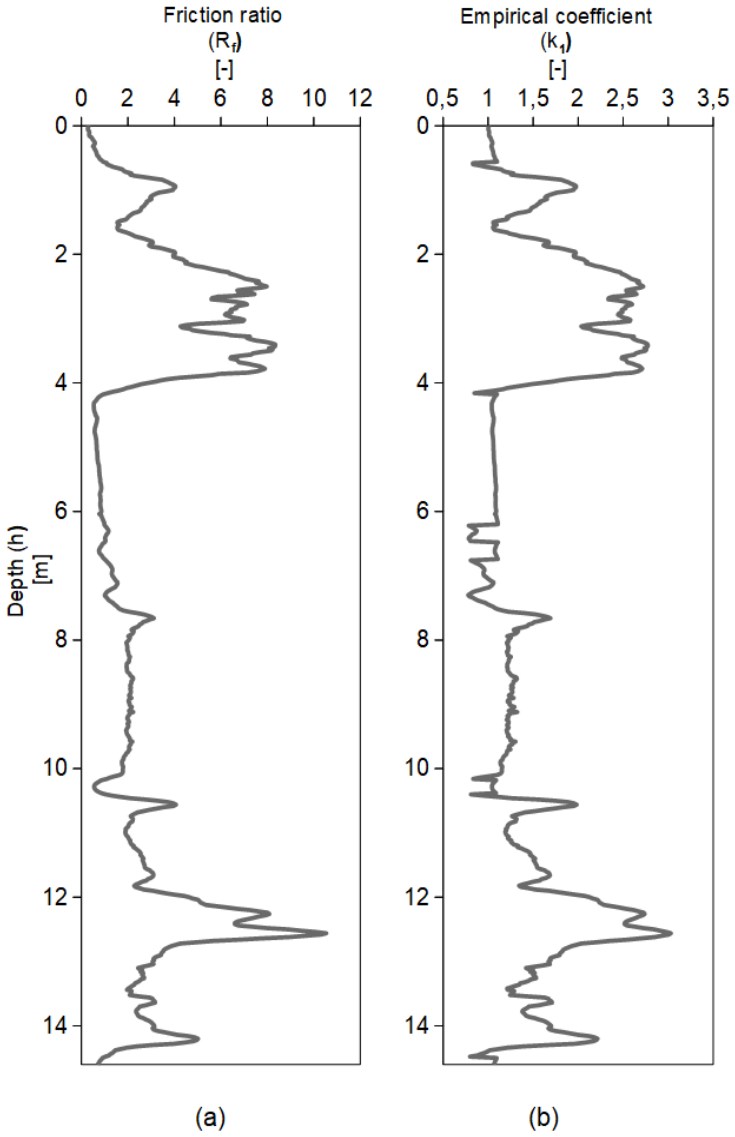

Figure 9.2. Values of a) friction ratio R_f b) coefficient k_1 in Togliani's method

The unit shaft resistance and total shaft resistance were calculated using Equations 2.6 and 2.7, and the resulting values are summarized below in Table 9.4.

Table 9.4. Calculated shaft resistance according to the Togliani's method

Pile length	*Calculated shaft resistance*
[m]	*[kN]*
8	*654*
11	*776*
14.6	*1031*

9.5 German method

In the German method, the bearing capacity of the shaft is determined based on nomograms (Fig. 2.1). For non-cohesive soils it is necessary to know the cone resistance q_c (see Fig.9.1.b) and for cohesive soils the undrained shear strength c_u (Fig.9.3).

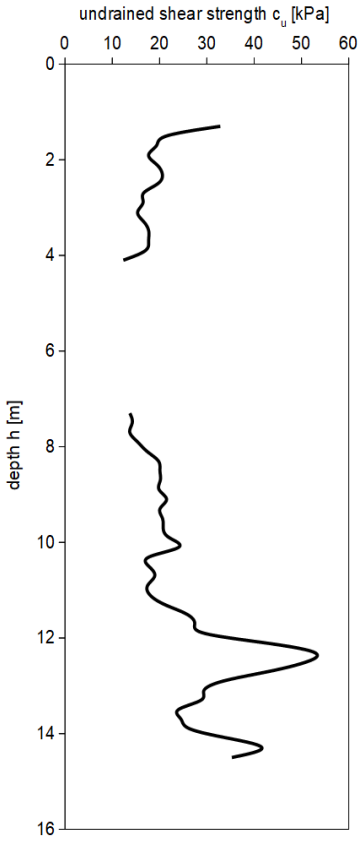

Figure 9.3. Values of undrained shear strength of analyzed soils

Nomograms in the German standard include 10 pile types. CMC piles are the most similar to Atlas piles in terms of technology. Therefore, curve 3 (see Fig. 2.1) based on the Atlas pile tests will be used in the calculations.

In the analyzed non-cohesive soils, up to a depth of 14.6 m, the cone resistance q_c is mostly below 7.5 MPa, just as the cohesive soils do not have a shear strength c_u of 60 kPa. In German recommendations it is stated that in this case a soil layer may only be taken into account if it is approved by a geotechnical expert and justified by the geotechnical conditions and the performance of the structure (Pfähle, 2012). Since the analyzed soils are soft but without negative friction, it was decided to extrapolate the graphs shown in Fig. 2.1 to apply the method to the given situation. The estimated resistance values are summarized in Table 9.5.

Table 9.5. Calculated shaft resistance according to the German method

Pile length	*Calculated shaft resistance*
[m]	*[kN]*
8	*568*
11	*686*
14.6	*856*

9.6 Unicone method

The Unicone method uses all three measurements from the CPTu sounding to perform the soil classification. In order to use this method, the effective cone resistance was determined (using Equation 2.14) and is shown in Fig. 9.4 with the gray line. Then, according to the q_E and f_s values (Fig. 9.1), the soil was classified using the soil profiling chart (Fig.2.2). Each soil type was assigned a side correlation coefficient which is shown in Fig. 2.3 with the red line.

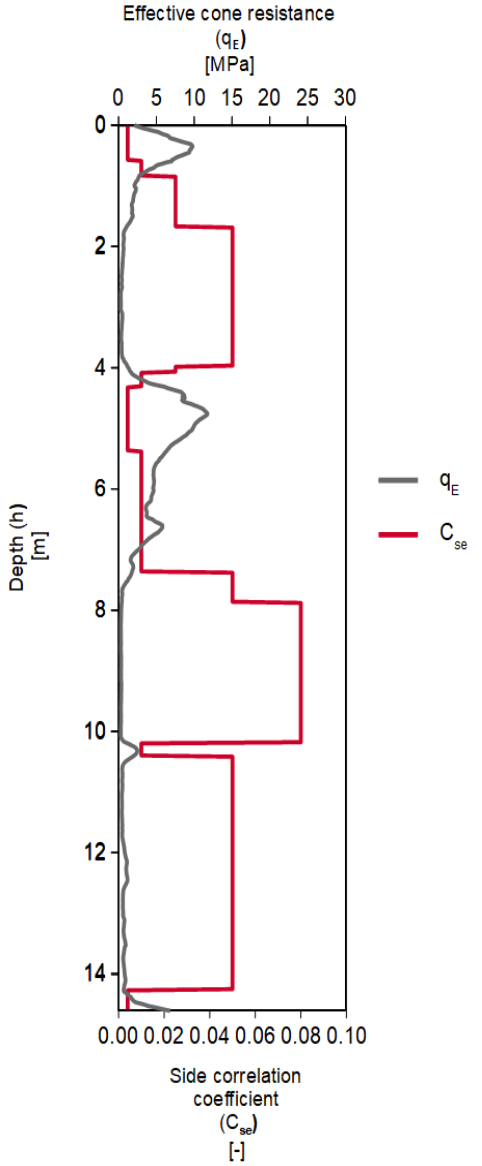

Figure 9.4. Effective cone resistance q_E and side correlation coefficient C_{se} in the Unicone method

The unit shaft resistance for each soil layer was then determined using Equation 2.15, followed by the total resistance values which are summarized in Table 9.6.

Table 9.6. Calculated shaft resistance according to the Unicone method

Pile length	*Calculated shaft resistance*
[m]	*[kN]*
8	*358*
11	*463*
14.6	*613*

9.7 SEU method

In the SEU method, the unit friction resistance is determined as a function of pore water pressure. Based on Figure 9.1.d and Equations 2.16 and 2.17, f_p was determined and is shown in Figure 9.5 below.

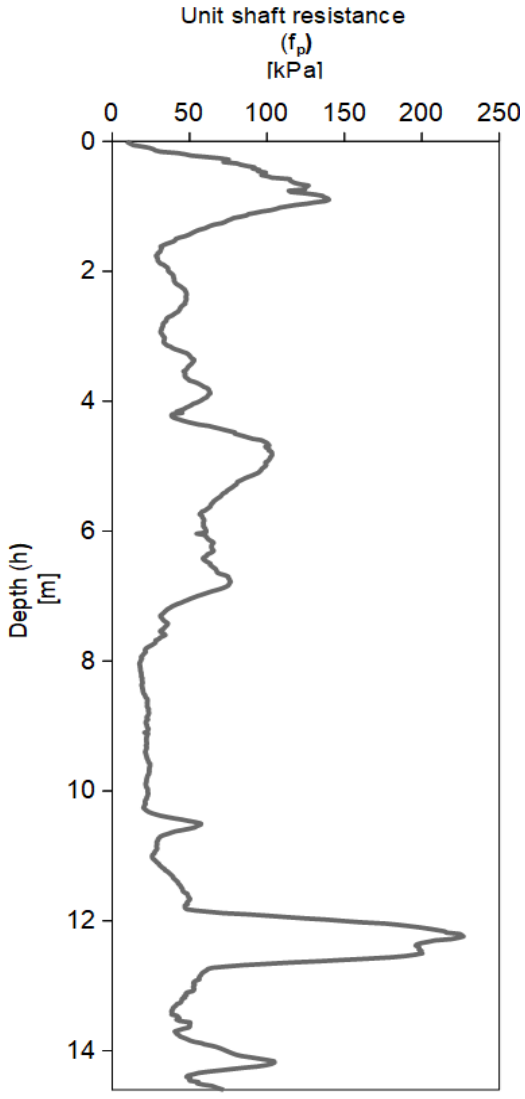

Figure 9.5. Unit shaft resistance in SEU method

The total pullout resistances were then determined and the values are summarized in Table 9.7.

Table 9.7. Calculated shaft resistance according to the SEU method

Pile length	*Calculated shaft resistance*
[m]	*[kN]*
8	*599*
11	*694*
14.6	*1058*

9.8 DMT method

For comparison of results, the DMT method also used averaged values of parameters measured in-situ. Figure 9.6 recalls the averaged DMT sounding results presented in Chapter 4.

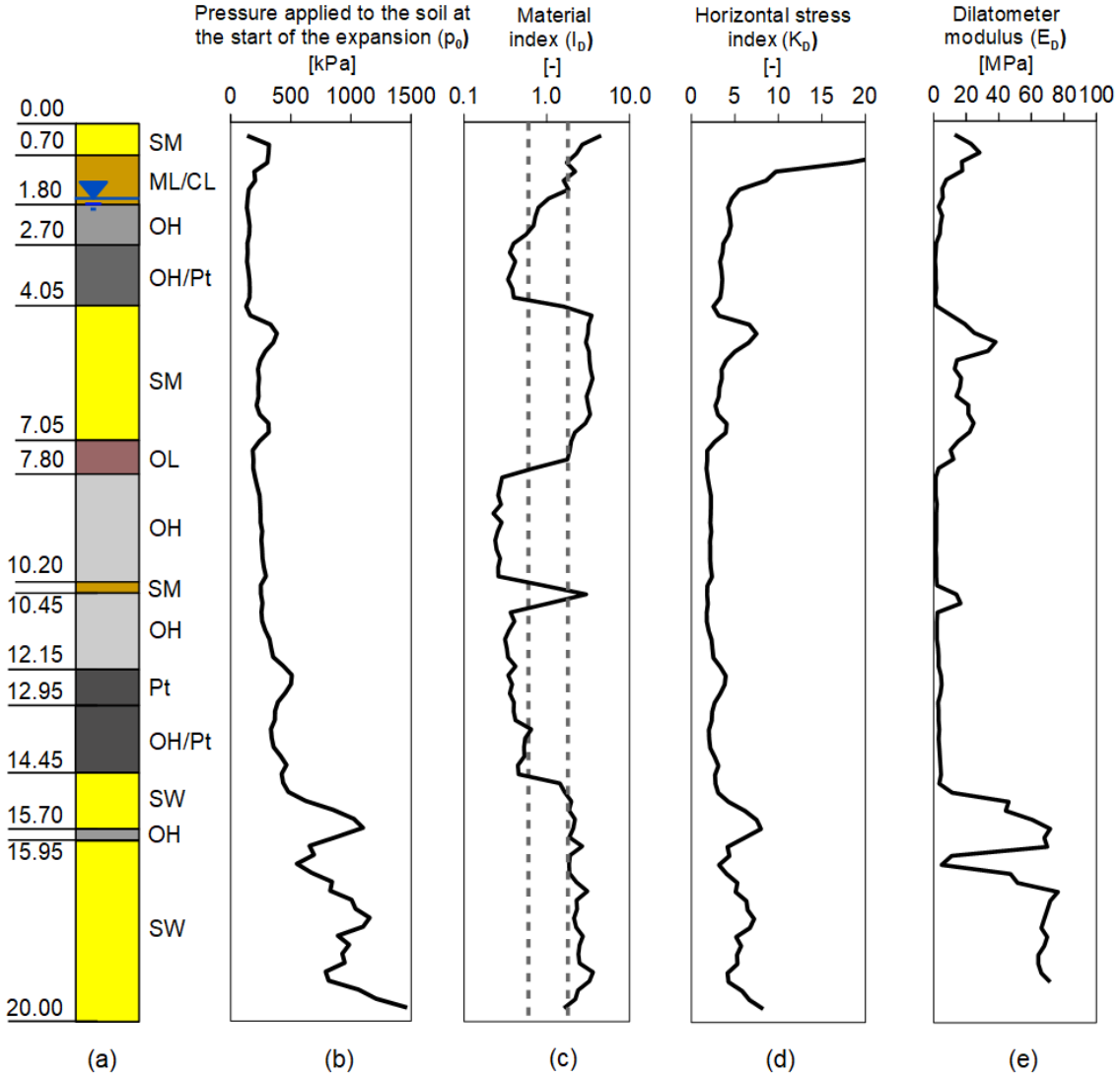

Soil type: CL = clay of low plasticity; ML = silt of low plasticity; OH = organic soil of high plasticity; OL = organic soil of low plasticity; Pt = Peat; SM = silty sand; SW= well-graded sand

Figure 9.6. Soil profile (a), and DMT sounding results (b)-(e) for Jazowa testing site.

Calculations were performed using both smooth and rough interface relationships according to the scheme presented in Table 8.2 in Chapter 8. The results of the calculations are summarized below.

Table 9.8. Calculated shaft resistance according to the DMT method

Pile length	*Calculated shaft resistance*	
	Smooth concrete	*Rough concrete*
[m]	*[kN]*	*[kN]*
8	*259*	*321*
11	*381*	*468*
14.6	*592*	*719*

The values obtained for the rough interface are about 20% higher.

9.9 Comparison of the results

The calculated shaft resistances values for 8,11 and 14.6-metres piles are presented in Figure 9.7 below.

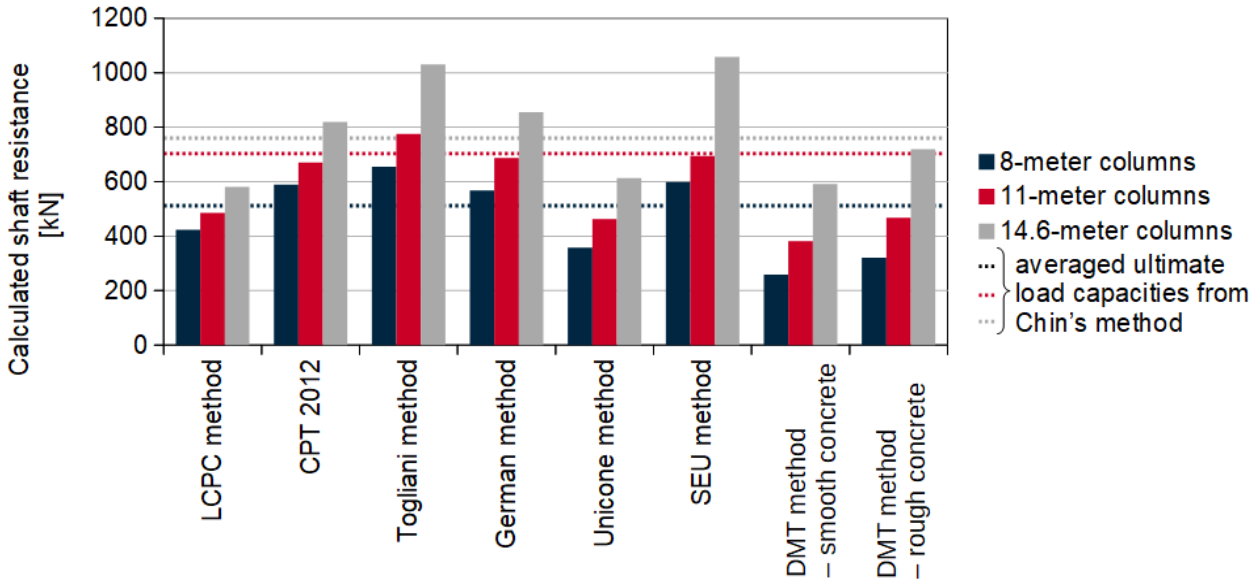

Figure 9.7. Comparison of the results.

Analyzing the results obtained, it can be noticed that in case of 8-meter floating columns the CPT 2012, Togiliani, German and SEU methods gave similar load capacity values, about 600 kN. The LCPC and Unicone methods gave values lower by about 100 kN. The DMT method gave the lowest bearing capacity values, with values for rough interface similar to those obtained with the Unicone method.

For 11-meter columns, the bearing capacity values obtained by the LCPC, Unicone and DMT methods (for rough interface) converge. The values from the relation for smooth concrete give bearing capacities about 100 kN lower, i.e. 400 kN. The bearing capacity obtained by the other methods is about 700 kN.

The bearing capacity of 14.6 m columns, based on the bearing layer, in the LCPC, Unicone and DMT methods (for smooth concrete) is about 600 kN. It is 50% higher in CPT 2012 and German method and almost 100% higher in Togliani and SEU method. The result from DMT method for rough concrete

stacks in between.

In conclusion, even the bearing capacities obtained by commonly used methods differ by up to 70-80 %. The results obtained with the DMT method lie at the lower boundary of the obtained results. Therefore, they provide a safe estimation of pile capacity. The reason for such divergence may be the fact that each of these methods has been calibrated on specific soil conditions, differing from the analyzed case. Most of them are based on empirical coefficients depending on the soil type and pile method, which may not be suitable for the soil conditions in northern Poland.

9.10 Recommendations and consideration for design

On the basis of the comparative analysis it is recommended to use in the calculations of bearing capacity the relationships proposed for the rough interface, which give results more similar to those obtained by other methods based on CPT soundings.

It should be kept in mind that the method was developed on the basis of a specific group of deltaic soils, characteristic for the regions of northern Poland. In case of application of this method in different soil conditions, it is recommended to calibrate the DMT model to local conditions in order to obtain similar results as for the Jazowa case.

It should also be remembered that during calibration of the method, only tests for pull-out piles were used, as well as the fact that the DMT method was developed for CMC column technology. No calculations for other types of columns/piles have been performed to date.

Chapter 10
Conclusions

This thesis focused on the design of ultimate limit state and serviceability limit state of concrete screw z piles. Currently used methods and the new proposal based on flat dilatometer test were discussed.

The newly developed method is based on the results of dilatometer soundings conducted on test fields before and after pile installation and on laboratory interface tests conducted in a direct shear box apparatus. Considerable installation effects due to screw auger pile installation were found by the interpretation of DMT tests. They are related to the changes of lateral stress level and vertical constrained modulus. These effects are specially pronounced in medium dense sands and overconsolidated clays, where net increase of lateral stress and constrained modulus are noticed. Only slight installation effects are observed in muds, while no effect or even a small decrease of these parameters can be noticed in peats, probably due to remolding of theirs structure during pile construction. One should also notice that the amount of installation effect is not only related to the soil type and its state but principally to the piling technology applied. Future studies of installation effects due to construction of different pile types will enhance the application of the proposed method.

Considering an analogy between the shaft friction mobilization on the pile segment and its representation in interface direct shear test, these installation effects were taken into account by adjusting the normal stress in the shear box apparatus. The interface tests permitted to determine skin friction mobilization curve and the value of maximum shear stress t_{max}. Quite good correlation was established between the maximum shear stress from the interface tests and p_0 reading from DMT tests prior to pile installation. The friction mobilization curves were normalized and described with tri-linear curve, where its inclination is expressed as a function of M_{DMT}. These findings will enable the application of dilatometer tests in the estimation of ultimate bearing capacity and in the determination of pile load-head displacement curve. One should notice that the interface tests were performed under constant normal load condition.

New method for determination of pile load-head displacement curve $Q - s$ based on transfer function $t - z$ and results of dilatometer tests was proposed.

The proposed $t-z$ curves provide promising $Q-s$ diagrams in the initial displacement range, which is usually the most significant from the practical point of view. These graphs coincide with the results obtained from the static load tests on the pull-out piles. In the context of ultimate bearing capacity, the results obtained by the proposed method provide a safe range of values of theoretical capacities with respect to the actual pile capacities demonstrated from the static test loads. Better approximation of Q-s diagram was obtained with direct shear tests with rough concrete-soil surface.

The aspect that distinguishes the developed method is the possibility of estimating the settlements and bearing capacities based only on one type of field tests. DMT soundings are quite popular in Poland and the basic measured parameters (p_0, p_1) are well suited for calculation of shaft and toe pile resistance. The measurements are taken sufficiently dense (i.e. each 20cm) to assure almost continuous soil profile. It is possible to operate directly on the results obtained from the soundings without the need of averaging the parameters for individual soil layers .

In this thesis, attention was also paid to the influence of individual factors on the ultimate bearing capacity of the pile, such as

- the effect of pile length on bearing capacity;
- an eventual increase of pile bearing capacity with time, with negligible set-up effect found;
- the effect of the loading path on pile pullout - a completely different course of the $Q-s$ plot was noticed in case of compression-tension and tension scheme.

10.1 Recommendations for further research

This research offers a great deal of future prospects and possibilities.

First of all, the currently carried out tests in the shear box apparatus were performed under conditions of constant normal stress. In fact, in dense sandy or cohesive stiff or semi-solid soils it would be necessary to take into account the increase of normal component of stress during shear. The estimated values of constant normal stiffness of pile-soil interface suggest that in medium to dense sands and in stiff clays the imposed lateral stiffness will be more appropriate boundary condition. This will permit more adequate simulation of pile-soil interface behavior and better coincidence between the method prediction and the results of pile loading tests at larger displacement, especially in medium to dense sands.

Secondly, it may be possible to attempt to create analogous $q-z$ curves, taking into account the mobilization of base resistance. This would require more detailed testing, preferably through the use of instrumented piles.

Better prediction of the Q-s curve from static load tests in the domain of larger displacement would be obtained:

- using interface direct shear test with CNS condition in medium dense to dense sands,
- increasing the displacement limit (4 mm in this study) at the interpretation of direct shear tests in case of soft soils).

Finally, an attempt to apply the presented method in different soil conditions or for other pile types and its possible calibration can be considered. This can introduce the installation effects in the design of different types of piles.

10.2 Limitations of the study

The proposed method was calibrated for the screw auger piles. It can be used in case of single pile as the effect of pile group is not included in the analysis.

The method should be used with caution in case of piles with high residual stress after installation (driven or pushed-in), which was also confirmed in this research where the piles with different loading scheme were analyzed. Moreover, intense driving could modify the parameters of pile-soil interface (i.e soil granulometry with grain crushing) which is not possible to reproduce in typical interface direct shear test.

In case of very long pushed-in piles some reduction of the shaft friction should be applied to take into account friction fatique.

Due to high stress level near the pile base the mobilization of shaft friction at this part of the shaft can not be reproduced correctly in the interface direct shear tests.

Bibliography

AFNOR, 2012. Justification des ouvrages ge´otechniques— Normes d'application nationale de l'Eurocode 7—Fondations profondes'' (Justification of geotechnical work—National application standards for the implementation of Eurocode 7—Deep foundations—in French), French standard NF P 94-262, AFNOR,Saint-Denis

Airey, D.W., Wood, D.M., 1987. An evaluation of direct simple shear tests on clay. Géotechnique 37, 25–35.

Aoki, N., Velloso, D. de A., 1975. An approximate method to estimate the bearing capacity of piles, in: Proc., 5th Pan-American Conf. of Soil Mechanics and Foundation Engineering. International Society of Soil Mechanics and Geotechnical Engineering Buenos …, pp. 367–376.

ASTM D2487, 2017. Standard Practice for Classification of Soils for Engineering Purposes (Unified Soil Classification System). ASTM International, West Conshohocken, PA.

ASTM D2974, 2014. Standard Test Methods for Moisture, Ash, and Organic Matter of Peat and Other Organic Soils. ASTM International, West Conshohocken, PA.

ASTM D3080, 2020. Test Method for Direct Shear Test of Soils Under Consolidated Drained Conditions. ASTM International. https://doi.org/10.1520/D3080_D3080M-11

Baguelin, F., Burlon, S., Bustamante, M., Frank, R., Gianeselli, L., Habert, J., Legrand, S., 2012. Justification de la portance des pieux avec la norme «fondations profondes» NF P 94-262 et le pressiomètre. Journ. Natl. Géotechnique Géologie L'ingénieur Bordx. 4–6.

Bałachowski, L., 2006. Scale effect in shaft friction from the direct shear interface tests. Arch. Civ. Mech. Eng. 6, 13–28. https://doi.org/10.1016/S1644-9665(12)60238-6

Balachowski, L., 1995. Différents aspects de la modélisation physique du comportement des pieux: Chambre d'Etalonnage et Centrifugeuse (PhD Thesis). Grenoble INPG.

Bałachowski, L., Międlarz, K., Konkol, J., 2018. Strength parameters of deltaic soils determined with CPTU, DMT and FVT, in: Cone Penetration Testing 2018. Presented at the 4th International Symposium on Cone Penetration Testing, CPT'18, CRC Press/Balkema, Delft, pp. 117–121.

Bjerrum, L., Landva, A., 1966. Direct simple-shear tests on a Norwegian quick clay. Geotechnique 16, 1–20.

Boukpeti, N., White, D.J., 2017. Interface shear box tests for assessing axial pipe–soil resistance. Géotechnique 67, 18–30. https://doi.org/10.1680/jgeot.15.P.112

Boulon, M., & Foray, P., 1986. Physical and numerical simulation of lateral shaft friction along offshore piles in sand. Proc 3rd Int Conf Numer. Methods Offshore Piling 127–147.

BS EN ISO 14688-2-2004 + A1-2013. Geotechnical investigation and testing. Identification and classification os soil. Principles for classification. The British Standards Institution.

Burlon, S., Frank, R., Baguelin, F., Habert, J., Legrand, S., 2014. Model factor for the bearing capacity of piles from pressuremeter test results–Eurocode 7 approach. Géotechnique 64, 513–525.

Bustamante, M., Gianeselli, L., 1982. Pile bearing capacity predictions by means of static penetrometer CPT. Presented at the 2nd European Symposium on Penetration Testing, Baklema, Amsterdam, Netherlands, pp. 493–500.

Cai, G., Liu, S., Puppala, A.J., 2011. Evaluation of Pile Bearing Capacity from Piezocone Penetration Test Data in Soft Jiangsu Quaternary Clay Deposits. Mar. Georesources Geotechnol. 29, 177–201. https://doi.org/10.1080/1064119X.2011.556887

Cambefort, H., 1964. Essai sur le comportement en terrain homogène des pieux isolés et des groupes de pieux. Éditions Eyrolles.

Cheng, X.H., Ngan-Tillard, D.J.M., Den Haan, E.J., 2007. The causes of the high friction angle of Dutch organic soils. Eng. Geol. 93, 31–44. https://doi.org/10.1016/j.enggeo.2007.03.009

Chin, F.K., 1970a. Estimation of the ultimate load of piles not carried to failure. Presented at the 2nd Southeast Asia Conference on Soil Engineering, Southeast Asian Society of Soil Engineering, Singapore, pp. 81–90.

Chin, F.K., 1970b. Estimation of the ultimate load of piles not carried to failure, in: Proceedings of 2nd Southeast Asia Conference on Soil Engineering. Presented at the 2nd Southeast Asia Conference on Soil Engineering, Southeast Asian Society of Soil Engineering, Singapore, pp. 81–90.

Clausen, C.J.F., Aas, P.M., Karlsrud, K., 2005. Bearing capacity of driven piles in sand, the NGI approach. 1st International Symposium Frontiers in Offshore Geotechnics: ISFOG.

Cox, C., Mayne, P.W., 2015. Soil Stiffness Constitutive Model Parameters for Geotechnical Problems: A dilatometer Testing Approach. Proc 3rd Int Conf Flat Dilatometer 393–400.

Desrues, J., Andò, E., 2015. Strain localisation in granular media. Comptes Rendus Phys., Granular physics / Physique des milieux granulaires 16, 26–36. https://doi.org/10.1016/j.crhy.2015.01.001

Doan, L.V., Lehane, B.M., 2018a. Shaft resistance of non-displacement piles in normally consolidated clay. Cone Penetration Test. 2018 Proc. 4th Int. Symp. Cone Penetration Test. CPT18.

Doan, L.V., Lehane, B.M., 2018b. Effects of clay fraction and roughness on tension capacity of displacement piles. Cone Penetration Test. 2018 Proc. 4th Int. Symp. Cone Penetration Test. CPT18.

Engin, H.K., 2013. Modelling Installation Effects - A Numerical Approach 227.

Eslami, A., Fellenius, B.H., 1997. Pile capacity by direct CPT and CPTu methods applied to 102 case histories. Can. Geotech. J. 34, 886–904.

Fakharian, K., Evgin, E., 1996. An automated apparatus for three-dimensional monotonic and cyclic testing of interfaces. Geotech. Test. J. 19, 22–31.

Fakharian, K., Vafaei, N., 2020. Effect of Density on Skin Friction Response of Piles Embedded in Sand by Simple Shear Interface Tests. Can. Geotech. J. cgj-2019-0243. https://doi.org/10.1139/cgj-2019-0243

Fleming, W.G.K., 1993. A new method for single pile settlement prediction and analysis. Géotechnique 43, 615–618.

Frank, R., 2017a. Some aspects of research and practice for pile design in France. Innov. Infrastruct. Solut. 2, 32. https://doi.org/10.1007/s41062-017-0085-4

Frank, R., 2017b. Some aspects of research and practice for pile design in France. Innov. Infrastruct. Solut. 2, 1–15.

Frank, R., 1985. Recent developments in the prediction of pile behaviour from pressuremeter results, in: Symp. From Theory to Practice on Deep Foundations. pp. 69–99.

Frank, R., 1975. ETUDE THEORIQUE DU COMPORTEMENT DES PIEUX SOUS CHARGE VERTICALE; INTRODUCTION DE LA DILATANCE.

Frank, R., Zhao, S.R., 1982. Estimation par les parame`tres pressiome´triques de l'enfoncement sous charge axiale de pieux fore´s dans des sols fins (in French: Assessment of the settlement under axial load of bored piles in fine-grained soils by means of pressuremeter parameters). Bull Liaison Labo P Ch 17–24.

Gambin, M., 1963. Calcul du tassement d'une fondation profonde en fonction des résultats pressiométriques. Sols Soils 7, 11–31.

Gambini, F., 1986. Manuale piloti. Scac Milano.

Gwizdala, K., 1984. Large diameter bored piles in non-cohesive soils. Determination of the bearing capacity and settlement from results of static penetration tests (CPT) and standard penetration test (SPT).

Hansen, J.B., 1970. A revised and extended formula for bearing capacity.

Hanzawa, H., Nutt, N., Lunne, T., Tang, Y.X., Long, M., 2007. A Comparative Study Between the NGI Direct Simple Shear Apparatus and the Mikasa Direct Shear Apparatus. Soils Found. 47, 47–58. https://doi.org/10.3208/sandf.47.47

Hirayama, H., 1990. Load-settlement analysis for bored piles using hyperbolic transfer functions. Soils Found. 30, 55–64.

Hossain, A.M., Andrus, R.D., 2016. At-Rest Lateral Stress Coefficient in Sands from Common Field Methods. J. Geotech. Geoenvironmental Eng. 142, 06016016. https://doi.org/10.1061/(ASCE)GT.1943-5606.0001560

Hvorslev, H.J., 1960. Physical components of the shear strength of cohesive soils. Proc Shear Strength Cohesive Soils ASCE 169–273.

Igoe, D.J.P., Gavin, K.G., O'Kelly, B.C., 2011. Shaft capacity of open-ended piles in sand. J. Geotech. Geoenvironmental Eng. 137, 903–913.

Institute, A.P., 1993. API Specification 13A. API.

Jardine, R.J., Chow, F.C., Overy, R., Standing, J., 2005. ICP design methods for driven piles in sands and clays. Thomas Telford Ltd., London.

Kempfert, H.-G., Becker, P., 2010. Axial pile resistance of different pile types based on empirical values, in: Deep Foundations and Geotechnical In Situ Testing. pp. 149–154.

Kempfert, H.-G., Becker, P., 2007. Grundlagen und Ergebnisse der Ableitung von axialen Pfahlwiderständen aus Erfahrungs-werten für die EA-Pfähle. Bautechnik 84, 441–449. https://doi.org/10.1002/bate.200710038

Komurka, V.E., Wagner, A.B, Edil, T.B, 2003. A Review of Pile Set-Up, in: Proceedings of 51st Annual Geotechnical Engineering Conference. Presented at the 51st Annual Geotechnical Engineering Conference, University of Minnesota, Minnesota, USA, pp. 105–130.

Konkol, J., 2017. Numerical analysis of pile installation effects in cohesive soils, PhD Thesis. ed. Gdansk University of Technology, Gdansk.

Konkol, J., 2015. Numerical estimation of the pile toe and shaft unit resistances during the installation process in sands. Stud. Geotech. Mech. 37, 37–44. https://doi.org/10.1515/sgem-2015-0005

Konkol, J., Międlarz, K., Bałachowski, L., 2019. Geotechnical characterization of soft soil deposits in Northern Poland. Eng. Geol. 259, 105187. https://doi.org/10.1016/j.enggeo.2019.105187

Krasiński, A., 2012. Proposal for calculating the bearing capacity of screw displacement piles in non-cohesive soils based on CPT results. Stud. Geotech. Mech. 34, 41–51.

Lechowicz, Z., 1997. Undrained shear strength of organic soils from dilatometer test. Ann. Wars. Agric. Univ. Land Reclam. 85–96.

Lehane, B.M., Jardine, R.J., 1994. Shaft capacity of driven piles in sand: a new design method. Proc. 7th Int. Conf. Behav. Offshore Struct. 23–36.

Lehane, B.M., Schneider, J.A., Xu, X., 2005. The UWA-05 method for prediction of axial capacity of driven piles in sand. Front. Offshore Geotech. ISFOG 683–689.

Lehane, B.M., White, D.J., 2005. Lateral stress changes and shaft friction for model displacement piles in sand. Can. Geotech. J. 42, 1039–1052. https://doi.org/10.1139/t05-023

Lim, J.K., Lehane, B., 2015. Time effects on shaft capacity of jacked piles in sand. Can. Geotech. J. 52, 1830–1838. https://doi.org/10.1139/cgj-2014-0463

Lim, J.K., Lehane, B.M., 2014. Characterisation of the effects of time on the shaft friction of displacement piles in sand. Géotechnique 64, 476–485. https://doi.org/10.1680/geot.13.P.220

Look, B., 2007. Handbook of geotechnical investigation and design tables, Balkema-proceedings and monographs in engineering, water and earth sciences. Taylor & Francis, London ; New York.

Loukidis, D., & Salgado, R. (2008). Analysis of the shaft resistance of non-displacement piles in sand. *Géotechnique*, *58*(4), 283-296.

Lunne, T., Berre, T., Strandvik, S., 1997. Sample disturbance effects in soft low plastic Norwegian clay. Presented at the Symposium on Recent developments in Soil and Pavement Mechanics, Baklema, Rio de Janeiro, pp. 81–102.

Makowski, J., 1997. Lower Vistula Dikes, historical development, present state and behaviour during high water periods. Instytut Budownictwa Wodnego PAN, Gdańsk.

Marchetti, S., 1980. In situ tests by flat dilatometer. J. Geotech. Geoenvironmental Eng. 106, 299–321.

Marchetti, S., Monaco, P., Totani, G., Calabrese, M., 2001. The Flat Dilatometer Test (DMT) in Soil Investigations, in: A Report by the ISSMGE Committee TC16. Presented at the International Conference on In Situ Measurement of Soil Properties and Case Histories, Bali, Indonesia, p. 41pp.

menard.pl, 2021, n.d. . Menard.pl. URL https://www.menard.pl/wzmacnianie-gruntu/technologie/kolumny-cmc (accessed 11.27.21).

Międlarz, K., Konkol, J., Ba\lachowski, L., 2019. Effective friction angle of deltaic soils in the Vistula Marshlands. Stud. Geotech. Mech. 41, 143–150.

Monaco, P., Amoroso, S., Marchetti, S., Marchetti, D., Totani, G., Cola, S., Simonini, P., 2014. Overconsolidation and Stiffness of Venice Lagoon Sands and Silts from SDMT and CPTU. J. Geotech. Geoenvironmental Eng. 140, 215–227. https://doi.org/10.1061/(ASCE)GT.1943-5606.0000965

Moormann, C., 2016. Design of piles – German practice 35.

Ng, K.W., Suleiman, M.T., Sritharan, S., 2013. Pile Setup in Cohesive Soil. II: Analytical Quantifications and Design Recommendations. J. Geotech. Geoenvironmental Eng. 139, 210–222. https://doi.org/10.1061/(ASCE)GT.1943-5606.0000753

Niazi, F.S., Mayne, P.W., 2013. Cone penetration test based direct methods for evaluating static axial capacity of single piles. Geotech. Geol. Eng. 31, 979–1009.

Ooi, L.H., Carter, J.P., 1987. A constant normal stiffness direct shear device for static and cyclic loading. Geotech. Test. J. 10, 3–12.

Pfähle, E.A., 2012. Deutsche Ges. f.

Potyondy, J.G., 1961. Skin Friction between variuos soils and construction materials. Géotechnique 11, 339–353. https://doi.org/10.1680/geot.1961.11.4.339

Pra-ai, S., Boulon, M., 2017. Soil–structure cyclic direct shear tests: a new interpretation of the direct shear experiment and its application to a series of cyclic tests. Acta Geotech. 12, 107–127. https://doi.org/10.1007/s11440-016-0456-6

Randolph, M.F., Wroth, C.P., 1981. Application of the failure state in undrained simple shear to the shaft capacity of driven piles. Geotechnique 31, 143–157.

Randolph, M.F., Wroth, C.P., 1979. Randolph, M. F., & Wroth, C. P. (1979). An analytical solution for the consolidation around a driven pile. Nternational J. Numer. Anal. Methods Geomech. 3, 217–229.

Seed, H.B., Reese, L.C., 1957. The action of soft clay along friction piles. Trans. Am. Soc. Civ. Eng. 122, 731–754.

Tabucanon, J.T., Airey, D.W., Poulos, H.G., 1995. Pile Skin Friction in Sands from Constant Normal Stiffness Tests. Geotech. Test. J. 18, 350–364. https://doi.org/10.1520/GTJ11004J

Terzaghi, K., Peck, R.B., 1948. Soil Mechanics in Engineering Practice. 2102 GeoFlorida 2010 Adv. Anal. Model. Des. GSP 199 556.

Togliani, G., 2008. Pile capacity prediction for in situ tests. Proc. Geotech. Geophys. Site Charact. 1187–1192.

Togliani, G., Reuter, G., 2015. Pile Capacity Prediction (Class C): DMT vs. CPTu. Proc. DMT'15 Rome June 14 16, 2015.

Tovar-Valencia, R.D., Galvis-Castro, A., Salgado, R., Prezzi, M., 2018a. Effect of Surface Roughness on the Shaft Resistance of Displacement Model Piles in Sand. J. Geotech. Geoenvironmental Eng. 144, 04017120. https://doi.org/10.1061/(ASCE)GT.1943-5606.0001828

Tovar-Valencia, R.D., Galvis-Castro, A.C., Prezzi, M., Salgado, R., 2018b. Short-Term Setup of Jacked Piles in a Calibration Chamber. J. Geotech. Geoenvironmental Eng. 144, 04018092. https://doi.org/10.1061/(ASCE)GT.1943-5606.0001984

Tsubakihara, Y., Kishida, H., 1993. Frictional behaviour between normally consolidated clay and steel by two direct shear type apparatuses. Soils Found. 33, 1–13.

Turner, J.P., Kulhawy, F.H., 1987. Experimental analysis of drilled foundations subjected to repeated axial loads under drained conditions. Rep. EL-S32S Electr. Power Res. Inst. Palo Alto Calif.

Uesugi, M., Kishida, H., Uchikawa, Y., 1990. Friction between dry sand and concrete under monotonic and repeated loading. Soils Found. 30, 115–128.

Verbrugge, J.C., 1981. Évaluation du tassement des pieux à partir de l'essai de pénétration statique. Rev. Fr. Géotechnique 75–82.

Vijivergiya, V.N., 1977. Load-movement characteristics of piles, in: 4th Symp. of Waterway, Port, Coastal and Occean Div., ASCE. pp. 269–284.

Wernick, E., 1978. Stresses and strains on the surface of anchors. https://doi.org/10.1051/geotech/1978003113

White, D.J., Bolton, M.D., 2005. Comparing CPT and pile base resistance in sand. Proc. Inst. Civ. Eng.-Geotech. Eng. 158, 3–14.

Więcławski, P., n.d. Prognozowanie pracy pali Vibro obciążonych osiowo z wykorzystaniem wyników sondowania CPT 132.

Zhang, Q.-Q., Zhang, Z.-M., He, J.-Y., 2010. A simplified approach for settlement analysis of single pile and pile groups considering interaction between identical piles in multilayered soils. Comput. Geotech. 37, 969–976. https://doi.org/10.1016/j.compgeo.2010.08.003